2018

Integrity Assessment Of Earthen Dams And Levees Using Cross-Plot Analysis Of Seismic Refraction And Electrical Resistivity Tomograms

Leti Teklu Wodajo
University of Mississippi

INTEGRITY ASSESSMENT OF EARTHEN DAMS AND LEVEES USING CROSS-PLOT ANALYSIS OF SEISMIC REFRACTION AND ELECTRICAL RESISTIVITY TOMOGRAMS

A Dissertation
presented in partial fulfillment of requirements
for the degree of Doctor of Philosophy
in the Department of Civil Engineering
The University of Mississippi

By

LETI T. WODAJO

May 2018

ABSTRACT

Geophysical methods provide a rapid, economical, non-invasive, and spatial coverage of the subsurface in terms of geophysical properties. On the other hand, geophysical methods can generate multiple geophysical anomalies. An anomaly on a seismic refraction or an electrical resistivity tomogram is an area that has different values compared to its surrounding. Geophysical anomalies in dams and levees can be due to the overall heterogeneity of the subsurface, structures such as principal spillways, artifacts of inversion software, or to a true compromised location, such as an air void due to internal erosion or seepage. Therefore, there is uncertainty involved with using geophysical methods where an anomaly does not necessarily represent a true compromised zone. Identification of true compromised zones requires an invasive geotechnical investigation, such as drilling.

To identify anomalies that are associated with true compromised zones, multiple types of geophysical surveys are commonly conducted. Although the use of multiple geophysical methods and qualitative side-by-side interpretation can reduce this problem to some degree, a more quantitative analysis in identifying the type of compromised zones is required. Such analysis can be achieved with the application of cross-plot analysis. With the use of cross-plot analysis, it is possible to relate and map results from multiple geophysical surveys to more commonly used geotechnical terms such as porosity and moisture content.

This research develops the use of cross-plot analysis using time-lapse seismic refraction tomography and electrical resistivity tomography for the assessment of earthen dams and levees.

The focus of this research is on the development of a method for quantifying the bounding seismic velocity and electrical resistivity values, which then divide the subsurface integrity conditions into different groups. A new approach of using preliminary and laboratory geophysical measurements to define cross-plot constraints is presented. This work will separately target different types of compromised zones, such as sand zones and dry compacted clay zones, by incorporating their unique seismic and electrical resistivity attributes into the cross-plot analysis. A new approach of cross-plot analysis using external physical constraints derived from geophysical surveys and theoretical models at the Francis Levee Site is also presented.

DEDICATION

This work is dedicated to God Almighty my creator,

my strong pillar, my source of knowledge and understanding.

To my dearest wife Liya and to my son Naod,

every good and perfect gift is from above and I'm always grateful to have you.

To my mother Sara, to my father Teklu, to my siblings

Bikila (big bro), Chuni, and Abiti totaw,

thank you for the love, support, and encouragement.

LIST OF ABBREVIATIONS AND SYMBOLS

a	Tortuosity
ARS	Agricultural Research Service
ASTM	American Society of Testing and Materials
CCR	Capacitively-coupled resistivity
CEC	Cation exchange capacity
CMPCC	Common Midpoint Cross-Correlation analysis
C_e	Conductivity due to the presence of clay fraction
C_w	Conductivity of pore fluid
E	Young modulus
ERT	Electrical resistivity tomography
F, F^*	Formation factor, formation factor of shaley sand
FEMA	Federal Emergency Management Agency
G	Shear modulus
G_d	Dry shear modulus
G_s	Saturated shear modulus
HERU	Hydraulic Engineering Research Unit

JARS	Joint analysis of refraction with surface-waves
K	Bulk modulus
K_g	Bulk modulus of saturating gas
K_l	Bulk modulus of saturating liquid
K_d	Bulk modulus of dry rock
K_f	Bulk modulus of saturating fluid
K_o	Bulk modulus of soil mineral grain
K_{sat}	Bulk modulus of saturated rock
LCR	Inductance (L), capacitance (C), and resistance (R)
LiDAR	Light Detection and Ranging
m	Cementation factor
MASW	Multichannel analysis of surface waves
MC	Moisture content
MGOS	Multiple Geode Operating System
n	Saturation exponent
NCLS	National Committee on Levee Safety

Q_v	Concentration of sodium exchange cations of the clay
S, S_w	Degree of saturation
SIRT	Simultaneous Iterative Reconstruction Technique
SRS	Stanford Research Systems
SRT	Seismic refraction tomography
TDR	Time domain reflectometer
USACE	United States Army Corps of Engineers
USBR	United States Bureau of Reclamation
USDA	United States Department of Agriculture
USSD	United States Society on Dams
v_p	P-wave seismic velocity
v_s	S-wave seismic velocity
υ	Poisson's ratio
ZAV	Zero-air-void
λ^e_{Na}	Maximum equivalent ionic conductance of sodium exchange ions
ρ	Soil mass density

ρ_b	Bulk electrical resistivity
ρ_{dry}	Dry density
ρ_f	Mass density of the fluid phase
ρ_g	Density of gas
ρ_l	Density of saturating liquid
ρ_o	Density of soil mineral grain
ρ_s	Density of solid phase
ρ_w	Electrical resistivity of the pore water, density of water
ϕ	Effective porosity
ψ	Axial modulus

ACKNOWLEDGMENTS

I would like to express my sincere gratitude to my research advisor Dr. Craig Hickey, interim director at the National Center for Physical Acoustics and Research Associate Professor of Physics and Geological Engineering, for his continuous encouragement and support over the years. His insight and guidance were invaluable in completing this research. My family and I are thankful to his wife, Rose Hickey, and two daughters Madison and Morgan, for their warm friendship and for becoming our adoptive family 8000 miles away from home!

I would also like to express my sincere gratitude to my academic adviser and committee member Dr. Chung Song, Associate Professor of Civil Engineering, for his valuable contribution, support, and encouragement. He has devoted his valuable time and energy in helping me navigate my graduate studies. I would also like to thank Dr. Elizabeth Ervin, Associate Professor of Civil Engineering, and Dr. Yacoub Najjar, Chair and Professor of Civil Engineering, for their interest and valuable comments on my work.

I would like to say thank you to everyone involved in this research especially to my fellow students past and present including Jared Case, Ted Watson, Blake Armstrong, Turner Arnold, and Gergő Arany, and NCPA employee J. D. Heffington for helping me during field data collection. Thank you for the thousands of hammer swings in the middle of the Mississippi Delta! I would also like to thank John Anderson for taking his valuable time and proofreading this manuscript.

I am as ever, especially grateful to my family, especially to my dear wife Liya, for bearing with me through it all. Thank you for helping me with the lab measurements and edits. To my son

Naod, who has been the light of our life for the last nineteen months, and has given me the extra motivation to get things done. To my mother Sara, father Teklu, and siblings Bikila, Lensa, and Amanuel, thank you for your continuous support and encouragement.

This research was funded by the Department of Homeland Security sponsored Southeastern Region Research Initiative (SERRI) at the Department of Energy's Oak Ridge National Laboratory (Project number. 90034), the United States Department of Agriculture (USDA) Award #58-6408-1-608, and the National Science Foundation and Colorado School of Mines, Partnership for International Research and Education (PIRE) project Award #OISE-1243539/400512.

Thank you!

Leti Teklu Wodajo

TABLE OF CONTENTS

LIST OF TABLES

LIST OF FIGURES

CHAPTER 1

INTRODUCTION

1.1 Motivation of Research

Earthen dams and levees are among the oldest manmade structures on Earth going as far back as 10,000 years (Bassell, 1904 and Cullen, 1962). These structures play a vital role in the day-to-day activities of nations. The purposes of dams include: recreational use, flood control, water supply, fish and wildlife, irrigation, and hydroelectric power generation (National Dam Inventory, 2009). Levees are used as flood control structures protecting urban areas from the overflowing of rivers and ocean waves.

The large number of dams and miles of levees in the United States and their risk of failure is alarming considering their age and engineering design. Out of the 75,000 earthen dams in the US, 56,000 are privately owned and do not undergo periodic assessment (National Dam Inventory, 2009). The US Army Corps of Engineers (USACE) controls 14,000 miles (22,530 kilometers) of levees. In addition to that, 8,000 miles (12,875 kilometers) of levees are under the responsibility of the US Bureau of Reclamation (USBR). A staggering 100,000 miles (160,934 kilometers) of levees are non-federal levees and under local government jurisdiction (National Committee on Levee Safety (NCLS), 2009).

Numerous catastrophic dam and levee failures in the past have caused the loss of life, destruction of properties, and environmental damages (Biswas et. al., 1971, NCLS, 2009). The

2005 New Orleans levee system failure due to Hurricane Katrina encapsulates the staggering damage associated with levee failures. More than 1 million people were displaced with more than 1 million residential structures damaged. More than 1,800 people lost their lives when close to 80% of New Orleans flooded. The Federal Emergency Management Agency (FEMA) spent more than 75 billion US dollars in emergency relief. An additional 15 billion US dollars was spent by the USACE to mitigate and upgrade the levee system and floodwalls surrounding New Orleans (NCLS, 2009, Seed et. al., 2005).

The safety of dams and levees is an international concern. In the Netherlands, 25% of the country is below mean sea level, and, without the protection of levees (also known as dikes or dykes), two-thirds of the country would be flooded daily (Van der Meer et. al., 2009, Ammerlaan, 2007). The entire country is protected by levees, and a total of 1735 levee failures are recorded between 1134 and 2006 (Van Bears et. al., 2009). According to World Bank's dam safety assessment in India, the lives of thousands of people living downstream of 25 high hazard dams are at imminent risk (Dam et al., 2011). According to International-Rivers (IR), there is no adequate information available on the integrity of many dams in the world (IR, 2009).

Like all manmade structures, dams and levees require proper and regular maintenance. A thorough inspection of dams and levees should go beyond visual inspection and address internal features that are not visible from the surface. Geophysical methods, such as seismic refraction tomography (SRT) and electrical resistivity tomography (ERT), have been extensively used for dam and levee investigations. These methods are ideal because they are non-invasive and economical compared to standard geotechnical methods, such as drilling techniques. Geophysical methods provide continuous spatial information compared to single point information obtained from borehole investigations.

While these methods provide valuable information about the subsurface, there is still room for improvement deriving more usable and easily understandable information by integrating the results of both methods. The motivation behind this research is the integration of seismic refraction and electrical resistivity tomography results with the application of time-lapse surveying and cross-plot analysis. By studying the different seismic and electrical attributes associated with seepage and piping, which is the second leading cause of dam and levee failure (Department of Ecology for the State of Washington, 2007), the strength of the two individual methods are combined to deduce more comprehensive information about the subsurface and present it in a manner decision makers can understand.

1.2 Research Objectives

The overall objective of this research is to advance the use of cross-plot analysis to combine time-lapse seismic refraction tomography and electrical resistivity surveys on dams and levees. More focus will be on the development of a method for determining the boundaries of seismic velocity and electrical resistivity values, which divide the subsurface conditions into different classes. These classifications will be based on the material integrity with the help of time-lapse surveys in the field and laboratory measurements. The current effort is to study loamy sand zones and dry compacted clay loam zones separately by studying their unique seismic and electrical resistivity attributes as they relate to seepage and piping.

1.3 Work Scope

This research is composed of seven chapters. The scope of each chapter is explained as follows.

Chapter 1 presents an introduction to the motivation of the research, the main research objective and the scope of the research.

Chapter 2 presents a literature review showing previous work conducted on dams and levees with the use of seismic refraction surveys, electrical resistivity surveys, and cross-plot analysis.

Chapter 3 presents an introduction to the Stillwater embankment model dam, results from conventional time-lapse seismic refraction tomography (SRT) and time-lapse electrical resistivity tomography (ERT) during the cyclic loading of the dam. A summary of the results and shortcomings of SRT and ERT surveys are included in the chapter.

Chapter 4 is an introduction to cross-plot analysis and its application on the Stillwater embankment dam during cyclic loading. The cross-plot analysis is divided into two parts targeting the loamy sand zone and the dry compacted clay loam zone separately. The application of time-lapse based restrictions on the cross-plot analysis is also presented. Observations on the shortcomings of cross-plot analysis are also included in the chapter.

Chapter 5 presents the establishment of constraints to improve the application of cross-plot analysis by including preliminary *a priori* data with the application of seismic velocity and electrical resistivity measurement and laboratory information.

Chapter 6 presents a real-world application of establishing cross-plot analysis constraints using external physical constraints derived from geophysical surveys and theoretical models.

Chapter 7 presents overall conclusions and recommendations for future research.

CHAPTER 2

LITERATURE REVIEW *

2.1 Introduction

In the United States there are approximately 100,000 miles of levees of which only 14,000 miles are owned by the federal government. The remaining 86,000 miles are under the control of state and local government and private owners (Keith et al., 2012). Out of the 100,000 miles of levees, documentation is only available for 14% of the total. Conducting invasive investigations over such a large distance of levees is not feasible. Therefore, there is a need for more expedient methods for the assessment of these structures using economical, non-invasive and less time-consuming methods. Geophysical methods, such as seismic refraction and electrical resistivity, provide a rapid, more economical, and non-invasive option of sub-surface investigation. These methods and others have been used separately and/or in combination to identify existing internal problems with dams and levees (Dahlin et al., 1995, Hickey et al., 2009; Kim et al., 2007, Ivanov et al., 2006; Song et al., 2005, Kilty et al., 1986, Liechty, 2010, Lin et al., 2014, Hickey et al., 2015, Wodajo, 2011).

* A book chapter with an in-depth summary on geophysical methods on earthen dams was published. Hickey, C., Römkens, M., Ph.D., Wells, R., and Wodajo, L., (2015) "Geophysical Methods for the Assessment of Earthen Dams, *Advances in Water Resources Engineering, Handbook of Environmental Engineering, Vol. 14, pp 297 – 359, ISBN: (Print) 978-3-319- 11022-6, (Online) 978-3-319-11023-3.*

2.2 Seismic Refraction Surveys on Earthen Dams and Levees

Seismic refraction surveying is used to map the subsurface seismic velocity distribution from recorded data using mechanical vibrations. Data is obtained by generating seismic energy at the surface at a known location and time, and recording propagation of refracted energy using a spatial array of geophones planted on the surface (Brosten et al., 2005).

Seismic refraction of soils is affected by elastic properties [shear modulus (G), bulk modulus (K), Young modulus (E), Poisson's ratio (υ)], physical properties (porosity, permeability, density, degree of saturation, pressure, and temperature), and lithological properties (grain size, grain shape, grain size distribution) (Uyanik, 2011). Seismic refraction tomography is based on the propagation of seismic waves through the subsurface. These seismic waves propagate through the soil without causing any major deformation (with very small-strain). Seismic refraction methods are more dependent on soil stiffness, which is the resistance of the body to deform under applied force. In this case the applied force is caused by the propagating wave (Clayton, 2011).

P-wave seismic refraction tomography is a method that maps the p-wave velocity distribution in the subsurface. P-wave, short for primary wave, is a type of body wave that propagates through a body by compressional and dilatational uniaxial strains in the direction of propagation. P-wave seismic velocity (v_p) can be written in terms of elastic moduli and mass density (ρ) of the soil as

$$v_p = \left[\frac{\psi}{\rho}\right]^{\frac{1}{2}} = \left[\frac{K + \frac{4}{3}G}{\rho}\right]^{\frac{1}{2}} \quad , \tag{2.1}$$

where ψ is axial modulus, K is bulk modulus, and G is shear modulus. For a fully saturated soil, the mass density of the soil (ρ) is given by,

$$\rho = (1 - \phi)\rho_s + \phi\rho_f, \tag{2.2}$$

where ϕ is effective porosity, ρ_s is the mass density of the solid phase, and ρ_f is the mass density of the fluid phase.

Saturation has an effect on the bulk modulus of porous materials. These effects can be formulated using Gassmann's equations in the low frequency regime (Han and Batzle, 2004).

$$K_{sat} = K_d + \Delta K_d\,, \tag{2.3}$$

where

$$\Delta K_d = \frac{K_o(1 - K_d/K_o)^2}{1 - \phi - K_d/K_o + \phi * K_o/K_f}\,, \tag{2.4}$$

and

$$G_s = G_d\,, \tag{2.5}$$

K_{sat} is the bulk modulus of the saturated rock, K_f is the bulk modulus of the fluid, K_o is the bulk modulus of the soil mineral grain, K_d is the bulk modulus of the dry rock, G_s is the saturated shear modulus, and G_d is the dry shear modulus of the soil. In Gassmann's formulations, water saturation does not affect the shear modulus of the porous medium.

For a partially saturated soil mass, seismic propagation velocity is affected by the degree of saturation (S), the bulk modulus of the saturating liquid (K_l), and the bulk modulus of the gas (K_g).

$$\frac{1}{K_f} = \frac{S}{K_l} + \frac{1-S}{K_g} \quad , \tag{2.6}$$

Where K_f is the effective bulk modulus of the fluid. The mass density (ρ) of a partially saturated soil mass is calculated by,

$$\rho = (1-\phi)\rho_o + \phi S\rho_l + \phi(1-S)\rho_g \, , \tag{2.7}$$

where ρ_o is density of the soil mineral grain, ρ_l is the density of the saturating liquid, and ρ_g is density of the gas.

Seismic velocities are related to the mechanical properties of soils through the elastic moduli as shown in the previous equations. Therefore, indirect investigation of the internal structures of dams and levees is possible by using seismic refraction surveys. Seismic refraction surveying is one of the most commonly used seismic methods for engineering investigations (USACE EM 1110-1-1802, 1995).

Yuan et al., (2012) conducted geophysical studies in two provinces in China. The objective of the studies was to use 3D seismic refraction imaging to investigate problematic areas and other known structures through a dam. The method involved using a simulated material model and estimating the travel time between each source and receiver through the model. The difference between the estimated travel time and the signal travel time obtained from receivers in 3D space was minimized by modifying the property distribution through the model. A survey was conducted on the upstream side of a clay dam. The velocity image obtained from the survey indicated the different velocities through the different parts of the dam. Another survey was conducted on a dam with a known culvert and spillway. The 3D image obtained from this survey indicated the location

and size of the culvert. The authors concluded that this method can be used for detecting seepage pathways and other defective areas through a dam.

Bedrosian et al., (2012) conducted geophysical investigations on the Martis Creek Dam located in Truckee Basin, California, with known potential of failure due to either seepage or an earthquake on nearby faults. Studies of the geologic structure of the area surrounding the dam were conducted focusing on the importance of a wider (regional-scale) understanding of the interpretation of smaller scale (engineering-scale) geophysical data. Multiple geophysical studies were conducted in the surrounding area of the dam including: seismic refraction and reflection, ERT imaging, airborne LiDAR, airborne magnetic field surveys, and magneto-telluric sounding. These studies indicated the presence of a thick package of sedimentary deposits interbedded with Plio-Pleistocene volcanic flows, both covered by glacial outwash. Seismic reflection, seismic tomography models, and magnetic field data were used to determine the distribution and chronology of the volcanic flows. It was determined that the interface between the sedimentary deposits and the overlaying glacial outwash has a major role in groundwater flow and observed seepage.

Moustafa et al., (2012) investigated a dam site located in Al-Lith Basin, Saudi Arabia, to identify the source and pathway of groundwater seepage. Seismic refraction and resistivity imaging were implemented for this investigation. Seismic data was collected using 40Hz geophones with 5m spacing. Surveys were conducted in three lines: the first line along the cofferdam, and two more lines on the downstream side parallel to the first line. Three shots were taken using a weight drop for each survey line. The first shot was at an offset of 10m from geophone 1, the second between geophone 24 and 25 and the last shot (reverse shot) was next to geophone 48. Seismic data was processed using time-term inversion and tomographic inversion.

The time-term inversion was used to obtain the initial velocity model assuming a vertically stratified subsurface without lateral change in velocity. The tomographic inversion was obtained using a ray-tracing technique and computing the travel time of the initial model. The model from the time-term inversion was modified until the difference between the computed travel time and field data was minimized. Results from the seismic tomographic inversion indicated the presence of four distinct velocity layers. Two main depressions filled with alluvium and fractured greenstones linked by narrow sharp uplifted walls were delineated using a refraction survey. These depressions act as buried channels crossing the dam site and causing seepage. Resistivity imaging conducted at the site indicated similar results.

Kim et al., (2011) conducted a study on the Daeryong earth-fill dam located in Korea. The dam, constructed in 1957, has been repeatedly grouted at different locations in the past to stop seepage. Grout was injected into the dam through boreholes drilled from the crest of the dam. P-wave refraction and surface wave surveys were conducted on the crest of the dam. The P-wave refraction survey was conducted using 4.5Hz geophones with 3m spacing and a 5Kg sledgehammer as the source. Three shots were taken at each source location. Surface wave data was also collected using the same geophone spacing and 3m shot intervals. The p-wave velocity tomogram was obtained from first-arrival times using the refraction data inversion algorithm known as the Simultaneous Iterative Reconstruction Technique (SIRT). The surface wave data was processed using the Common Midpoint Cross-Correlation analysis (CMPCC) method which was modified from the MASW technique. Investigation of porosity and water saturation was conducted by gridding both p- and apparent s-wave velocity data into a mesh and calculating the Vp/Vs ratio and apparent dynamic Poison's ratios with the assumption of an isotropic media. Both p-wave and apparent s-wave velocity sections indicated the variation in depth of boundaries

between fill and core and also between core and bedrock. Seepage pathways through the clay core of the dam were indicated as areas of high apparent dynamic Poisson's ratios (>0.44). Combining p-wave travel time tomography and dispersion inversion of Rayleigh waves was a simple and easy way of detecting potential seepage and high porosity zones within and under an earthen dam.

Ivanov et al., (2007) made a comparison between conventional refraction-tomography methods and the joint analysis of refraction with surface-waves methods (JARS). Steps in the JARS method include first determining the s-wave velocity using MASW and then obtaining a pseudo-Vp model by rescaling the Vs estimates using assumptions about the Vp/Vs trend. Both the conventional refraction-tomography methods and the JARS method were tested on two levees located in Southern Texas and Southern New Mexico.

The survey on the Southern Texas site was conducted using two 2D, two-component (2C) survey lines with a geophone spacing of 0.9 m with two receivers (10Hz vertical geophone and 14Hz horizontal geophone) at each location. Two different sources, a 7.25Kg sledgehammer and a mechanical weight drop, were used with a source offset of 1.8m with off-end shots and additional shots extending out to a distance equivalent to the maximum depth of investigation. At the Southern New Mexico site, an array of 10Hz vertical geophones with a spacing of 0.6m were used. Similar sources to those used in the Southern Texas site are also used here, with a source spacing of 2.4m with shots extending beyond the 120 geophone spread to a distance equivalent to the maximum depth of investigation. The JARS method was able to image low velocity layers and zones that were not visible in the conventional method. The JARS method also revealed horizontal layering patterns and channel-like features consistent with geologic expectations.

2.3 Electrical Resistivity Surveys on Earthen Dam and Levees

Electrical resistivity measures the conductivity (ability) or resistivity (inability) of a material to transport electricity. Electrical resistivity surveys measure the electrical resistivity distribution in the subsurface by injecting electric current and measuring electric potential differences with the use of multiple electrodes planted on the surface (Morgan, 2001). In the case of soils, electrical resistivity mainly depends on the mineralogy of the soil, which can be clay content, porosity, degree of saturation, water content, type of pore fluid, and permeability (Garcia-Bengochea et. al., 1979, Abu-Hassanien et. al., 1996, Johansson et al., 1996). Although electrical resistivity of soils also depends on the particle shape, orientation, and alignment, it is not as strongly correlated with the stiffness of the soil as it is with moisture content, clay content, porosity, and salt-water salinity (Cosenza et al., 2006).

For a fully saturated soil without clay, Archie (1942) formulated his first law between porosity (ϕ) and bulk resistivity (ρ_b) as,

$$F = \frac{\rho_b}{\rho_w} = \phi^{-m} \quad , \tag{2.8}$$

where F is the formation factor, ρ_w is the resistivity of the pore water, and m is the cementation factor (1.8 – 2 for sands). Equation 2.8 shows that for a fully saturated clean sand, porosity is inversely proportional to electrical resistivity. This is due to better electrical conduction of the clean sand as its water holding capacity increases.

For partially saturated clean sand, Archie's second law is given by,

$$\rho_b = \rho_w \cdot a \cdot (\phi^{-m} \cdot {S_w}^{-n}) \quad , \tag{2.9}$$

where a is tortuosity (typically set to 1), S_w is the degree of saturation and n is the saturation exponent (2 for water). Equation 2.9 shows that, at constant porosity, electrical resistivity increases with increasing saturation. For constant saturation, there is only a small change in electrical resistivity with increasing porosity.

For a more generalized application, Waxman-Smits model for electrical resistivity incorporates the effect of clay content. Archie's first law is only applicable to soils where there is no clay. When clay is present, electric current is not transmitted only through the pore fluid but also along the surface of the clay mineral (Waxman and Smits, 1968). For a fully saturated soil sample, the Waxman-Smits formula, given by Eq. 2.10 – 2.13, incorporates the conductivity (inverse of resistivity) due to the presence of clay fraction (C_e), the conductivity of the pore fluid (C_w), and the formation factor of shaley sand (F^*), which is approximated by Archie's first law.

$$C_o = \frac{1}{F^*}(C_w + C_e)\,, \tag{2.10}$$

where the conductivity of the clay fraction is given by,

$$C_e = \frac{\lambda_{Na}^e}{1000} \cdot Q_v\ . \tag{2.11}$$

The maximum equivalent ionic conductance of the sodium exchange ions (λ_{Na}^e), measured in $cm^2 \cdot equiv^{-1} \cdot Ohm^{-1}$, is experimentally determined. Waxman and Smits (1968) determined λ_{Na}^e to be 39.6 $cm^2 \cdot equiv^{-1} \cdot Ohm^{-1}$ with confidence level of 90%. The concentration of sodium exchange cations of the clay (Q_v) is given by,

$$Q_v = \frac{CEC(1-\phi)\rho_o}{\phi}\ , \tag{2.12}$$

and has units of ($\mathrm{equiv} \cdot \mathrm{liter}^{-1}$). CEC is the cation exchange capacity determined from the types of clay minerals present in the soil sample. When multiple types of clay minerals are present in the clay fraction of the soil, effective CEC for the clay fraction is determined by,

$$\mathrm{CEC}_{\mathrm{mixture}} = \sum_{\mathrm{i}=1}^{\mathrm{n}} \frac{\mathrm{Mass}_{\mathrm{clay\ type}}}{\mathrm{Total\ mass}_{\mathrm{clay}}} \cdot \mathrm{CEC}_{\mathrm{clay\ type}} \,. \tag{2.13}$$

Electrical resistivity measurements are sensitive to changes in saturation and are commonly used for the detection of seepage in earthen dams and levees. Aal et.al., (2004) showed that a wet or seepage affected area of a dam's subsurface is associated with a low resistivity value. Loke et al., (1995) showed that application of 2D electrical resistivity inversions provide reliable models that can be used to represent the subsurface. Loperte et al., (2015) conducted electrical resistivity measurements to investigate possible water infiltration on a rock-filled dam affected by the presence of fractures. Areas of the dam affected by seepage were localized using electrical resistivity tomography. Loke (1999, 2004) showed that sensitivity of electrical resistivity measurements to changes in saturation could be used to determine depth of water table.

For identifying seepage in earthen dams and levees, and for continuous monitoring (in space) of their subsurface, electrical resistivity methods have been extensively used and are the preferred methods (Butler et al, 1990; Abuzeid et al., 1994; Okko et al., 1994; Panthulu et al, 2001; Zhou et al., 2003; Kim et al., 2004; Lim et al., 2004; Song et al., 2005; Cho et al., 2007; Sjödahl et al, 2008; Case, 2012; Lin et al, 2013; Al-Fares, 2014, Chinedu et al., 2014; Lin et al., 2014). Although the preferred method compared to seismic refraction methods, it is less sensitive to changes in stiffness (Samouëlian et al., 2005).

2.4 Cross-Plot Analysis

Cross-plot analysis has been extensively used in the oil industry for formation evaluations and lithological delineations since the 1960s (Fertl, 1981; Krief et al., 1990; Shahin et al., 2009; Liu et al., 2016; Anyiam et al., 2017; Holmes et al., 2017). Cross-plot analysis using multiple input parameters, such as electrical resistivity, nuclear, and acoustic logging, have been used in determining lithological reservoir characteristics.

Hayashi et al., (2010) conducted a study focusing on the application of cross-plot analysis to levee assessment. For this application, Hayashi et al., (2010) used shear wave velocity and electrical resistivity as the quantifying parameters. Shear strength and permeability play a major role in determining the vulnerability of a levee to seepage and erosion. S-wave velocity is affected by the shear strength and is directly related to the shear modulus of the soil. Porosity of the soil relates to the shear modulus and can be estimated from the s-wave velocity. Soil electrical resistivity is affected by the grain size distribution and clay content. Permeability is also affected by grain size distribution, saturation, soil type, and porosity. Determining the resistivity of the soil therefore can provide more information about the permeability of the soil.

This cross-plot method was applied to a levee located in the Shikoku area in Japan. The surface-wave data was collected using a land streamer with 24 geophones at 1m spacing. This data was processed using CMP cross-correlation analysis and MASW. Electrical resistivity of the levee was determined using the capacitively-coupled resistivity (CCR) method which uses capacitors as electrodes. Results from the study indicated that for a given s-wave velocity, higher resistivity was an indicator of sandy soil whereas lower resistivity was an indicator of clayey soil. For a given resistivity, higher s-wave velocity was an indicator of a high (tight) degree of compaction whereas a lower s-wave velocity was an indicator of a low (loose) degree of compaction. Therefore, low s-

wave velocity and high resistivity is an indication of dangerous (loose, sandy) conditions whereas high S-wave velocity and low resistivity indicates a safe (tight, clayey) levee condition.

Inazaki et al., (2011) used cross-plot analysis to combine individual s-wave velocity and electrical resistivity data collected at different sites and produced a map of permeability distribution and N-value. In order to produce these maps, prior geotechnical data such as N-value was required. For example, in order to relate s-wave velocity and N-value, SPT measurement to obtain the N-value and s-wave measurement to get the s-wave velocity need to be conducted. Since SPT is a point measurement, s-wave velocity values at the same locations are needed to have an accurate correlation between the two. A point s-wave velocity measurement can be done using suspension P-S velocity logging. When conducting seepage and piping vulnerability studies on water retaining structures such as dams and levees, conducting invasive surveys should be the last resort since drilling holes in these structures might add to the existing problems.

Hayashi and Suzuki (2004), Inazaki (2007), and Imamura et al., (2007) have showed similar application of cross-plot analysis where degrees of compaction (loose or dense) are divided using correlations between s-wave velocity values and N-values, and soil types (fine or coarse) are divided using resistivity measurements and by comparing to borehole data.

2.5 Summary

Geophysical methods provide economical and non-invasive options of spatial sub-surface investigation. These methods and others have been used separately and/or in combination to identify existing internal problems with dams and levees.

Both seismic refraction tomography (SRT) and electrical resistivity tomography (ERT) have been used separately or side-by-side to identify subsurface seepage through the body of dams

and levees. Using two or more geophysical methods helps reduce anomalies. The common method of interpretation using these methods is to process and interpret each method separately and compare results for similarities and differences. This is a qualitative approach usually done by searching for anomalies in tomograms showing significant changes in value and explaining what physical condition in the subsurface might cause these changes.

A more complete and semi-qualitative approach of interpreting two or more geophysical methods is by using cross-plot analysis. For example, cross-plot analysis using seismic refraction and electrical resistivity is an approach where different soil types and conditions of dams and levees are classified based on their seismic velocity and electrical resistivity values. Instead of analyzing the results from each method separately, a four quadrant criteria based on seismic velocity and electrical resistivity boundaries is formulated. These boundaries create a four-quadrant system of classification of the internal soil structure of dams and levees. Based on the measured seismic velocity and resistivity at a given location and where that point falls within the four quadrants (safe, probably safe, compromised, and probably compromised), the soil type and integrity of the dam or levee at that location is estimated.

CHAPTER 3

3. GEOPHYSICAL MEASUREMENTS AT STILLWATER MODEL DAM *

3.1 Introduction

In this chapter, application of time-lapse seismic refraction and electrical resistivity measurements on a quarter-scale model embankment dam will be presented. The model dam is constructed with two compromised zones within the dam.

3.2 Introduction to the Stillwater Model Dam

In order to implement time-lapse seismic refraction and electrical resistivity measurements, with the application of cross-plot analysis, to monitor changes in the internal structure of earthen dams caused by seepage and internal erosion, an experimental quarter-scale dam was constructed at the USDA-ARS Hydraulic Engineering Research Unit (HERU) located in Stillwater, Oklahoma.

Construction of the model dam was completed in September, 2010, with a height of 1.22 m (4 ft), a width of 2 m (6.5 ft), and a length of 8.5 m (28 ft). Figure 3.1 shows the cross-section of the dam.

* A section of this chapter was published in a peer-reviewed journal. Rittgers, J. B., Revil, A., Mooney, M. A., Karaoulis, M., Wodajo, L., and Hickey, C. J., (2016), "Time-lapse Joint Inversion with Automatic Joint Constraints," Geophysical Journal International, vol. 207(3), pp 1401-1419.

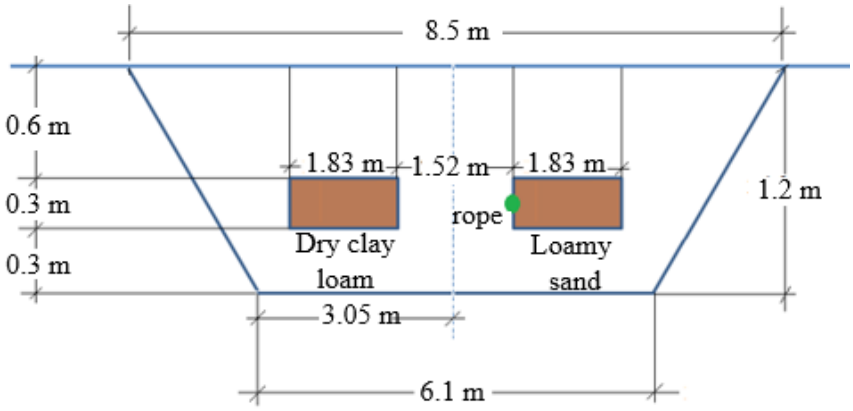

Figure 3.1: Cross-section of model embankment dam.

Laboratory tests were conducted on the clay loam used to construct the dam to determine the optimum water content and the maximum dry density (Hanson et al., 2005). Optimum moisture content (OMC) for the clay loam is 13%, and the maximum dry density is 1906 Kg/m^3. Compacting the dam at the optimum moisture content makes the dam impermeable and stiff and therefore less susceptible to seepage. The main part of the dam was constructed in 11 equal lifts and compacted at the optimum moisture content. Figure 3.2 shows a picture of the dam after construction was completed.

Figure 3.2: Picture of the model embankment dam.

Two compromised zones, a dry compacted clay loam and a loamy sand zone, where placed within the dam as shown in Figure 3.1. These zones measuring 1.83 m (6 ft) x 0.3 m (1ft) run the entire width of the dam and are covered with only 0.9 m (3 ft) of compacted clay loam on the upstream face of the dam. These zones are placed within the dam to represent zones that are susceptible to seepage and piping. The dry compacted clay loam zone was constructed using the same material as the main dam but compacted at a lower moisture content of 10% (3% less than the optimum moisture content). Therefore, this zone has a higher porosity compared to the main dam body. The loamy sand zone is used to represent a highly permeable material within a dam. Loamy sand zones usually do not occur within dams, and this zone is meant to represent the occurrence of sand below the foundation of a dam. In the model, the loamy sand is placed within the body of the dam to simplify construction.

During construction, in situ sensors were inserted at the center of the two compromised zones and at 0.6 m (2 ft) to the right of the loamy sand zone. Figure 3.3 shows the locations of these sensors within the model dam. These sensors are used to monitor changes in temperature and moisture associated with seasonal changes (seepage from rainfall) or seepage due to the loading and unloading of the dam. The sensor pack includes a thermocouple to measure changes in temperature and a time domain reflectometer (TDR) to measure changes in moisture content. The placement of the sensors allows measurements of temperature and moisture content both in lateral and vertical directions.

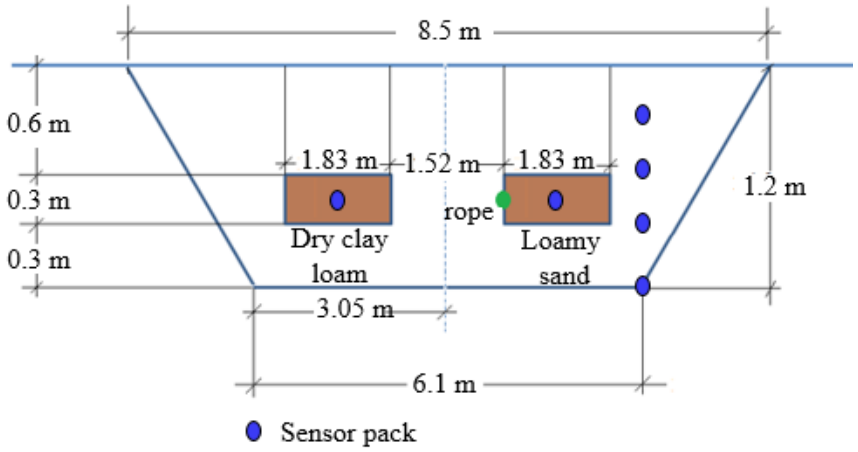

Figure 3.3: Sensor pack locations within the model embankment dam.

3.3 Seismic Refraction Survey, Equipment and Acquisition

Multiple p and s-wave seismic refraction surveys were conducted on the crest of the model embankment dam. Seismic records were collected using 10 Hz, 635 Ohm, GS32CT vertical (p-wave) geophones and horizontal (s-wave) 10 Hz, 600 Ohm, GS20DM geophones. Forty-eight of each vertical and horizontal component geophones were used with a spacing of 0.34 m covering a length of 15.98 m. Figure 3.4 shows the schematic of the model embankment dam and layout of geophones.

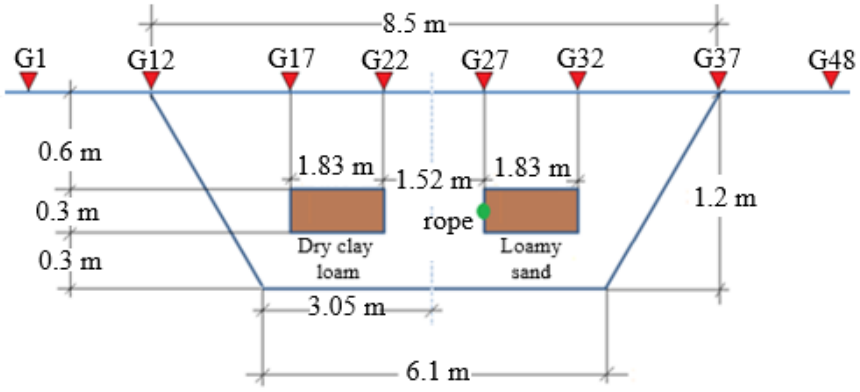

Figure 3.4: Schematic of model embankment dam and geophone layout.

A 5 lb sledge hammer with a trigger attached to the hammer handle was used as a seismic source. A 10 cm x 10 cm aluminum plate was used as a source plate for p-wave refraction surveys and an aluminum source plate with spikes at the bottom was used for s-wave refraction surveys. Figure 3.5 shows a picture of equipment used for seismic refraction surveys.

Figure 3.5: Equipment for seismic refraction survey.

A Geode™ and a field laptop with the Multiple Geode Operating System (MGOS™) were used to collect the ground vibration induced by the sledge hammer and recorded using the geophones. Figure 3.6 shows a schematic of the seismic refraction survey field setup.

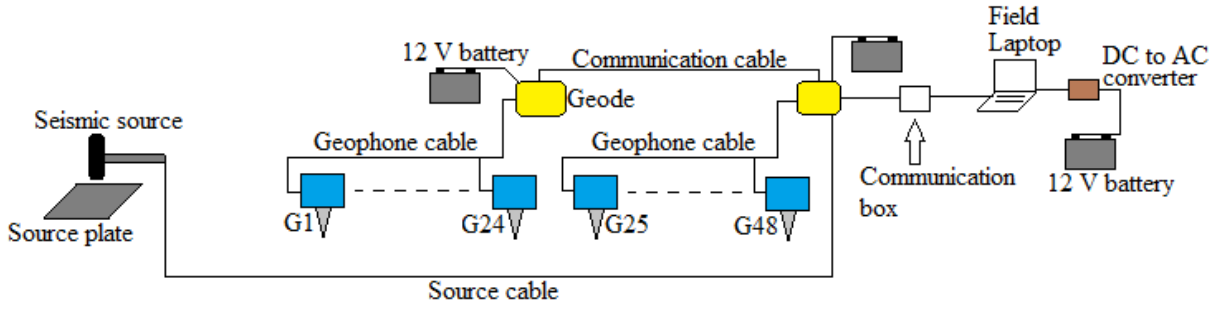

Figure 3.6: Schematic of seismic refraction survey field setup.

For both the p- and s-wave refraction surveys, a geophone spacing of 0.34 m was used. Data was collected with a sample interval of 62.5 µsec and a record length of 1 sec. Data was collected with shots in-between every geophones and half geophone spacing off the first and last geophone. Multiple shots were recorded at each shot location.

3.4 Electrical Resistivity Survey, Equipment and Acquisition

Electrical resistivity surveys were conducted on the crest of the model embankment dam using the SuperSting^{TM} R8/IP resistivity meter. Figure 3.7 shows a picture of equipment used for electrical resistivity surveys.

Figure 3.7: Equipment for electrical resistivity survey.

Figure 3.8 shows Schematic of the model embankment dam and the layout of electrodes is shown in Figure 3.8. Fifty-six stainless steel electrodes with 0.18 m spacing were used to cover a length of 9.9 m.

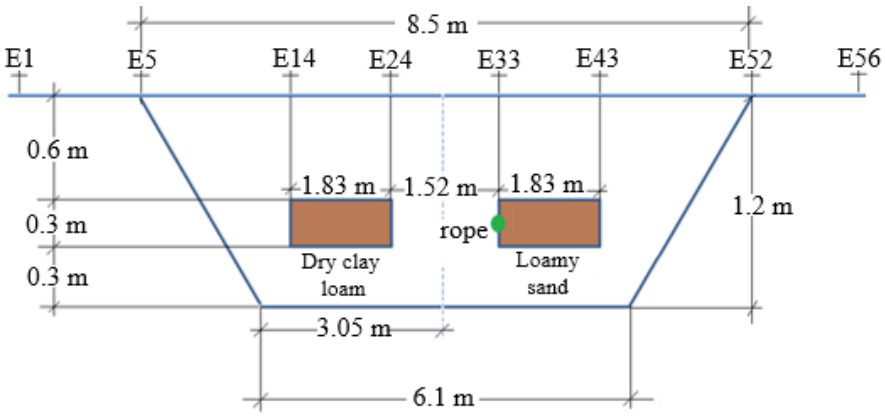

Figure 3.8: Schematic of model embankment dam and electrode layout.

A dipole-dipole electrode configuration was used for the electrical resistivity surveys. The electrical resistivity resolution obtained from the dipole-dipole electrode configuration was better in identifying the two compromised zones compared to the Schlumberger and inverted Schlumberger electrode configuration (Case, 2012).

Electrode configuration and survey parameters, such as number of stacking (number of cycle) and maximum error, were created and saved to a command file using AGI administrator software and loaded to SuperSting^{TM} R8/IP resistivity meter. A commercially available inversion software, EarthImager 2D, was used to process all the electrical resistivity data.

3.5 Time-Lapse P-Wave Seismic Refraction Tomography and Electrical Resistivity Tomography Surveys

Multiple seismic refraction and electrical resistivity surveys were conducted on the model embankment dam over a period of two years. These surveys were conducted at five different times over the two year period as shown in Table 3.1. In this table, the loading condition refers to whether the model embankment dam was filled or drained. For survey period 1, which was conducted at the end of November 2010, time-lapse seismic refraction and electrical resistivity surveys were conducted while the dam went through a complete cyclic loading (unloaded-loaded-

unloaded-reloaded). For survey periods 2, 3, and 4, consecutive surveys were conducted starting with the dam unloaded and keeping the dam loaded until the end of the survey period. On the fifth survey period, consecutive surveys were conducted during the failing of the dam through an internal erosion of the loamy sand zone.

Table 3.1: Seismic refraction and electrical resistivity survey periods and loading conditions for the model embankment dam.

Survey period	Start date	End date	Reservoir loading condition
1	Nov. 29, 2010	Dec. 02, 2010	Full loading and unloading cycle
2	March 14, 2011	March 16, 2011	Unloaded - loaded
3	May 23, 2011	May 27, 2011	Unloaded - loaded
4	August 1, 2011	August 2, 2011	Unloaded - loaded
5	April 16, 2012	April 19, 2012	Unloaded - loaded

Results from the first survey period (Nov. 29 – Dec. 02, 2010) will be presented in the following sections. A total of five p-wave seismic refraction and five electrical resistivity surveys were conducted during survey period 1. Table 3.2 summarizes the surveys conducted during the cyclic loading and unloading of survey period 1.

Table 3.2: Summary of cyclic loading of the dam during survey period 1.

P-wave seismic refraction survey	Electrical resistivity survey	Survey date	Reservoir loading condition
P1	R1	November 29, 2010	Not loaded
P2	R2	November 30, 2010	Loaded for 18 hours
P3	R3	December 1, 2010	Loaded for 44 hours & 20 min.
P4	R4	December 2, 2010	Unloaded
P5	R5	December 2, 2010	27 min. after reloading

The November 2010 surveys were conducted over a period of 5 days. For the first surveys (P1 and R1) and the fourth surveys (P4 and R4), the dam was empty. For the remaining surveys the model dam was loaded to a height of 0.98m (3.2ft), which was 0.36m (1.2ft) above the two compromised zones. Figure 3.9 shows pictures taken during the five surveys.

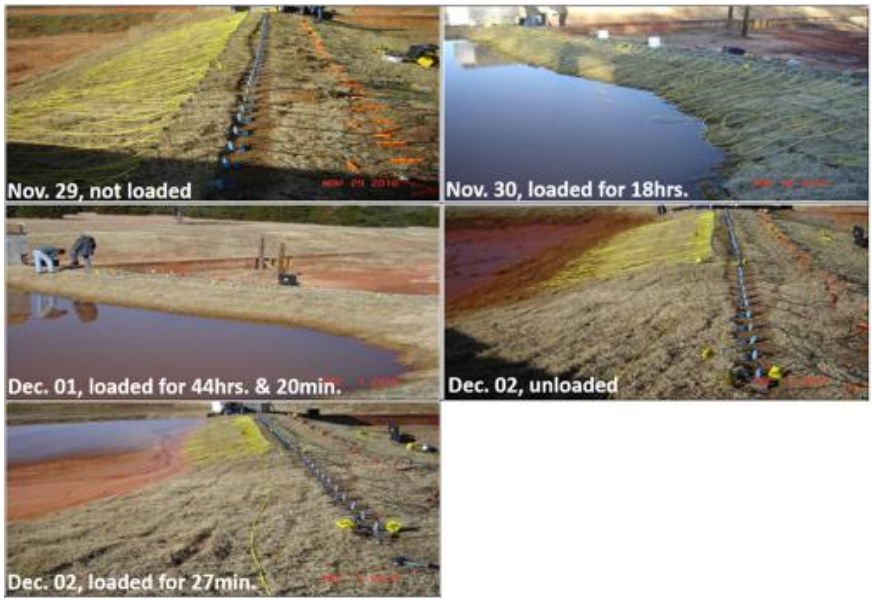

Figure 3.9: Pictures taken during the cyclic loading and unloading of the dam.

Figure 3.10a shows a sample p-wave seismic refraction end shot gather for survey period 1 when the dam was not loaded. The red line indicates the first arrival picks for the shot gather. A sample of the measured apparent resistivity pseudosection for the same survey time is shown in Figure 3.10b. The pseudosection is not the true representation of resistivity distribution in the subsurface; it is converted to a true resistivity by an inversion process and used for analysis and interpretation.

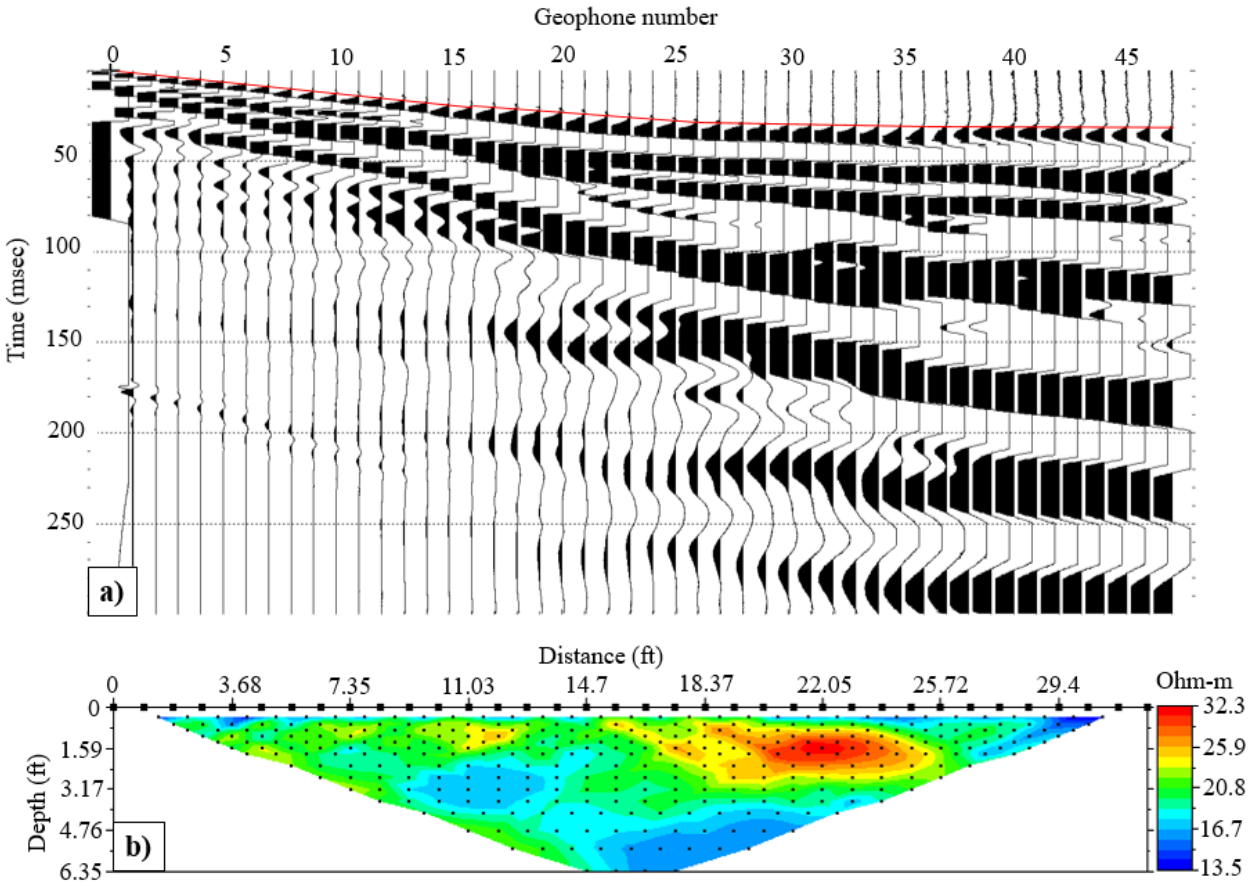

Figure 3.10: a) Example of an end shot gather for survey period 1, initial survey before loading the dam, b) measured apparent resistivity pseudosection for survey period 1 initial survey before loading the dam.

3.6 Moisture Content Readings

Lateral variations in moisture content (TDR readings) during the cyclic loading of the model dam during survey period 1 is shown in Figure 3.11. These values are point measurements taken at different times during cyclic loading and unloading. Moisture content readings from TDR sensors are in terms of volumetric water content, which is the ratio of volume of water to volume of soil. Since moisture content is the measure of the quantity of water contained in the soil, dry soil should have a moisture content of 0. For a fully saturated soil, water will fill all the pores of the soil; therefore the moisture content should be equal to the porosity of the soil. Figure 3.11 shows that the loamy sand zone remains drier compared to the dry compacted clay loam zone and the dam body (clay loam) throughout survey period 1. Although the dam body (clay loam) was compacted with higher moisture than the dry compacted clay loam, the high moisture reading in the dry compacted clay loam is caused by a heavy rainfall that occurred in early November. Due to under-compaction, the dry compacted clay loam has higher porosity than the dam body (clay loam), and rain water can easily infiltrate through it leading to higher moisture content. Even though more water infiltrates through the loamy sand due to high porosity, it is not retained for long due to the high permeability of the loamy sands.

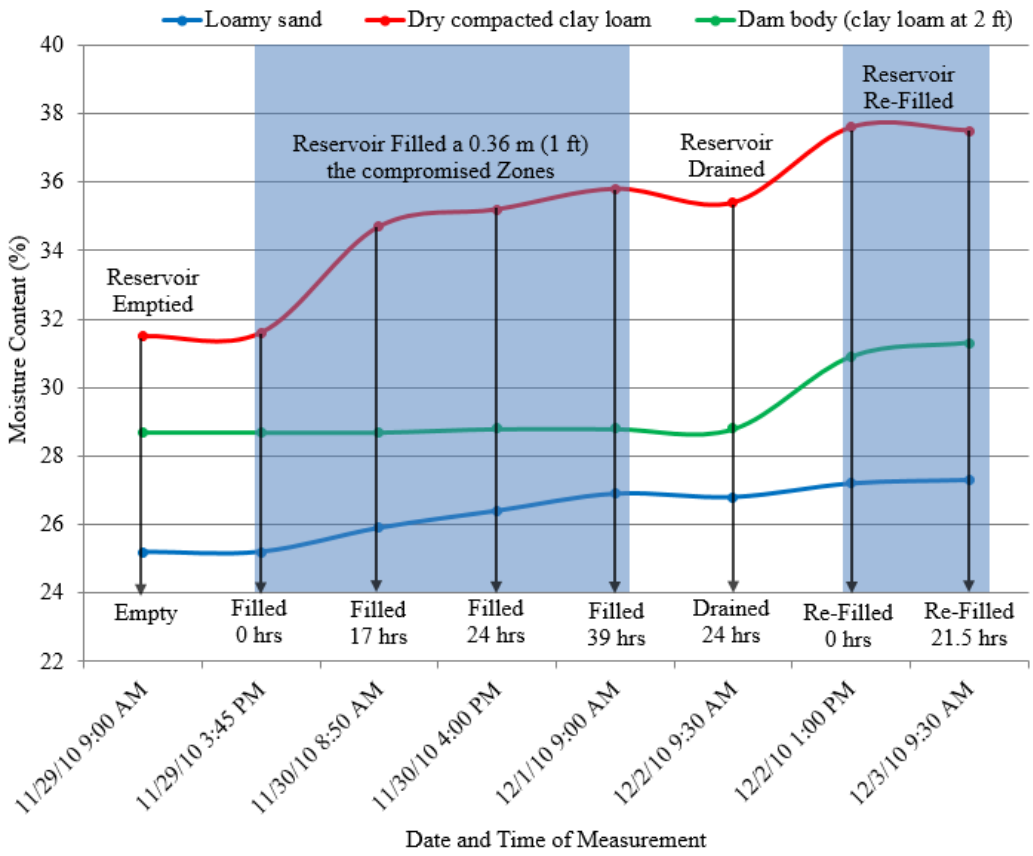

Figure 3.11: Lateral variation in moisture content during survey period 1.

3.7 P-wave SRT Results During Cyclic Loading

All p-wave refraction surveys are processed using a commercially available software, Rayfract™. Results of the inversions (p-wave velocity and ray coverage tomograms) are plotted using the commercially available software, Surfer™. All p-wave velocity values are in meters per second (m/s).

3.7.1 P-wave seismic refraction survey 1 (Dam not loaded)

P-wave velocity tomogram and the corresponding ray coverage tomogram for the first survey when the dam is unloaded (reservoir empty) are shown in Figure 3.12. On this figure and all subsequent p-wave velocity and ray coverage tomograms, the location of the dry compacted

clay loam is shown with the box on the right and the location of the loamy sand is shown with the box on the left. The shape of the dam is also superimposed on all tomograms.

The low velocity of the dam body compared to the surrounding native ground indicates the shape of the dam. The loamy sand is indicated with a low velocity and a corresponding low ray coverage. This is expected because of the high porosity of the loamy sand. An area of low ray coverage is observed at 5 m distance between the ground surface and 0.4 m depth. It is not clear if this an artifact or a problem anomaly associated with the abutment.

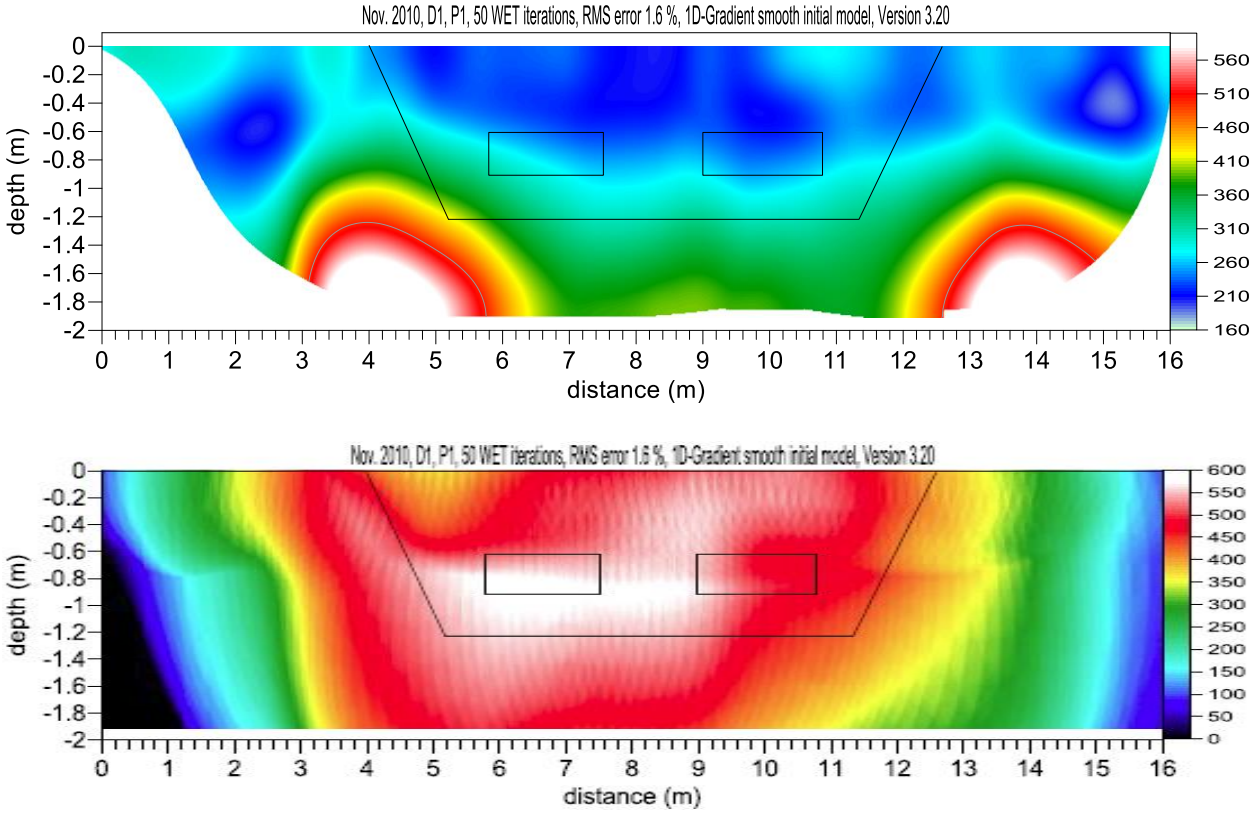

Figure 3.12: P-wave velocity (m/s) and ray coverage tomogram when the reservoir was empty (unloaded).

3.7.2 P-wave seismic refraction survey 2 (Loaded for 18hrs.)

P-wave velocity tomogram and the corresponding ray coverage tomogram when the dam has been loaded for 18 hours (reservoir filled) are shown in Figure 3.13. Significant change is observed in both the velocity and ray coverage tomograms. There is a decrease in p-wave velocity above the dry compacted clay loam and loamy sand zones. An increase in p-wave velocity is observed at the bottom of the loamy sand zone. One reason for the decrease in velocity just above the zones could be that water is infiltrating through the two zones and a gap is forming between the top surface of the two zones and the adjacent surface of the dam. Another possible reason for the change in the velocity distribution could be the change in stress distribution caused by the water load. The ray coverage tomogram shows low coverage at the top of the two compromised zones. This supports the assumption that a gap is forming between the top surface of the zones and the adjacent surface of the dam.

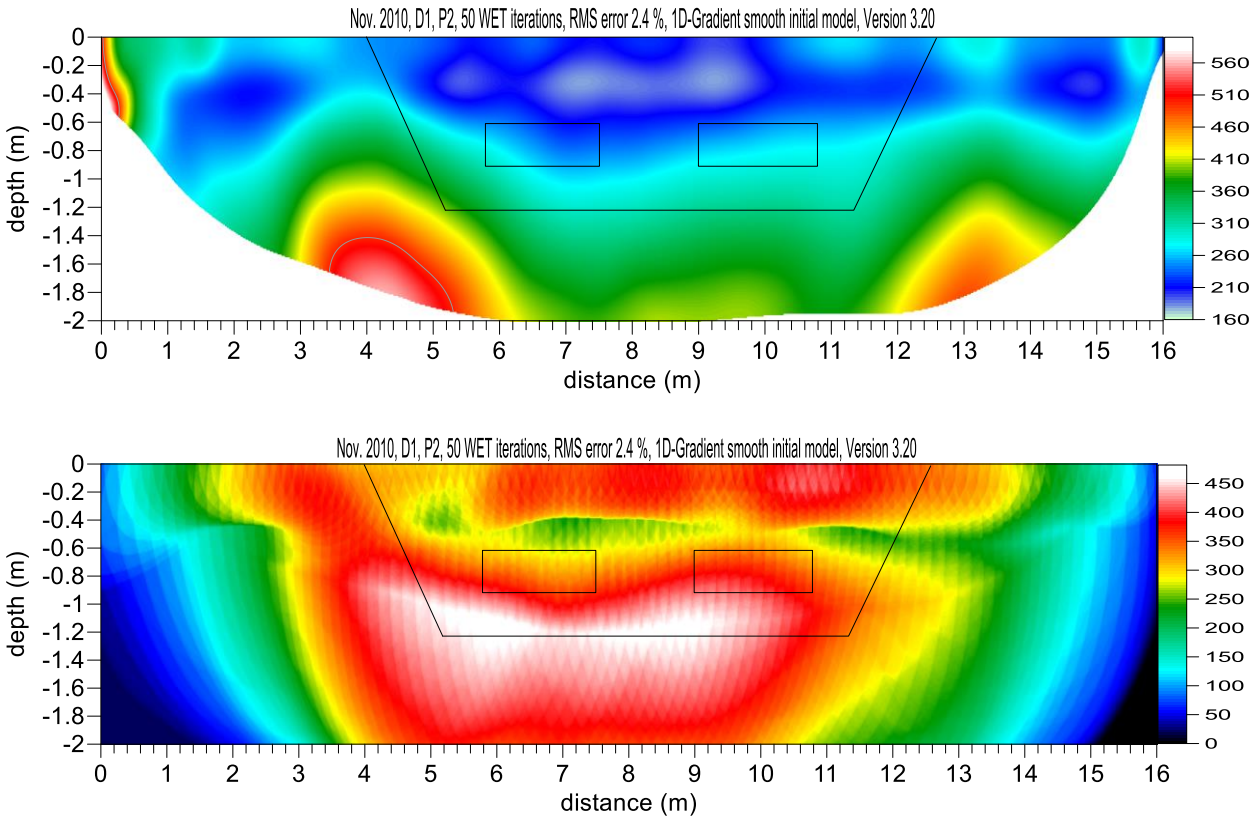

Figure 3.13: P-wave velocity (m/s) and ray coverage tomogram when the dam was loaded for 18hrs.

The low ray coverage area at 5 m distance and 0.4 m depth is more clearly visible when the dam is loaded. The same location has a low p-wave velocity. This could be an indication of seepage through the interface of the dam and the abutment.

3.7.3 P-wave seismic refraction survey 3 (Loaded for 44hrs. and 20min.)

P-wave velocity tomogram and the corresponding ray coverage tomogram when the dam has been loaded for 44 hours and 20 minutes is shown in Figure 3.14. Both the p-wave velocity and ray coverage tomogram show similar features as the previous survey. There is an area of low ray coverage on the right abutment. This could be an indication of seepage through the interface of the dam and the abutment.

The low ray coverage and low p-wave velocity area at 5 m distance and 0.4 m depth is more prominent. A small wet area at the left abutment is observed validating the assumption of a seepage path through the interface of the dam and the abutment.

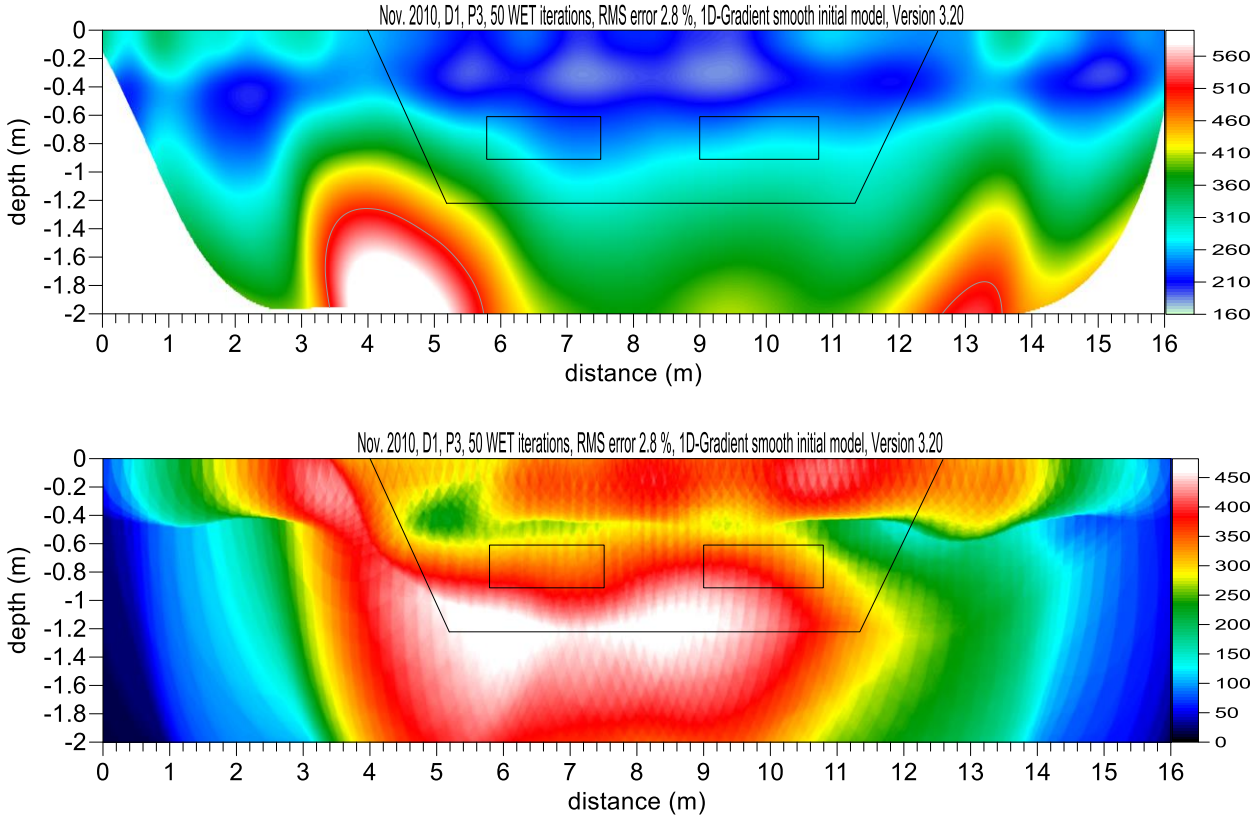

Figure 3.14: P-wave velocity (m/s) and ray coverage tomogram when the dam was loaded for 44hrs and 20min.

3.7.4 P-wave seismic refraction survey 4 (Unloaded)

P-wave velocity tomogram and the corresponding ray coverage tomogram of the model embankment dam after overnight unloading is shown in Figure 3.15. There is a decrease in area of low velocity above the dry compacted clay loam compared to the previous survey. The low velocity and low ray coverage area on the right abutment is more prominent.

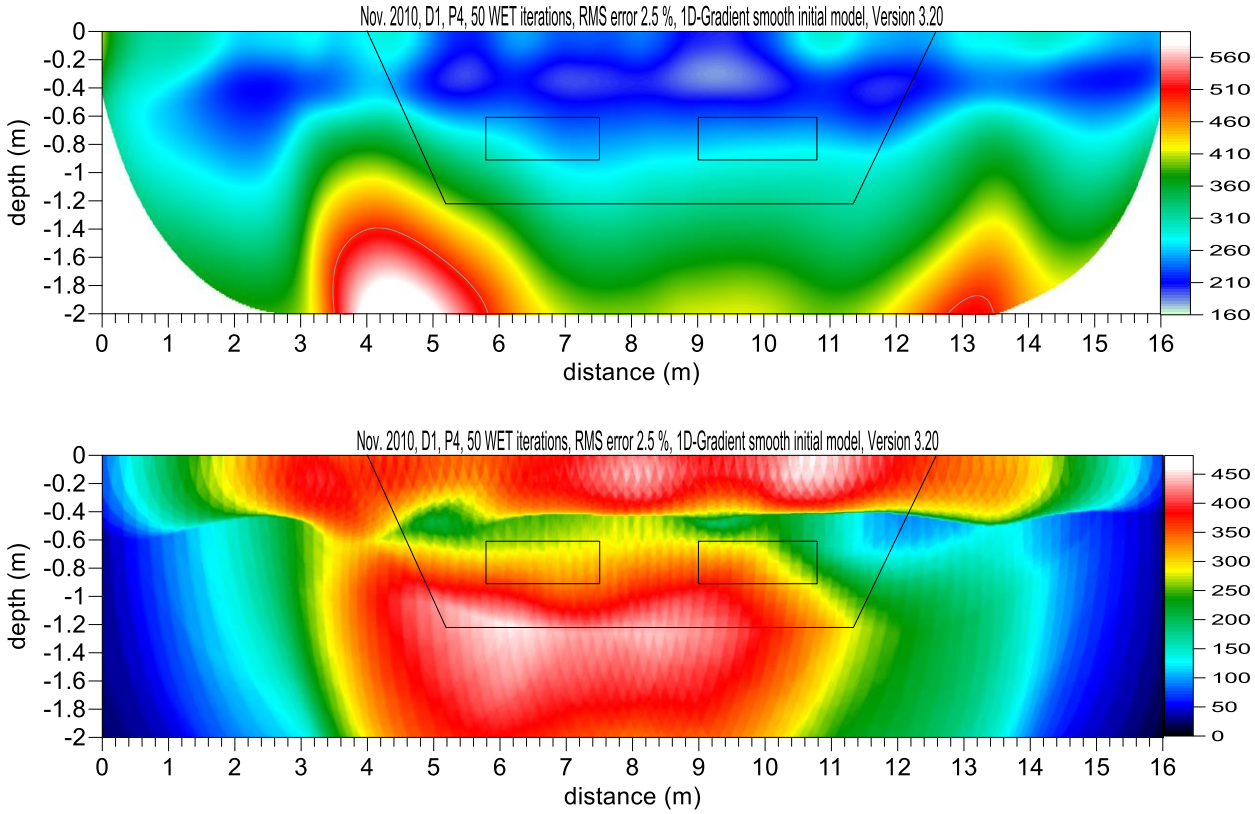

Figure 3.15: P-wave velocity (m/s) and ray coverage tomogram when the dam was unloaded.

3.7.5 P-wave Seismic Refraction Survey 5 (27min. after reloading)

P-wave velocity tomogram and the corresponding ray coverage tomogram 27 minutes after reloading the dam are shown in Figure 3.16. There is no significant difference in both the p-wave velocity and the ray coverage tomogram. The survey was conducted only 27 minutes after the reloading of the dam was completed which might not be sufficient time to notice any major difference.

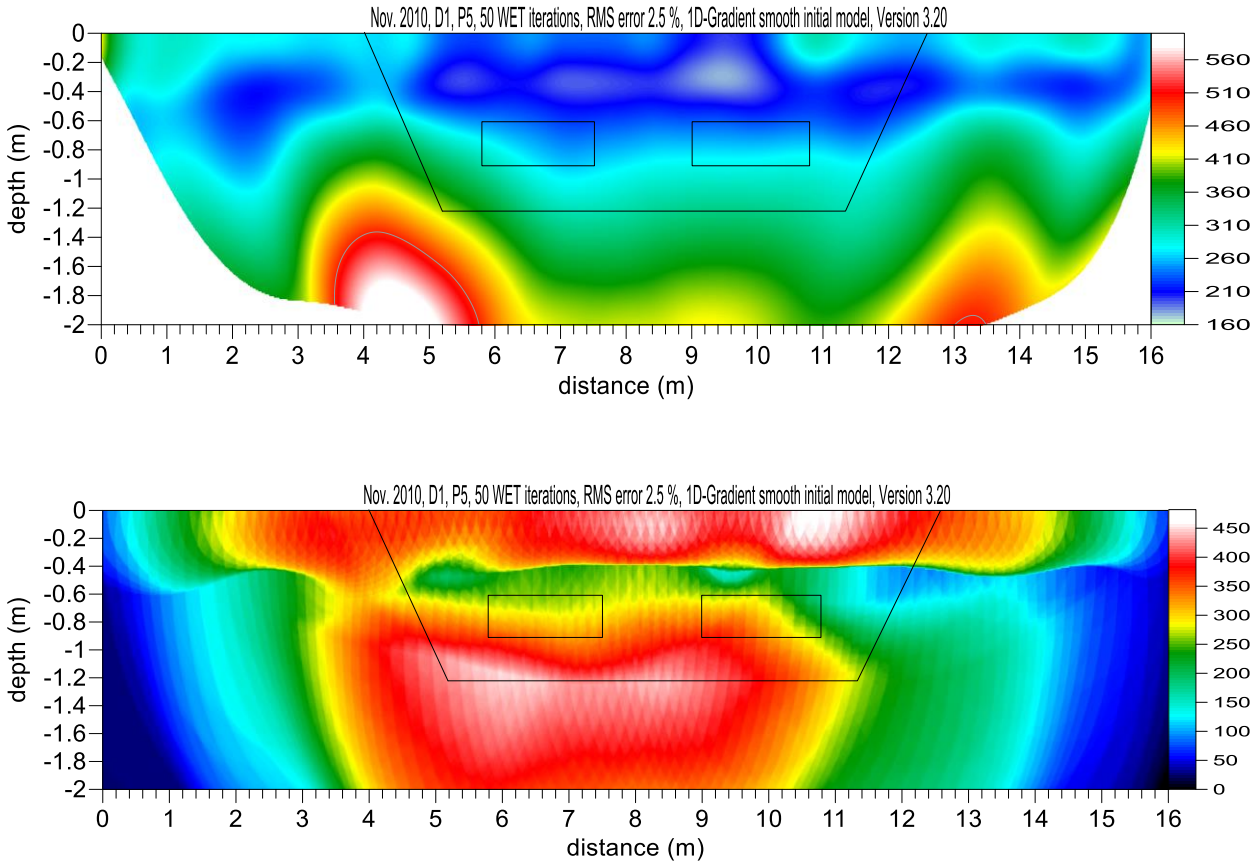

Figure 3.16: P-wave velocity (m/s) and ray coverage tomogram 27min. after reloading.

3.7.6 Comments on the p-wave seismic refraction surveys

Seismic refraction tomography on earthen dams and levees is more effective when there is a significant change in stiffness. This can be seen in the Stillwater model dam results where the general shape of the dam is identified from the native ground. This is because the native ground has been in situ longer and is stiffer than the dam body. The dam body is constructed from excavated clay loam and compacted in multiple layers. Therefore, the contrast in the stiffness of the dam body and native ground shows up as a velocity boundary indicating the shape of the dam. Another example is that the SRT results show some indication of the two compromised zones when the model dam was loaded. As the loading time increases and piping progresses, porosity

increases and the pores are not fully saturated; stiffness decreases, and those locations show up as low velocity zones in the tomograms.

Although the general shape of the dam and indication of the two compromised zones was observed for the model dam experiment, there is a consistent problem of the anomalies showing up at shallower depths than expected. The lateral placement of these anomalies is at the correct location compared to the actual location of the targets (the two compromised zones), but the vertical location of the same anomalies is at shallower depth than the actual targets.

The results from seismic refraction surveys show that the method lacks the resolution to correctly indicate the vertical location of the different zones. Similar problems have been observed on actual dams where principal spillways appear shallower than expected (Wodajo, 2011). Therefore, conducting seismic refraction tomography at locations where information on the geometry of the subsurface is not available might lead to incorrect interpretations, especially in identifying the actual depth of the targets.

When conducting seismic refraction tomography on actual dams and levees, efforts should be made to incorporate depth information in the processing stage of the data. For example, when conducting a survey on an earthen dam, the depth of the principal spillway pipe from as built drawings can be used to adjust the tomogram or as prior information during data processing. Another example is, when conducting seismic refraction surveys on levees where there are no principle spillways going through the levee, depth correction can be made if ground water elevation can be obtained from well information or other sources in the area.

3.8 ERT Results During Cyclic Loading

Electrical resistivity surveys were conducted alongside seismic refraction surveys. All electrical resistivity values are given in Ohm-meter (Ohm-m). Similar to the p-wave velocity tomograms, the location of the loamy sand zone is shown with a box on the right and the location of the clay loam zone is shown with a box on the left.

3.8.1 Electrical resistivity survey 1 (Dam not loaded)

Electrical resistivity tomogram for the first survey when the dam is unloaded (empty) is shown in Figure 3.17. The resistivity of the dam close to the surface is higher than the resistivity at the bottom of the dam. Location of the loamy sand zone is indicated with a high resistivity. In addition to the natural high resistivity of sandy soils, this is expected because the loamy sand is drier than the dry compacted clay loam zone and dam body (clay loam) as shown in the TDR sensors plot. Although the compromised dry compacted clay loam is wetter than the dam body (clay loam), it is not clearly indicated in the electrical resistivity tomogram.

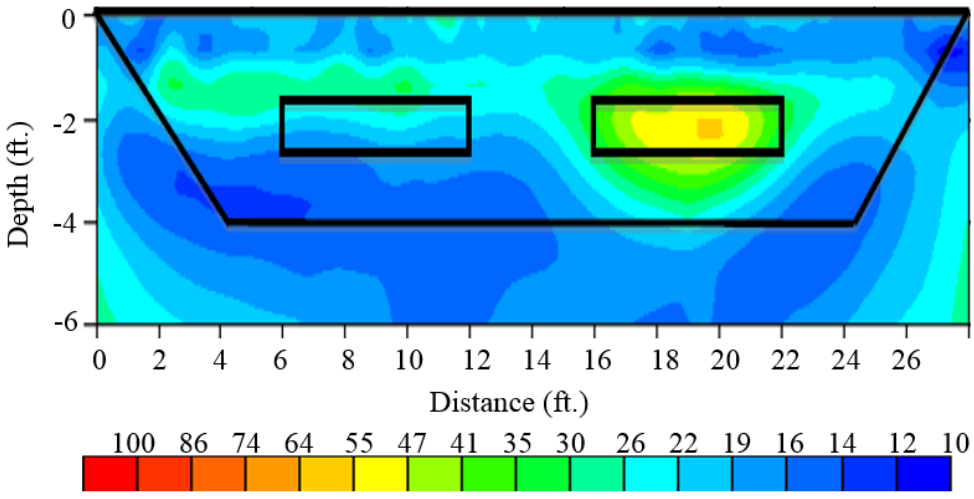

Figure 3.17: Electrical resistivity tomogram (Ohm-m) when the reservoir was empty (unloaded).

3.8.2 Electrical resistivity survey 2 (Loaded for 18hrs.)

Electrical resistivity tomogram when dam has been loaded for 18 hours is shown in Figure 3.18. The tomogram shows that the resistivity in the loamy sand zone is decreasing which is an indication that water is seeping into the zone. TDR sensor in the loamy sand shows an increase in moisture content which supports the decrease in resistivity. There is a decrease in resistivity at the bottom of the dry compacted clay loam which is also associated with an increase in moisture content due to seepage. TDR sensor reading also shows an increase in moisture content within the dry compacted clay loam.

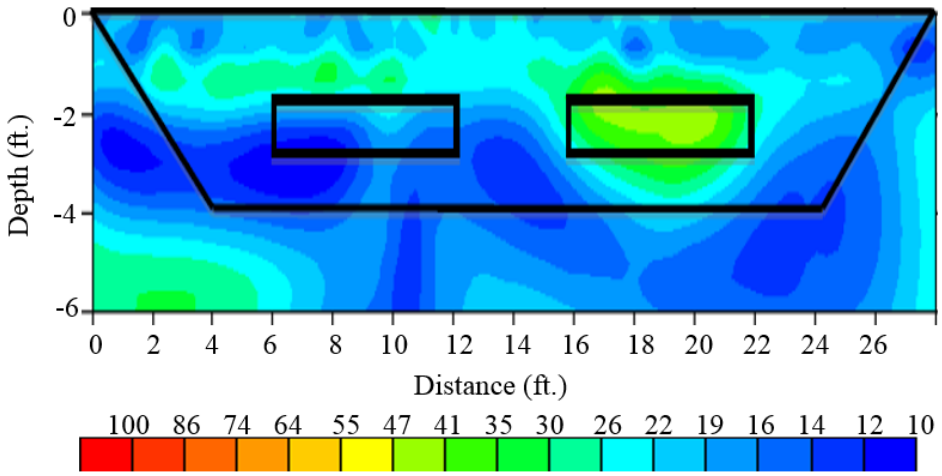

Figure 3.18: Electrical resistivity tomogram (Ohm-m) when the dam was loaded for 18hrs.

3.8.3 Electrical resistivity survey 3 (Loaded for 44hrs. and 20min.)

Electrical resistivity tomogram when the dam has been loaded for 44 hours and 20 minutes is shown in Figure 3.19. There is no significant change in the electrical resistivity tomogram compared to the previous survey. Moisture content readings for the two zones and the dam body remain almost constant between 18 hours of loading and 44 hours of loading. This could explain why there is no significant change in the tomograms.

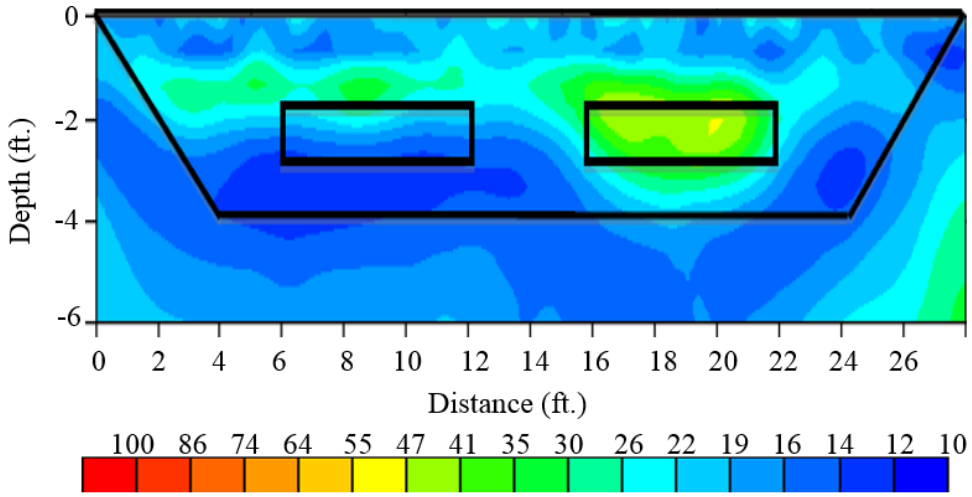

Figure 3.19: Electrical resistivity tomogram (Ohm-m) when the dam was loaded for 44hrs. and 20min.

3.8.4 Electrical resistivity survey 4 (Unloaded)

Electrical resistivity tomogram of the model embankment dam after unloading it overnight is shown in Figure 3.20. TDR sensor readings indicate a slight decrease in moisture content in both zones and the dam body due to unloading. The dry compacted clay can now be identified with a low resistivity zone. The previous high resistivity of the loamy sand zone has dropped to the resistivity of the dam body which makes it difficult to identify the zone. Two low resistivity zones are shown on both abutments which could be an indication of water seepage through the interface of the abutment and the dam body. Even though the dam is empty at the time of this survey, it is not believed that enough time has passed for the water that seeped through the dam when the dam was loaded to dissipate.

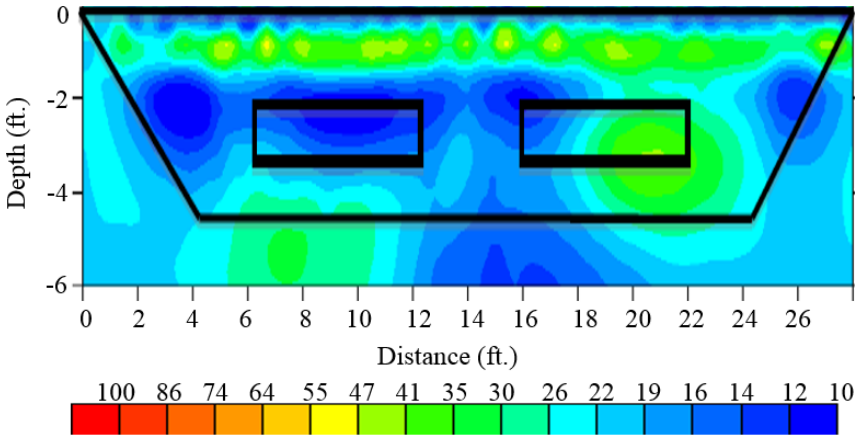

Figure 3.20: Electrical resistivity tomogram (Ohm-m) when the dam was unloaded.

3.8.5 Electrical resistivity survey 5 (27min. after reloading)

Electrical resistivity tomogram 27 minutes after reloading the dam is shown in Figure 3.21. There is an increase in the moisture content of the two zones and the dam due to the reloading of the dam. The resistivity tomogram better indicates the increase in moisture content in the loamy sand than in the dry compacted clay. At only 27 minutes after loading it is believed that more seepage is taking place between the interface of the loamy sand zone and the dam than through the interface of the dry compacted clay loam and the dam. This is because the interface between the loamy sand and the dam is more permeable due to the difference in material and compaction effort.

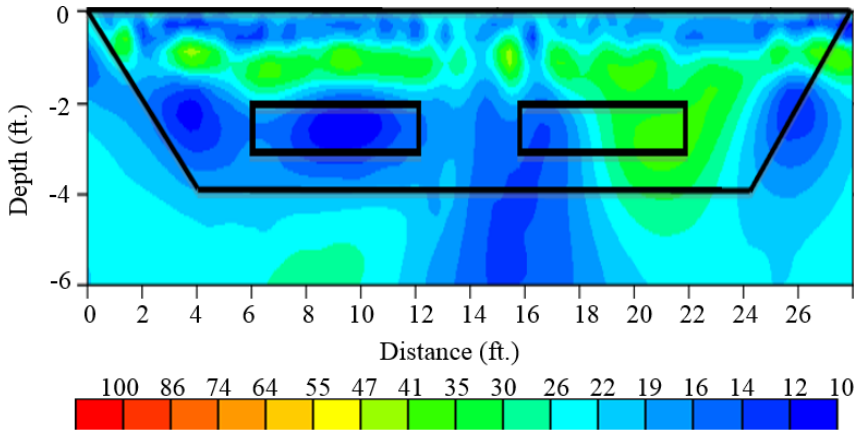

Figure 3.21: Electrical resistivity tomogram (Ohm-m) 27min. after reloading.

3.8.6 Comments on the electrical resistivity surveys

Electrical resistivity of soils is not as strongly correlated with the stiffness of the soil as it is with moisture content, clay content, porosity, and salt water salinity (Cosenza et al., 2006). The sensitivity of electrical resistivity to mineralogy can be seen on the Stillwater model dam survey before loading; where the loamy sand zone is clearly identified from the surrounding clay as a high resistivity anomaly. Stillwater results also show that electrical resistivity is more sensitive to moisture content. As moisture content increases with loading time, the initial high resistivity of the loamy sand starts to decrease.

The fact that electrical resistivity is more dependent on moisture content than stiffness is evident by observing the dry compacted clay loam zone. Before the model dam was loaded, even though the dry compacted clay loam has lower stiffness than the surrounding dam body, it is not identified in the electrical resistivity tomogram. Once the model dam is loaded and adequate time has passed for the water to reach the dry compacted clay loam, a low resistivity anomaly appears in the resistivity tomogram indicating the dry compacted clay loam zone.

Another example of the weak correlation between electrical resistivity and soil stiffness can be observed when considering the shape of the model embankment dam. Compared to seismic refraction tomography, electrical resistivity offers less information on the general shape of the dam. Unless there is seepage (moisture content or piping) or change in mineralogy between different interfaces of the subsurface, it is difficult to identify different geometries within the subsurface using electrical resistivity surveys.

Even though electrical resistivity is lacking in identifying the shape of the dam, the lateral and vertical placement of the two compromised zones in the resistivity tomograms are more accurate compared to that of the velocity tomograms.

3.9 Summary

Time-lapse seismic refraction tomography and electrical resistivity tomography were conducted on a model embankment dam during a full loading and unloading cycle. The model dam was constructed with two compromised zones; dry compacted clay loam zone and loamy sand zone.

The p-wave refraction survey conducted a short time after loading shows substantial changes that might be associated with stress redistribution within the embankment. After a longer period of loading time, the effects of seepage are evident in the tomograms but they are not collocated with the actual location of the compromised zones. These anomalies, with a slight decrease in p-wave velocity, are present at shallower depths than expected.

Water seepage reduces the high resistivity of the loamy sand in the tomograms to the baseline resistivity of the dam. The resistivity of the dry compacted clay loam also decreases with cyclic loading. This evidence helps validate the time-lapse ERT method for detecting seepage inside a dam. Since electrical resistivity is more sensitive to small changes in moisture content, conducting electrical resistivity surveys right after the completion of construction can be used to check if the dam was compacted with uniform moisture content.

Both seismic refraction tomography and electrical resistivity surveying provide valuable information for earthen embankment dam and levee investigation. Seismic refraction methods perform better when there is a good contrast in the stiffness of the different parts of the subsurface

including compromised and safe zones. Seismic refraction methods provide valuable information in identifying different boundaries in the subsurface, but it is difficult to identify different soil types and the vertical depth accuracy is poor. Electrical resistivity surveys on the other hand are more sensitive to changes in mineralogy and water content but not as sensitive to changes in stiffness.

A more comprehensive information assessment of the integrity of earthen embankment dams and levees could be obtained by combining the strengths of seismic refraction tomography and electrical resistivity surveys. One approach of obtaining this is by finding common traits that affect both the seismic and electrical properties of soils. Cross-plot analysis based on seismic and electrical attributes to seepage and piping can be used as a starting point for this approach.

CHAPTER 4

4. CROSS-PLOT ANALYSIS ON THE STILLWATER MODEL DAM

4.1 Introduction

In the previous chapter, time-lapse p-wave seismic refraction and electrical resistivity measurements were conducted on the Stillwater model dam. Although these methods provide valuable information on the integrity assessment of dams and levees, a more complete assessment requires combining the strength of individual methods.

In this chapter, a new application of cross-plot analysis using the time-lapse p-wave seismic refraction and electrical resistivity measurements on the Stillwater model dam will be presented.

4.2 Introduction to Cross-plot Analysis

Cross-plot analysis using seismic refraction and electrical resistivity results is an approach where different soil types and conditions of dams and levees are classified based on their seismic velocity and electrical resistivity values (Hayashi et al., 2010). Instead of analyzing the results from each method separately, a four quadrant criteria based on the ranges of seismic velocity and electrical resistivity are used. Based on the measured seismic velocity and resistivity at a given location and where that point falls within the four quadrants, the soil type and integrity of the dam or levee at that location is estimated.

An illustration of a cross-plot criteria based on seismic and electrical attributes for seepage and piping is shown in Figure 4.1. In the quadrant labeled 1, with low p-wave velocity and high

resistivity, the dam is classified to be in poor condition. This is because low p-wave velocity is associated with poor compaction (low stiffness) and high porosity, whereas high resistivity is associated with low clay content or a high porosity unsaturated sand. Therefore, the combination of these factors would classify a dam as being in a poor condition. Criteria for a good dam condition is shown in quadrant 4 with high p-wave velocity and low resistivity. A combination of well compacted soil with low porosity (high p-wave velocity) and high clay content (low resistivity) is considered a good dam condition. Although low resistivity can also be associated with high porosity brine saturated sand, this is not a likely condition in dams and levees.

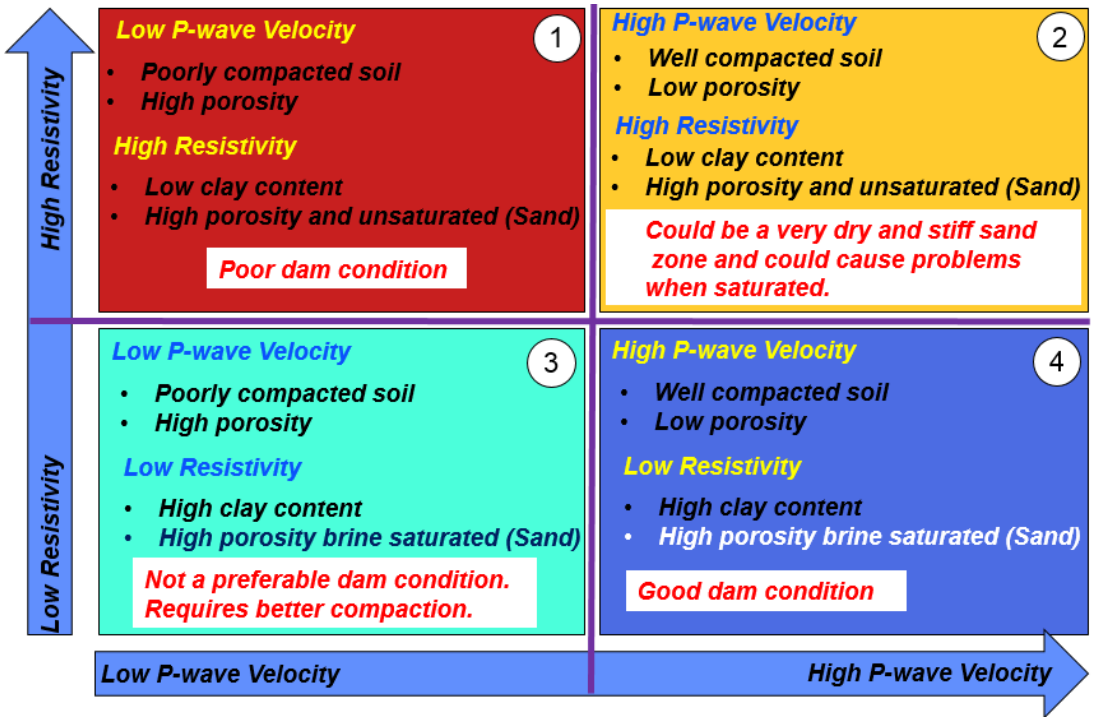

Figure 4.1: Cross-plot analysis using seismic velocity and electrical resistivity values.

Although the cross-plot analysis using the criteria shown in Figure 4.1 can be used as a general guide, it requires some modification based on the type of the compromised zone (poorly compacted clay zone or sand zone). For example, after long loading time and rainwater infiltration, it is difficult to find a dry compacted clay zone with high electrical resistivity. This is because

clays have surface conductance that significantly lowers their electrical resistivity value (Abu-Hassanien et. al., 1996) and the additional saturation from wetting further drops their electrical resistivity. Therefore, referring to Figure 4.1, the electrical resistivity of a saturated dry compacted clay zone will not fall in quadrant 1 and could even drop lower than the electrical resistivity of a well-compacted saturated clay in quadrant 4. Therefore, based on Figure 4.1, a dam in poor condition with a saturated dry compacted clay zone with low electrical resistivity and low p-wave velocity falls in quadrant 3 and not in quadrant 1. On the other hand, the cross-plot criteria shown in Figure 4.1 can be directly applied for targeting sand zones. Even though the resistivity of the sand zone can also drop over time with saturation, it will not drop lower that the resistivity of a saturated clay zone.

4.3 Cross-plot Analysis Targeting the Stillwater Loamy Sand Zone

To test the concept of cross-plot analysis, the Stillwater dam p-wave velocity and electrical resistivity tomograms are re-gridded so that each plot has the same number of grid points (nodes). Figure 4.2 shows the re-gridded p-wave velocity and electrical resistivity tomograms for the November survey 1 (unloaded dam).

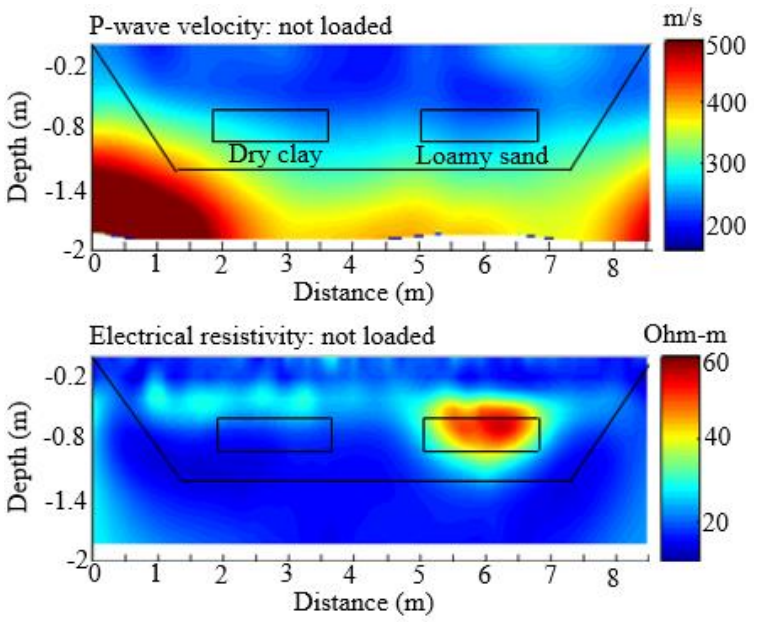

Figure 4.2: Re-gridded p-wave velocity and electrical resistivity tomograms for November survey 1.

Once the tomograms are re-gridded, the anomaly associated with the loamy sand zone is selected. This selection is made by closely observing the p-wave and electrical resistivity tomogram and identifying the anomaly in each tomograms associated with the loamy sand zone. Anomalies associated with the compromised zones can be identified with good accuracy because the locations of the compromised zones are known beforehand. However, in real field studies this is not the case. The top plot of Figure 4.3 shows the loamy sand zone anomaly from the p-wave tomogram and the bottom part shows the loamy sand zone anomaly from the electrical resistivity tomogram. The location of the anomaly from the p-wave tomogram does not fall inside the box labeled loamy sand due to the vertical accuracy problem associated with p-wave refraction surveys. The size of the window used to select the anomaly on both tomograms is the same. The safe zone (SF) in Figure 4.3 is a zone within the model embankment dam that is considered safe. The location of the safe zone is the same for both the p-wave and electrical resistivity tomograms and does not change for all loading conditions.

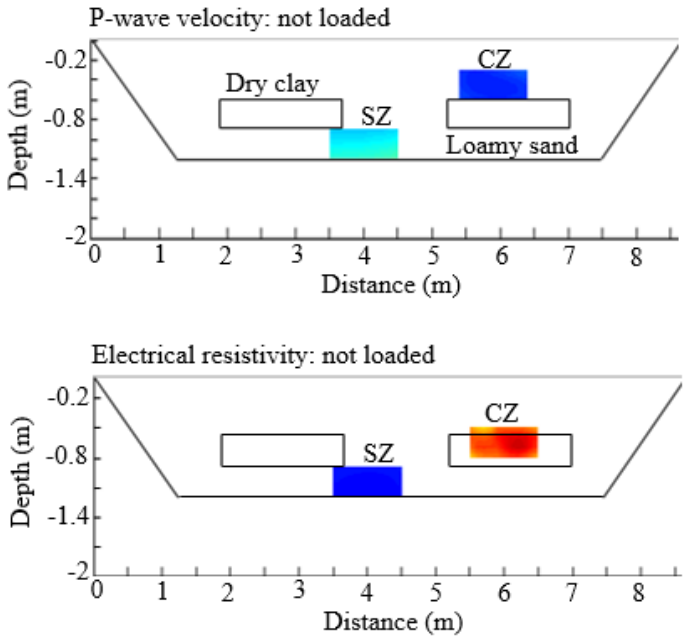

Figure 4.3: Location of the loamy sand anomaly and a safe zone (SZ) for November survey 1.

After the compromised and safe zones are selected, a scatter plot is produced as shown in Figure 4.4. The red markers in Figure 4.4 are associated with the loamy sand anomaly windows and the blue markers are associated with the safe zones. A clear separation between the loamy sand and the safe zone is indicated in the scatter plot. This is expected because loamy sand typically has higher electrical resistivity and lower p-wave velocity compared to clay loam. The next step is to generate the scatter plots for all the loading conditions on one figure to study dependence on the time the survey is completed.

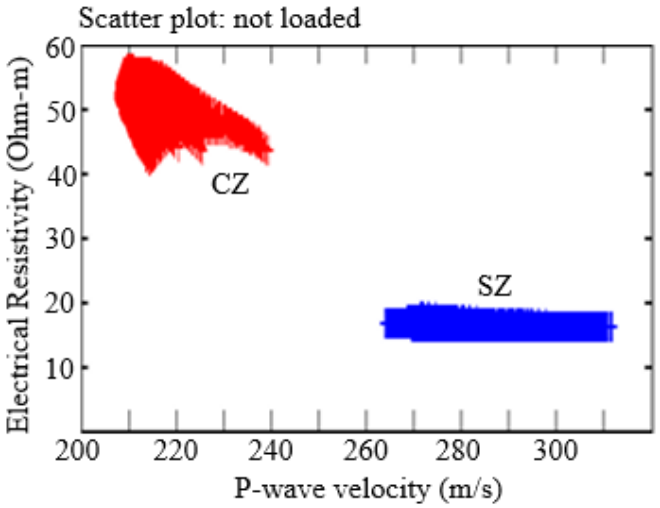

Figure 4.4: Scatter plot for the compromised (loamy sand) and safe zones for November survey 1.

The scatter plots for all the loading conditions from the November cyclic loading surveys are shown in Figure 4.5. The scatter plot shows there is a clear separation between the compromised (loamy sand) zone and the safe zone. The percent change in resistivity and velocity from the safe to the loamy sand zone is about 150% and 46%, respectively. The compromised (loamy sand) zone shows a decrease in resistivity with longer loading time whereas there is no significant change in velocity after the first loading. Both resistivity and velocity of the safe zone show no significant change for different loading conditions which could be due to the short experiment time for water to infiltrate to the safe zone.

The most important decision in the cross-plot analysis is selecting the bounding values of electrical resistivity and seismic velocity that divide the four quadrants of the scatter plot. Case 1 shown by the red line in Figure 4.5 is a narrow (targeted) selection of boundary values and can be used if there is prior information that most of the dam is in a safe condition. Case 2 shown by the green line in Figure 4.5 on the other hand is a conservative (high factor of safety) selection and assumes most of the dam could be in a compromised condition. Therefore, based on the boundaries selected, the cross-plot analysis could have low or high factors of safety.

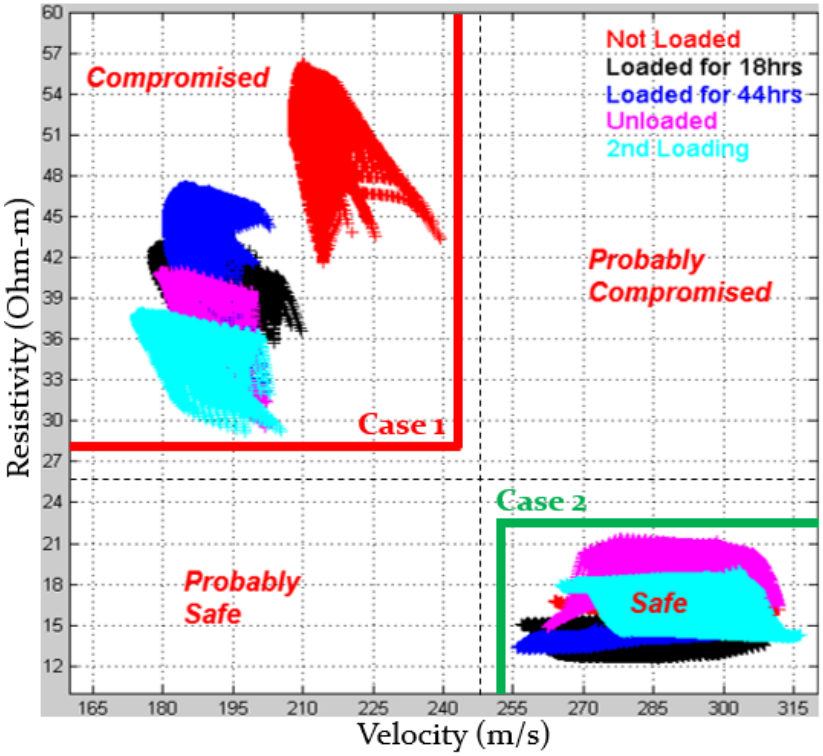

Figure 4.5: Scatter plot for all the loading conditions for the November cyclic loading (targeting the loamy sand zone).

Figure 4.6 shows the electrical resistivity and p-wave velocity values used for the November cyclic loading cross-plot analysis focusing on the loamy sand zone. Considering prior information that the loamy sand zone is a localized problem compared to the overall size of the dam, values of 28 Ohm-m for electrical resistivity and 240 m/s for p-wave velocity are used. These values are picked from observation of the scatter plot and in order to have a tight boundary focusing on the loamy sand zone.

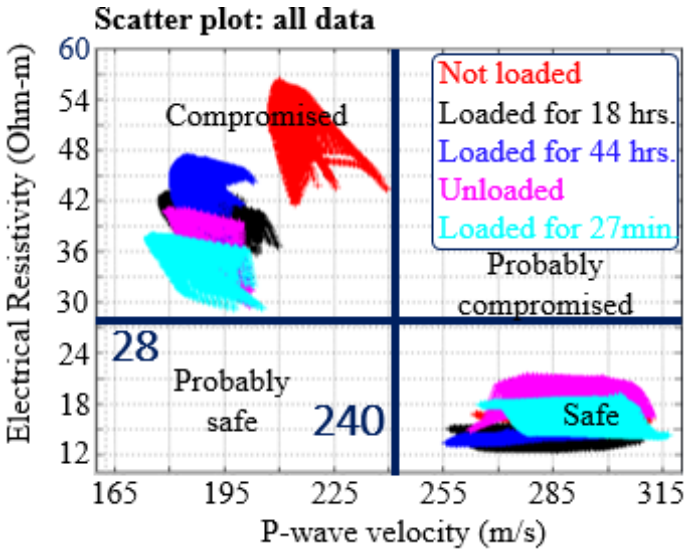

Figure 4.6: Boundary selection for cross-plot analysis (targeting the loamy sand zone).

Once the boundary values are selected, the next step is to use the re-gridded electrical resistivity and p-wave velocity tomograms and build cross-plot maps of the entire dam. For each and every pair of identical grid points on both tomograms, the electrical resistivity and p-wave velocity values are checked in which quadrant they fall on the scatter plot. Therefore, depending on the quadrant in which the velocity-resistivity pair is located, it is color coded to produce the cross-plot map of the entire dam.

The cross-plot map targeting the loamy sand zone for the November survey 1, when the dam was not loaded, is shown in Figure 4.7. The top part of the figure shows the 2D cross-section map. The bottom part, which is the plan view, is produced using the 2D cross-section map and plotting the worst condition in the vertical direction. The plan view is important because it provides the lateral location of compromised zones and therefore avoids the depth uncertainty associated with seismic refraction surveys.

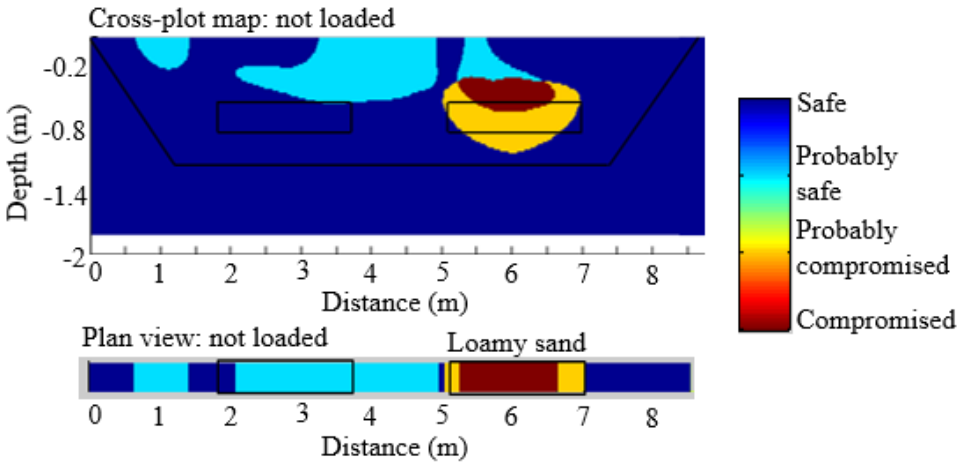

Figure 4.7: Cross-plot map targeting the loamy sand zone for November survey 1.

Plan view from the cross-plot analysis of the November cyclic loading surveys is shown in Figure 4.8. For the first three surveys (not loaded, loaded for 18 hrs. & loaded for 44 hrs.), the location of the loamy sand zone is identified as a compromised location whereas the rest of the dam is indicated as safe or probably safe. For the last two surveys (unloaded and loaded for 27 mins.), most parts of the dam are indicated as highly compromised. This is due to high electrical resistivity values at the near surface for the whole length of the dam (Figures 3.19 and 3.20). The high resistivity could be due to the unloading of the dam and water leaving the body of the dam and leaving behind air filled void spaces. Considering the plan view of last two surveys, it is difficult to identify the location of the compromised (loamy sand) zone.

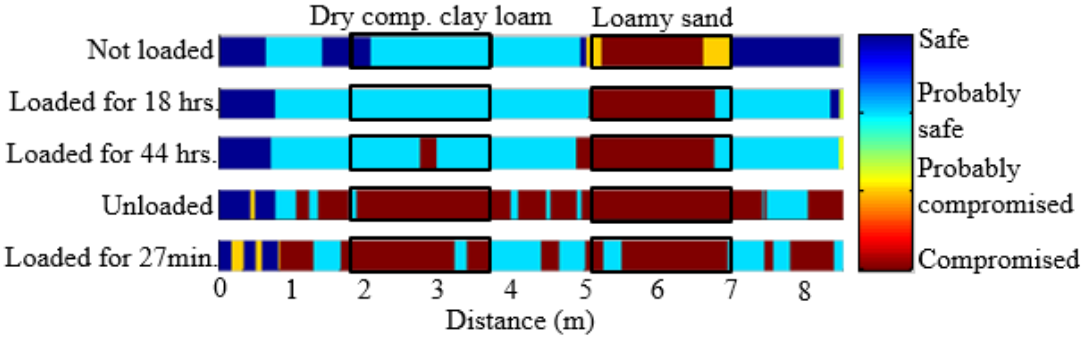

Figure 4.8: Loamy sand zone cross-plotting results for cyclic loading of the dam.

4.4 Cross-Plot Analysis Targeting the Loamy Sand Zone with Time-Lapse Restriction on Resistivity

Cross-plot analysis can be refined by utilizing the time-lapse aspect of the November cyclic loading surveys. One of the observations made from the scatter-plot, Figure 4.6, is that the resistivity value of the compromised (loamy sand) zone decreases as the loading time increases. This is due to the introduction of water associated with seepage into the loamy sand zone which reduces resistivity. Therefore, by adding the restriction that resistivity should decrease with loading time and keeping the resistivity and velocity boundaries the same, the compromised (loamy sand) zone can be better targeted. Figure 4.9 shows the plan view result obtained by applying the temporal restriction on resistivity. The result shows that the loamy sand zone is clearly identified as a highly compromised zone for all loading conditions.

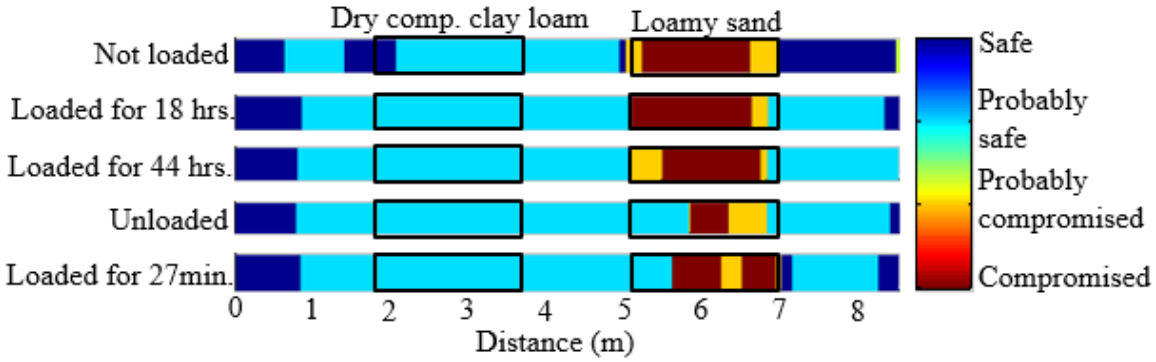

Figure 4.9: Loamy sand zone cross-plotting results with restriction on resistivity.

4.5 Cross-Plot Analysis Targeting the Dry Compacted Clay Loam Zone

Cross-plot analysis targeting the dry compacted clay loam zone was also performed for the November cyclic loading surveys. While the overall process remains the same for the cross-plot analysis targeting the loamy sand zone, different criteria are used to define the four quadrants of the scatter plot. Clays are naturally conductive; therefore, low resistivity is expected when

targeting clays. Dry compacted clay loams have low bulk modulus which leads to low seismic velocity values. Therefore, dry compacted clay loam is expected to have low resistivity due to the intrinsic conductivity of clays and low p-wave velocity due to the under compaction.

When dry compacted clay loam and clay loam compacted at OMC are exposed to additional wetting over the same amount of time, the electrical resistivity of the dry compacted clay loam drops lower than the electrical resistivity of the clay loam compacted at OMC. This is because more water can easily get into the dry compacted clay loam. Over longer loading time, p-wave velocity of the dry compacted clay loam is also expected to decrease due an increase in saturated density. Figure 4.10 shows the scatter plot used for targeting the Stillwater dry compacted clay loam. The scatter plot classification takes into consideration that the dry compacted clay zone will be saturated due to rainfall and cyclic loading of the dam.

Low p-wave velocity and low resistivity, represented by the quadrant labeled 3 in Figure 4.10, represents a compromised dry compacted clay loam zone that has been affected by wetting. The quadrant labeled 2 with high p-wave velocity and higher resistivity represents a safe clay loam zone compacted at OMC.

The scatter plot shown in Figure 4.10 shows a good separation in p-wave velocity between the dry compacted clay loam and the safe zone (dam body). The percent change in p-wave velocity from the safe clay loam to dry compacted clay loam is 46%. Based on the scatter plot, a p-wave velocity of 211 m/s is used in order to have a tight constraint on the dry compacted clay loam zone.

There is no significant separation in electrical resistivity between the dry compacted clay loam zone and safe clay loam compacted at OMC. The percent change in electrical resistivity from the safe clay loam to the dry compacted clay loam is 25%. Short loading time could be the reason for the overlap in electrical resistivity between the dry compacted clay loam and the clay loam

compacted at OMC. For trying the cross-plot analysis, an electrical resistivity value of 15 Ohm-m, the highest resistivity measured in the dry compacted clay loam, is picked as the electrical resistivity boundary. Visual inspection of Figure 4.10 shows that this boundary classifies parts of the safe zones into the probably safe quadrant. Therefore, in order to pick better boundaries, longer loading times should be allowed for the electrical resistivity of the dry compacted clay loam to drop below that of the clay loam compacted at OMC.

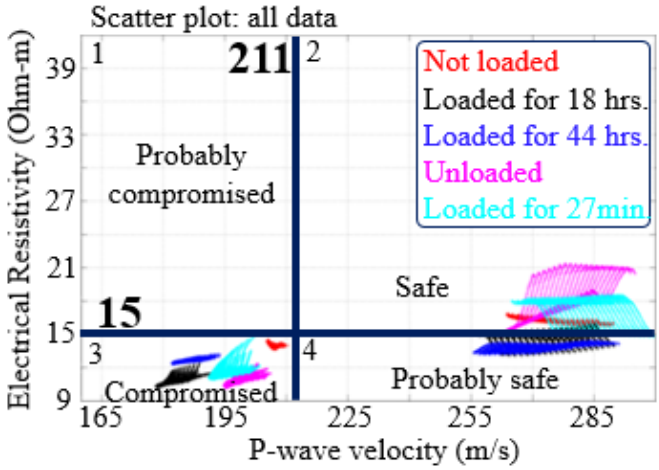

Figure 4.10: Scatter plot for all the loading conditions for the November cyclic loading (targeting the dry compacted zone).

The plan view results from the cross-plot analysis targeting the dry compacted clay loam zone is shown in Figure 4.11. The result shows no clear distinction of the dry compacted clay zone. Additional measurement after extended loading time could be required for an improved identification of the dry compacted clay zone.

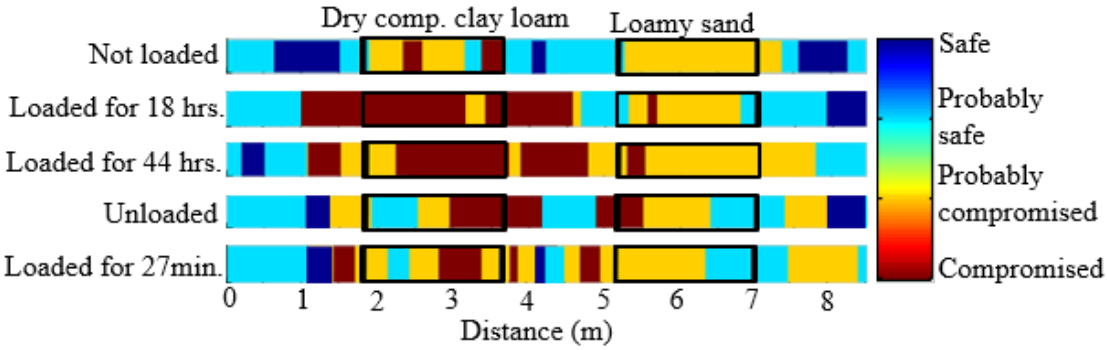

Figure 4.11: Dry compacted clay loam zone cross-plotting results for cyclic loading of the dam.

4.6 Summary

Cross-plot analysis can be used to combine the strengths of seismic refraction and electrical resistivity surveys and provide a simplified visualization for the integrity assessment of dams and levees. One of the advantages of implementing cross-plot analysis is that the end result, the cross-plot 2D map or plan view, is presented in non-technical terms, such as “safe” and “compromised” with no numerical values to interpret. This will enable non-technical personnel to read the result and have an understanding of the integrity of the dam or levee.

Although the end product is easy to read and understand, a clear understanding of the individual seismic refraction and electrical resistivity constraints used to conduct the cross-plot analysis is required. Most importantly, cross-plot analysis is based on identifying how different compromised zones (targets) manifest in both seismic refraction and electrical resistivity tomograms, and what common seismic/electrical attributes of the compromised zones can be utilized.

Cross-plot analysis results from the Stillwater embankment dam showed that dry compacted clay loam is not clearly isolated from the clay loam compacted at OMC. Measurements after a much longer loading time could be required for the electrical resistivity of the dry compacted clay loam to drop much further. The compromised loamy sand zone is correctly

identified using cross-plot analysis with the added restriction that electrical resistivity should decrease with loading time. Therefore, time-lapse measurements are required and provide valuable information especially for identifying loamy sand zones using cross-plot analysis.

Cross-plot analysis does not resolve problems that are inherent to the seismic refraction and electrical resistivity surveys. For example, depth accuracy problems of seismic refraction surveys are transferred to the cross-plot 2D cross-section maps. Anomalies associated with compromised zones do not always appear at the same exact location on both the seismic refraction and electrical resistivity tomograms. Therefore, if proper adjustment is not made addressing accuracy issues, cross-plot analysis could provide misleading information because grid points of an anomaly on one tomogram are not paired to the right grids on the other tomogram.

One of the difficulties associated with seismic refraction and electrical resistivity cross-plot analysis is determining the seismic velocity and electrical resistivity values that divide the four quadrants of the scatter plot. In the case of the Stillwater embankment dam, the location of the two compromised zones were known, which allowed identifying the associated anomalies on the tomograms. On surveys conducted on real dams and levees, this prior information is not always available; therefore, it is difficult to distinguish between anomalies in the tomograms associated with actual compromised zones from other anomalies. There is a need for more research on how these boundary values can be determined.

CHAPTER 5

5. ESTABLISHING CONSTRAINTS FOR CROSS-PLOT ANALYSIS USING PRELIMINARY AND LABORATORY GEOPHYSICAL MEASUREMENTS *

5.1 Introduction

The previous chapter discussed how the proper application of seismic refraction and electrical resistivity cross-plot analysis depends on the proper selection of seismic velocity and electrical resistivity boundaries.

In this chapter, a new approach of establishing cross-plot boundaries using preliminary data and laboratory measurements will be presented. For this purpose, preliminary and laboratory geophysical measurements on the Stillwater dam are used. In addition to that, a study to check if seismic velocity and electrical resistivity laboratory measurements can differentiate between three groups of soil types on the USDA soil texture triangle will be presented. The three groups of soils are classified based on regions of recommended and not recommended soil types for earthen dam construction.

5.2 Preliminary P-wave Velocity and Electrical Resistivity Measurements at Stillwater Dam

After the placement of the two zones at the Stillwater model dam was completed, preliminary p-wave seismic surveys using 3C geophones and Wenner array electrical resistivity surveys using four electrodes were conducted at the same time on the two zones and the dam body.

* A paper on a section of this chapter is in preparation. Wodajo, L.T., and Hickey, C.J., "Establishing Constraints for Cross-plot Analysis using Preliminary Geophysical Measurements: A Study at Stillwater model dam." *Journal of Environmental and Engineering Geophysics.*

The preliminary measurement setups on the dry compacted clay loam zone are shown in Figure 5.1.

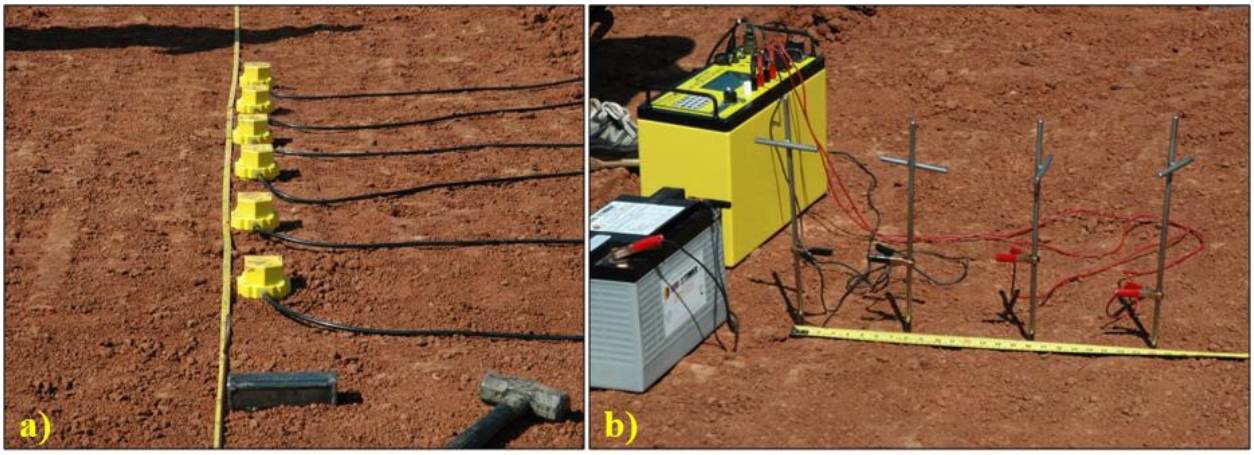

Figure 5.1: a) Preliminary p-wave seismic refraction measurement and b) preliminary electrical resistivity measurement on the dry compacted clay loam zone.

Results from the preliminary measurements are summarized in Table 5.1. Compared to the dam body compacted at OMC of 13%, the loamy sand zone and the dry compacted clay loam zone have a 15.5% and 4.2% decrease respectively in p-wave velocity. The loamy sand zone and dry compacted clay loam zone have a 344% and 111% increase respectively in electrical resistivity.

Table 5.1: Preliminary seismic velocity and electrical resistivity values during construction.

	Loamy sand	**Dry compacted clay loam**	**Dam body (clay loam)**
P-wave velocity (m/s)	223	253	264
Electrical resistivity (Ohm-m)	80	38	18

For simplification, the main part of Stillwater dam excluding the two compromised zones will be referred to as clay loam. This part is made from clay loam soil compacted at optimum moisture content and therefore represents the safe part of the dam. The dry compacted zone will be referred to as dry compacted clay loam.

5.2.1 Cross plot analysis using preliminary measurements on the clay loam

From preliminary measurements on the clay loam, a pair of seismic and electrical resistivity values within the safe part of the dam is obtained. As shown in Figure 5.2, these values can be used as cross-plot analysis boundaries to establish safe zones within the dam. In order to obtain p-wave velocity and electrical resistivity in the safe zone, a more compacted zone (higher confining stress) with higher moisture content is required. Such conditions could be possible due to the addition of overburden pressure from completion of the dam and overtime wetting of the dam from reservoir and rainwater infiltration. Therefore, p-wave velocity and electrical resistivity pairs that fall in the safe quadrant can be considered as safe with a high level of confidence. Cross-plot analysis with such conservative constraint (high degree of safety) creates difficulty in differentiating true compromised zones from false alarms. Some parts of the clay loam from the Stillwater field measurements (tomograms) are predicted as probably compromised. This might be a problem of using only one preliminary data point and could be improved by using an average of multiple preliminary surveys at different locations on the clay loam.

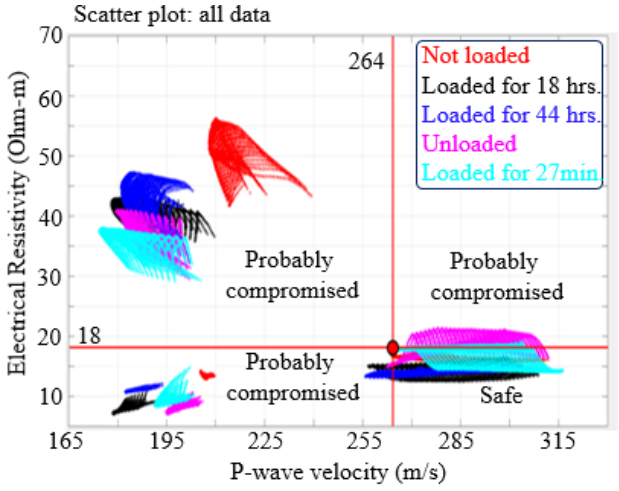

Figure 5.2: Cross-plot analysis based on preliminary measurements on the clay loam used to look for similar safe zones. Scatter plots of the clay loam, loamy sand, and dry compacted clay loam from field measurements (Chapter 4) are replotted for reference.

An example of using the preliminary values of the clay loam (dam body) is shown in Figure 5.3 for the second loading of the dam. As expected, the majority of the dam is classified as compromised due to the very conservative constraints (high factor of safety).

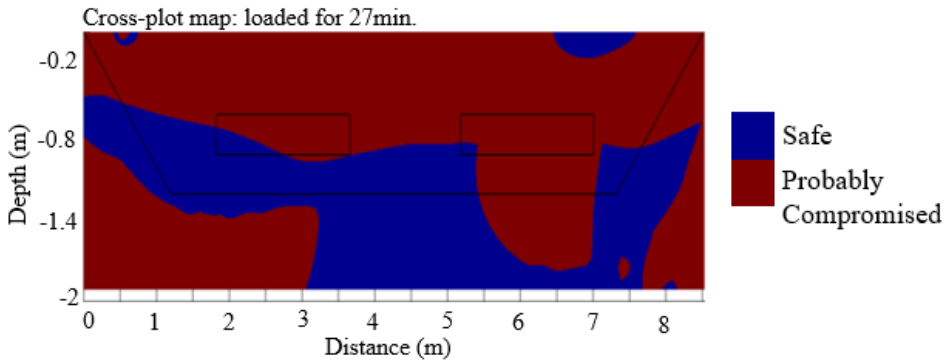

Figure 5.3: Cross-plot section based on the preliminary values of the clay loam.

5.2.2 Cross-plot analysis targeting the loamy sand zone using preliminary measurements on loamy sand

Cross-plot analysis using p-wave velocity and electrical resistivity values from preliminary measurements on the loamy sand zone is shown in Figure 5.4. For reference, the scatter plot and cross-plot boundary targeting the loamy sand zone used in Chapter 4 is also shown in Figure 5.4. Based on the preliminary values of the loamy sand, the scatter plot is divided into probably safe and compromised quadrants. The preliminary electrical resistivity of the loamy sand zone (80 Ohm-m) is higher compared to the cyclic loading field measurement data. The preliminary measurements were conducted in September immediately after the zones were placed but before the dam construction was completed. The field measurements, on the other hand, were conducted in November after the whole dam was constructed. Lower resistivity in the November field measurement is expected due to saturation caused by rainwater infiltrating into the loamy sand zone. Preliminary p-wave velocity of the loamy sand zone (223m/s) falls within the range of the not loaded field measurement as expected but the electrical resistivity is higher.

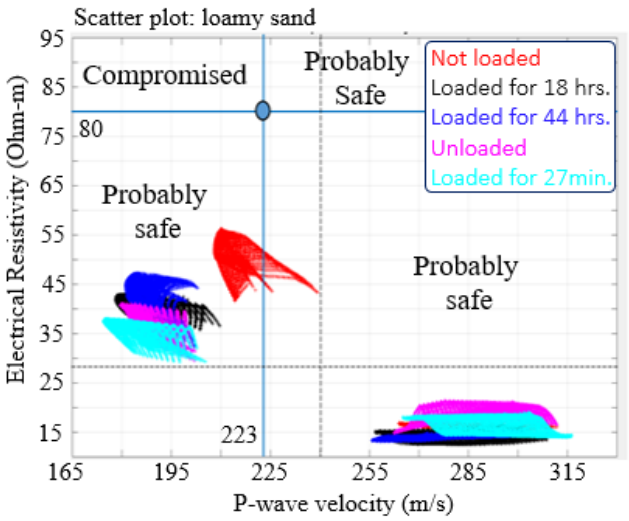

Figure 5.4: Cross-plot analysis targeting the loamy sand zone using preliminary p-wave and electrical resistivity values of the loamy sand zone as boundaries.

Since the preliminary measurement on the loamy sand zone represents the worst case, any velocity and resistivity pair that falls in the compromised zone is most likely compromised with a high degree of certainty. In order to have higher resistivity and lower p-wave velocity, the loamy sand has to be drier and under compacted (looser). Such conditions might occur if the loamy sand was eroded during wet periods due to internal erosion and measurements were performed in drier seasons where water saturation decreases. In actual dams, where water is impounded most of the time, the electrical resistivity is expected to decrease as loading time increases. A similar result is shown in the Stillwater data in Figure 5.4. Therefore, as shown in Figure 5.4, using the loamy sand preliminary electrical resistivity values for the cross-plot analysis, the loamy sand zones would classify as probably safe instead of compromised.

Since the preliminary electrical resistivity of the loamy sand (80 Ohm-m) is expected to decrease with increased loading time, laboratory measurements can be used to determine a representative resistivity of a saturated loamy sand.

From laboratory electrical resistivity measurements on the Stillwater loamy sand at OMC, bulk electrical resistivity (ρ_b) of 62 Ohm-m, saturation (S_w) of 68%, and porosity (ϕ) of 31.5% are obtained. Using these values and Archie's second law for a partially saturated sand (Eq. 2.9), engineers can approximate the electrical resistivity of the saturating water (ρ_w). Using a tortuosity (a) of 1, a cementation factor (m) of 2, and saturation exponent (n) of 2, the electrical resistivity of the saturating water (ρ_w) is 2.84 Ohm-m. This value is between the highest value of resistivity for salt water and lowest value of resistivity for fresh water (Samouëlian et al., 2005). To estimate how much the electrical resistivity of the loamy soil drops when fully saturated ($S_w = 1$), Archie's first law (Eq. 2.8) is used while keeping porosity (ϕ) constant at 32%. Keeping the same cementation factor (m) of 2 and using 2.84 ohm-m for the electrical resistivity of the saturating water (ρ_w), the electrical resistivity of the loamy sand at full saturation is approximately 28.7 Ohm-m. Reducing the electrical resistivity boundary of the loamy sand, from the preliminary 80 Ohm-m to the saturation-adjusted value of 28.7 Ohm-m, will move the saturated loamy sand zones to the compromised quadrant.

An example of using the saturation adjusted preliminary values of the loamy sand is shown in Figure 5.5 for the second loading of the dam. The majority of the dam is classified as probably safe due to the low factor of safety of the boundaries.

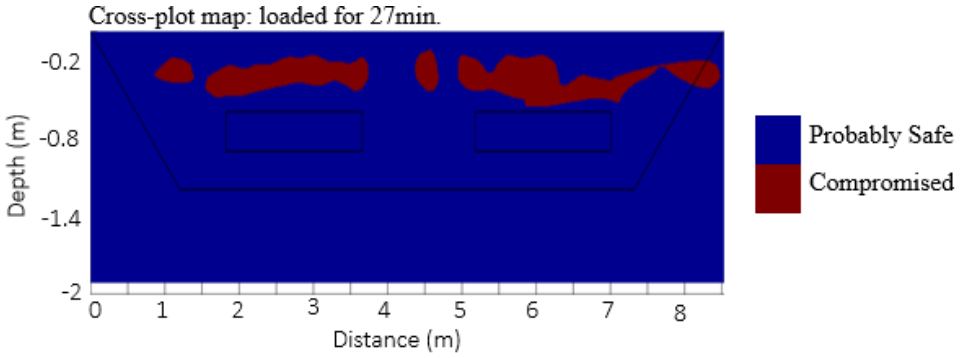

Figure 5.5: Cross-plot based on saturation adjusted preliminary values of the loamy sand.

5.2.3 Combined cross plot analysis using preliminary measurements on the clay loam and loamy sand

Using preliminary p-wave velocity and electrical resistivity of both the loamy sand (compromised zone) and clay loam (safe zone), cross-plot analysis targeting the loamy sand zone is shown in Figure 5.6. For the loamy sand, instead of the preliminary 80 Ohm-m electrical resistivity, the saturation adjusted value of 28.7 Ohm-m is used.

In order for cross-plot analysis targeting the loamy sand zone to work, both p-wave velocity and electrical resistivity should separate the loamy sand zone and the clay loam into different quadrants. Therefore, both p-wave velocity and electrical resistivity boundary values can be chosen anywhere in the yellow shaded zone in Figure 5.6. As the intersection point of the velocity and resistivity boundaries moves towards point A (safe zone), the constraint becomes a high factor of safety. On the other hand, as the constraint moves closer to point B, the constraint becomes a low factor of safety. Therefore, the choice in the boundaries can ultimately be loosely related to a factor of safety.

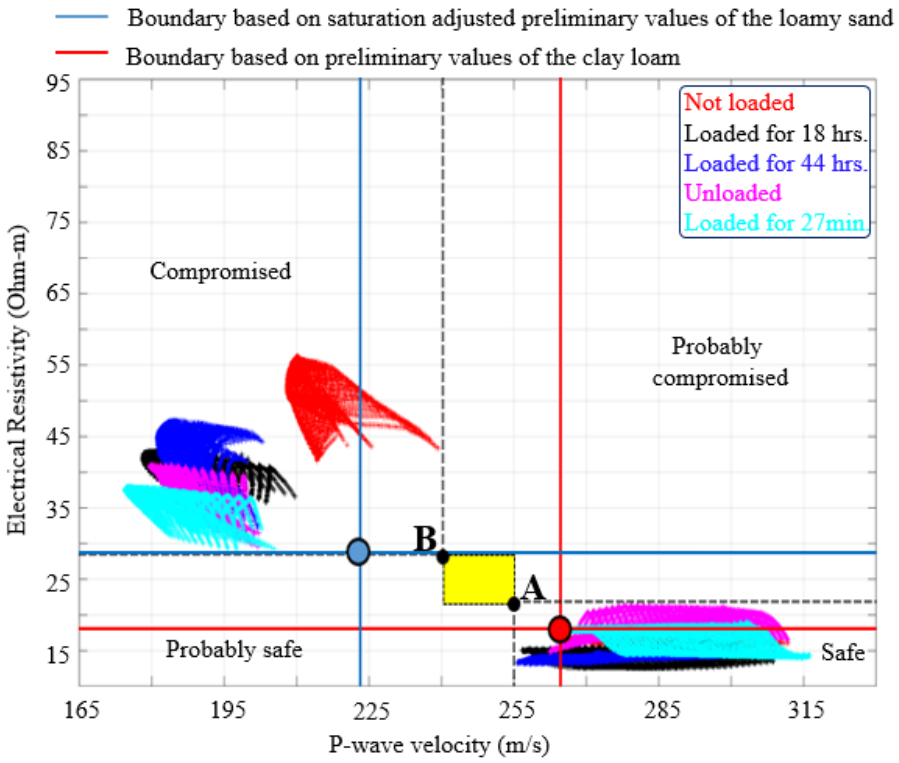

Figure 5.6: Cross-plot analysis targeting the loamy sand zone using preliminary p-wave velocity and electrical resistivity values of the loamy sand and clay loam. Preliminary electrical resistivity of the loamy sand is adjusted for saturation.

For the loamy sand, the preliminary p-wave velocity (223 m/s) is outside the shaded region while the saturation adjusted electrical resistivity (25.4 Ohm-m) is within the shaded region. Preliminary p-wave velocity (254 m/s) and electrical resistivity (18 Ohm-m) of the clay loam fall outside the shaded region but are close to point A. The average of the preliminary p-wave velocity of the loamy sand and clay loam, which is 243.5 m/s, falls within the shaded region. Therefore, one possible option is to use the average p-wave velocity and saturation adjusted electrical resistivity values as boundaries for targeting the loamy sand zone.

5.2.4 Cross plot analysis using preliminary measurements on dry compacted clay loam

Cross-plot analysis targeting the dry compacted clay loam using preliminary measurements on the dry compacted clay loam is shown in Figure 5.7. Compared to the clay loam, the dry

compacted clay loam has a higher electrical resistivity due to the lower water content and lower p-wave velocity due to lower bulk and shear modulus.

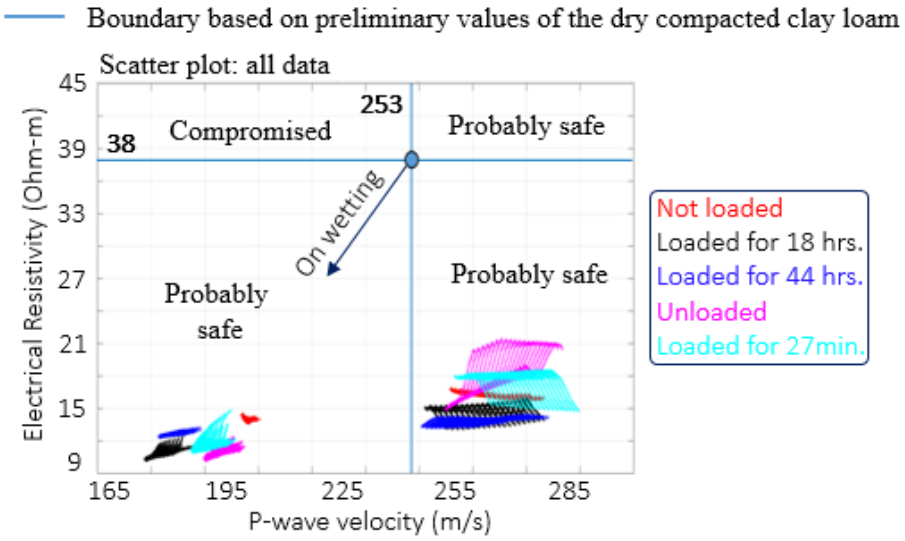

Figure 5.7: Cross-plot analysis targeting the dry compacted clay loam using preliminary p-wave and electrical resistivity values of the dry compacted clay loam as boundaries.

Since the preliminary measurements are conducted immediately after construction, the zones are not affected by additional wetting from rainwater infiltration. This leads to a low factor of safety constraint. Therefore, p-wave and electrical resistivity pairs that fall in the compromised quadrant are compromised with high degree of certainty.

Over longer loading times, p-wave velocity of the dry compacted clay loam is expected to decrease due to an increase in saturated density. Electrical resistivity is also expected to drop with increased saturation. Therefore, using the preliminary measurements of the dry compacted clay loam as the cross-plot analysis boundaries does not place the field measured dry compacted clay loam into the compromised quadrant. Laboratory measurements and the Waxman-Smits model (Eqs. 2.10 – 2.13) could be used to estimate the drop in electrical resistivity due to saturation. In

order to determine the cation exchange capacity (CEC) of the clay minerals for the Waxman-Smits model, an X-ray diffraction test on a sample of the clay loam is required.

A modified cross-plot analysis for targeting saturated dry compacted clay loam is shown in Figure 5.8. In the figure, after longer loading time, the preliminary measurement value on the dry compacted clay loam (blue circle) will move closer to point B. Similarly, after longer loading time, the preliminary measurement value on the clay loam (red circle) will move closer to point A. The close proximity of the preliminary value on the clay loam (red circle) to point A is an indication that the fluctuation due to saturation in the clay loam is small. This is associated with the proper compaction of the clay loam at optimum moisture content. In order for cross-plot analysis to work, point B in Figure 5.8 should be lower than point A. This creates a separation in resistivity between the compromised and safe quadrant. Since electrical resistivity drops much faster in the dry compacted clay loam than the clay loam compacted at OMC, point B could drop below point A if measurement is taken after a much longer loading time. This will provide a better boundary selection in resistivity for the cross-plot analysis. An important observation is that p-wave velocity clearly separates the dry compacted clay loam from the clay loam compacted at OMC.

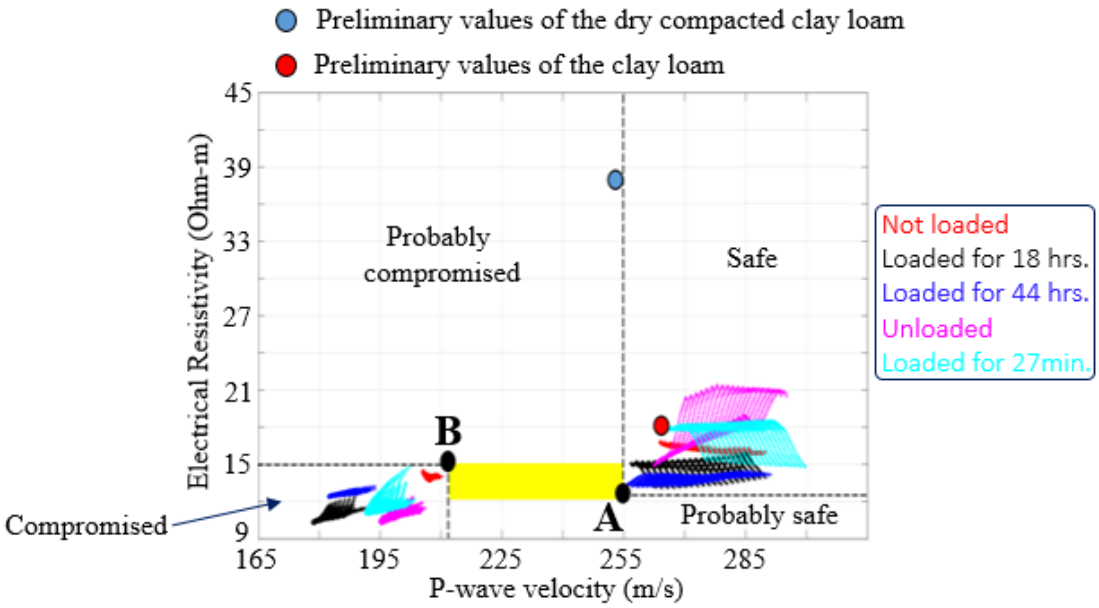

Figure 5.8: Cross-plot analysis targeting the saturated dry compacted clay loam zone.

5.3 Laboratory Seismic Velocity and Electrical Resistivity Measurements on the Stillwater Dam Soils

In this section, p-wave velocity and electrical resistivity measurements on the Stillwater dam soils are presented. These measurements were conducted to provide additional information to interpret field data. The lab measurements were conducted on the Stillwater clay loam and loamy sand. According to the sieve results, the clay loam consists of 30% sand, 43% silt, and 27% clay by mass. For the loamy sand, the material was divided into 84% sand, 9% silt, and 7% clay by mass.

A modified version of the standard proctor test described by the American Society of Testing and Materials (ASTM) D-698 was used to determine the maximum dry density and the corresponding optimum moisture content for each soil type. Table 5.2 shows the compaction effort used for the standard proctor test. The standard Proctor compaction method was chosen for sample preparation because it is used to define compaction specifications for dam constructions. After

compaction, about 50 gm of soil sample was oven dried at a temperature of 100-110 ^{o}C for 16 to 24 hours until the weight stabilized. The mass of the soil after oven drying was used to determine the actual moisture content after compaction using the gravimetric method (Black, 1965).

Table 5.2: Standard proctor tests, modified from Das (2009).

Proctor test	Mold			hammer weight (Kg)	hammer drop height (mm)	# of layers	blows per layer
	Volume (cm^3)	Height (mm)	Diameter (mm)				
Standard	943	116.43	101.6	2.49	304.8	3	25
Note: all measurements conducted using soil passing U.S. No. 4 sieve.							

For a given compaction effort, it is postulated that at low moisture content the friction between the soil grains is high and insufficient water is available to lubricate the particles to allow them to be rearranged into a dense soil. On the other hand, at very high moisture content, energy has little effect on the compaction because the water is incompressible and supports the compaction force without the soil being densified (Drnevich et al., 2007). Compacting soil above optimum moisture content leads to lower stiffness and permeability (Nicholson, 2015). For a given soil type and compaction effort, the maximum dry density defines the optimum moisture content. At higher compaction efforts, maximum dry density is attained at lower optimum moisture content. For this study, a modification of the proctor test mold, shown in Figure 5.9, and the arrangement used by Kaliniski et al., (1993) was used.

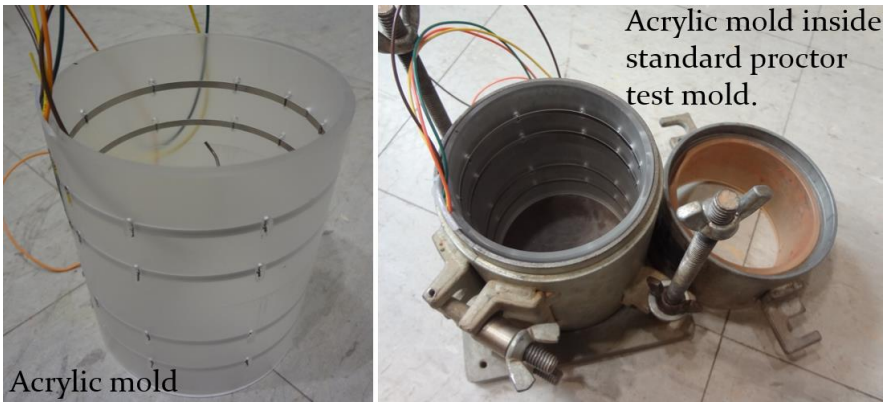

Figure 5.9: Acrylic mold with four electrodes.

The height of the acrylic mold is 116.43 mm with an inside diameter of 94 mm for a total volume of 808 cm^3. This is a 14% reduction in volume compared to the standard proctor test mold. Therefore, the proctor test compaction effort needs to be adjusted for the acrylic mold in order to compensate for the reduction in cross-sectional area. In order to determine the new compaction effort (blows per layer), soil from the Stillwater embankment dam was compacted inside a proctor mold (with no acrylic mold) with the standard 25 blows per layer and the standard compaction curve was plotted. Next, a battery of the same soil was compacted inside the acrylic mold, and the number of blows per layer was adjusted until the results matched the standard compaction curve with no acrylic mold. Figure 5.10 shows how the standard compaction curve without an acrylic mold is well aligned with an adjusted compaction effort of 19 blows per layer with an acrylic mold. The adjusted 19 blows per layer was considered equivalent to the standard compaction energy for tests conducted in this study.

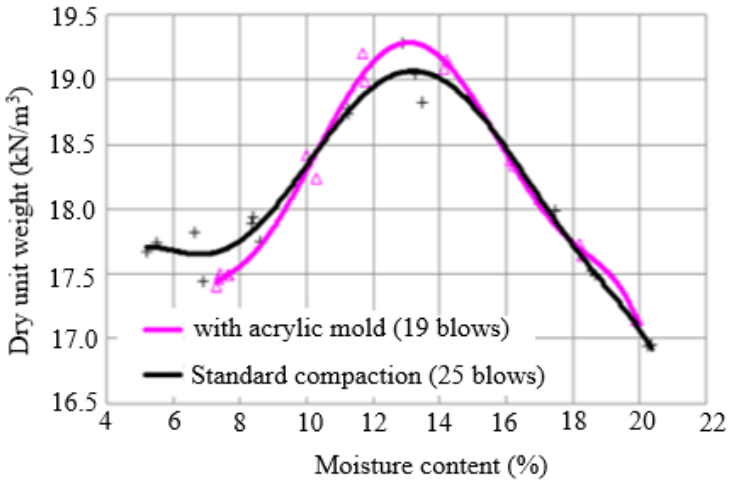

Figure 5.10: Adjusted compaction effort compared to standard compaction effort.

5.3.1 Electrical resistivity measurement

Electrical resistivity measurements have been widely used to characterize geotechnical and hydrogeological parameters (Abu-Has sanein et al., 1996, Bryson, 2005, Bryson et al., 2009, Kalinski et al., 1993, McCarter, 1984, Samouëlian et al., 2005). Electrical resistivity measurements require the use of current and potential electrodes. Fowels (1980) measured the electrical resistivity of soils compacted inside the Miller soil box. Current is passed through the soil through two metal ends and the potential difference is measured between two pins inserted along the length of the box. Soil samples compacted into a circular mold have also been widely used to measure electrical resistivity of soils in the lab (Rhoades et al., 1977, Kalinski et al., 1993, Borsic et al., 2005, Sreedeep et al., 2005).

Kalinski et al., (1993) used a circular eight-electrode resistivity cell arrangement as an alternative to the Miller soil box. The eight electrodes are equally spaced around the circumference of a nonconductive cell. Using this arrangement, the measurement is taken with a set of four adjacent electrodes with the outer two electrodes as current electrodes and the inner two electrodes

as potential electrodes. Eight separate measurements are taken on one soil sample and the average of the eight measurements is taken as the final resistivity of the soil sample.

The nonconductive acrylic cylinder mold shown in Figure 5.9 includes four stainless steel ring electrodes (Hickey, 2012). The acrylic mold is designed to fit inside the standard proctor test mold. The outer two rings are used to inject current while the inner two rings measure the potential difference. By using four ring electrodes that continuously cover the circumference of the soil sample, this arrangement reduces the eight measurements and averaging required in the Kalinski et al., (1993) to just one measurement. Figure 5.11 shows the electrical resistivity lab measurement setup.

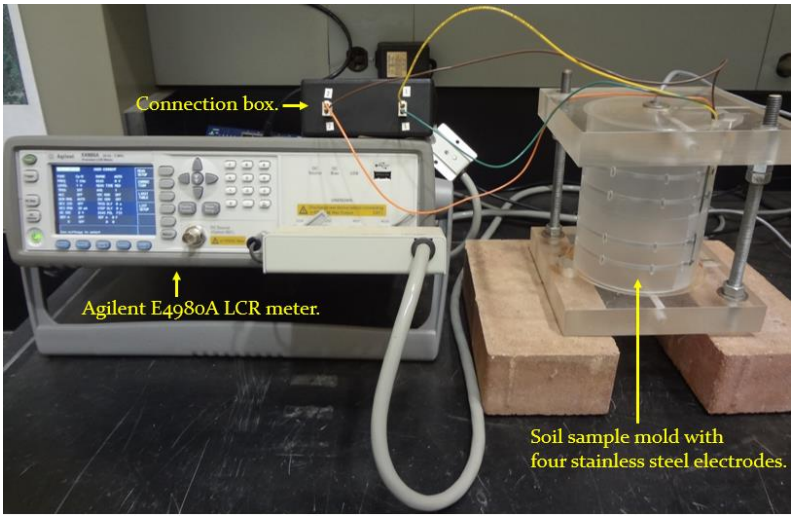

Figure 5.11: Electrical resistivity lab measurement setup.

Calibration for electrical resistivity measurement was conducted using an Agilent E4980A LCR meter with the acrylic mold to measure the resistance (Ω) of the sample. This measured resistance was then be converted to true resistivity using equations derived from calibration curves. Different concentrations of sodium chloride (NaCl) solutions can be used to establish a calibration curve. The measured resistance of the solution using the acrylic mold was plotted with the

corresponding true resistivity of the solution obtained with the use of a handheld conductivity meter.

5.3.2 Seismic velocity measurement

In addition to the electrical resistivity measurement, seismic velocity measurements were also conducted on the same soil sample in the acrylic mold. Seismic velocity measurements were made with the use of bender elements (Lee et al., 2005). Bender elements have been widely used for laboratory measurements of shear wave velocities, which are used for determining the shear modulus of soils (Dyvik et al., 1985, Jovicic, et al., 1996, Pennington et al., 2001, Leong et al., 2009, Chan et al., 2010, Fioravante et al., 2001, Mattsson et al., 2005).

Signal transmitter and receiver bender elements are comprised of two piezoelectric transducers separated by a metal shim (Chan, 2012). Bender elements can generate both P and S waves depending on the phase of voltage supplied to the transmitter. By introducing a voltage that is out of phase to the individual bender elements, shear waves are created due to the bending motion parallel to the surface of the soil sample. Applying an in-phase voltage will produce p-waves which propagate normal to the surface of the soil sample (Deniz, 2008). Both the transmitted and received signals can be viewed and recorded on an oscilloscope in order to pick the first arrival time. Seismic velocity through the soil is then determined by dividing the distance between the transmitter and the receiver with the travel time of the signal.

In this study, the transmitter and receiver bender elements are attached to the opposite ends of the soil sample while inside the acrylic mold. Figure 5.12 shows the seismic velocity lab measurement setup. A good contact between the bender elements and the soil sample is required in order to have good signal transmission.

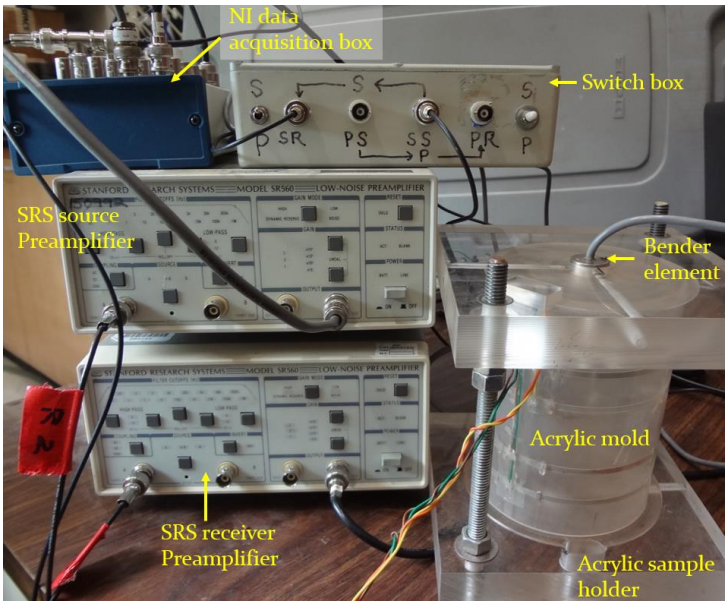

Figure 5.12: Seismic velocity lab measurement setup.

A Stanford Research Systems (SRS) source preamplifier with a maximum allowable gain of 50 and an input source amplitude of 0.1V was used to amplify the source signal. A SRS receiver preamplifier was used to amplify and frequency filter the received signal. A National Instruments (NI) data acquisition box was connected to a laptop with a LabVIEW program. The LabVIEW program was used to control the acquisition and calculation of the seismic velocities. A half cycle of a 3 kHz sine wave with an amplitude of 0.1V was used as the input source impulse. The propagation velocity through the soil was calculated by dividing the distance between the bender elements [height of the standard proctor mold (116.43mm)] by the difference between the reference time of the source pulse and the first arrival of the received signal. The program acquires multiple measurements before displaying one velocity reading and similar velocity readings can be taken successively. The final velocity value of the soil sample was taken as the average of these readings.

5.3.3 Lab measurements on the Stillwater clay loam

The Proctor curve plot for the Stillwater clay loam is shown in Figure 5.13. The soil has an OMC of 13% and a maximum dry density of 1906 Kg/m^3. The main body of the Stillwater dam is compacted at the OMC. The dry compacted zone is compacted at 10% moisture content and has a dry density of 1812 kg/m^3. The zero-air-void (ZAV) line represents an ideal condition of 100% saturation where all the air in the soil is expelled during compaction.

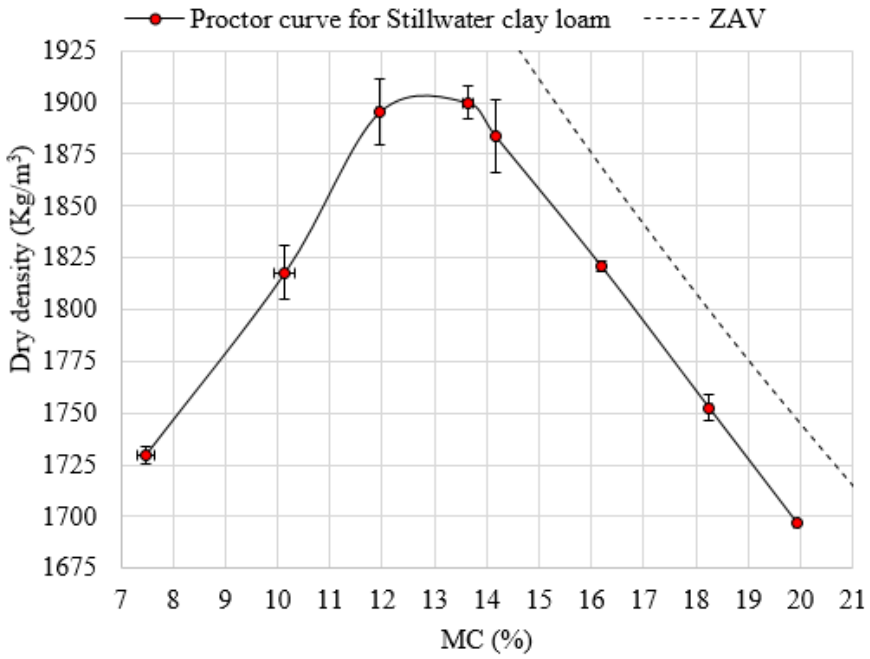

Figure 5.13: Proctor curve plot for Stillwater clay loam.

It should be noted that a proctor compaction is a complicated process, where both the saturation and porosity change for each data point on the proctor curve. Using the dry density (ρ_{dry}) and moisture content (MC) for each data point in the proctor curve, saturation (S) is calculated using,

$$S = \frac{MC \cdot \rho_o \cdot \rho_{dry}}{\rho_w \left(\rho_o - \rho_{dry}\right)} \cdot 100\% , \qquad (5.1)$$

where the soil mineral density (ρ_o) is taken as 2650 Kg/m^3 and the density of water (ρ_w) is 1000 Kg/m^3. Porosity (ϕ) is calculated using,

$$\phi = \left(1 - \frac{\rho_{dry}}{\rho_o}\right) \cdot 100\% \ . \qquad 5.2$$

P-wave velocity measurement results for the clay loam are shown in Figure 5.14. P-wave velocity is monotonic with a maximum near OMC. At the OMC of 13%, p-wave velocity is 955 m/s, and is 855 m/s at 10% moisture content (Figure 5.14a). A study conducted by Lu et al. (2009) showed that saturation levels have an effect on the speed and attenuation of seismic waves. At low saturation, a decrease in p-wave velocity was observed with an increase in saturation. A p-wave velocity versus saturation plot, Figure 5.14(b), shows a decrease in velocity after the OMC. Figure 5.14(c) shows that porosity reaches a minimum near the OMC as the soil grains can easily rearrange and become compact due to water lubrication. With the addition of more water above the OMC, the saturating fluid carries the compaction load and the soil begins to flow causing an increase in porosity as is typically expected.

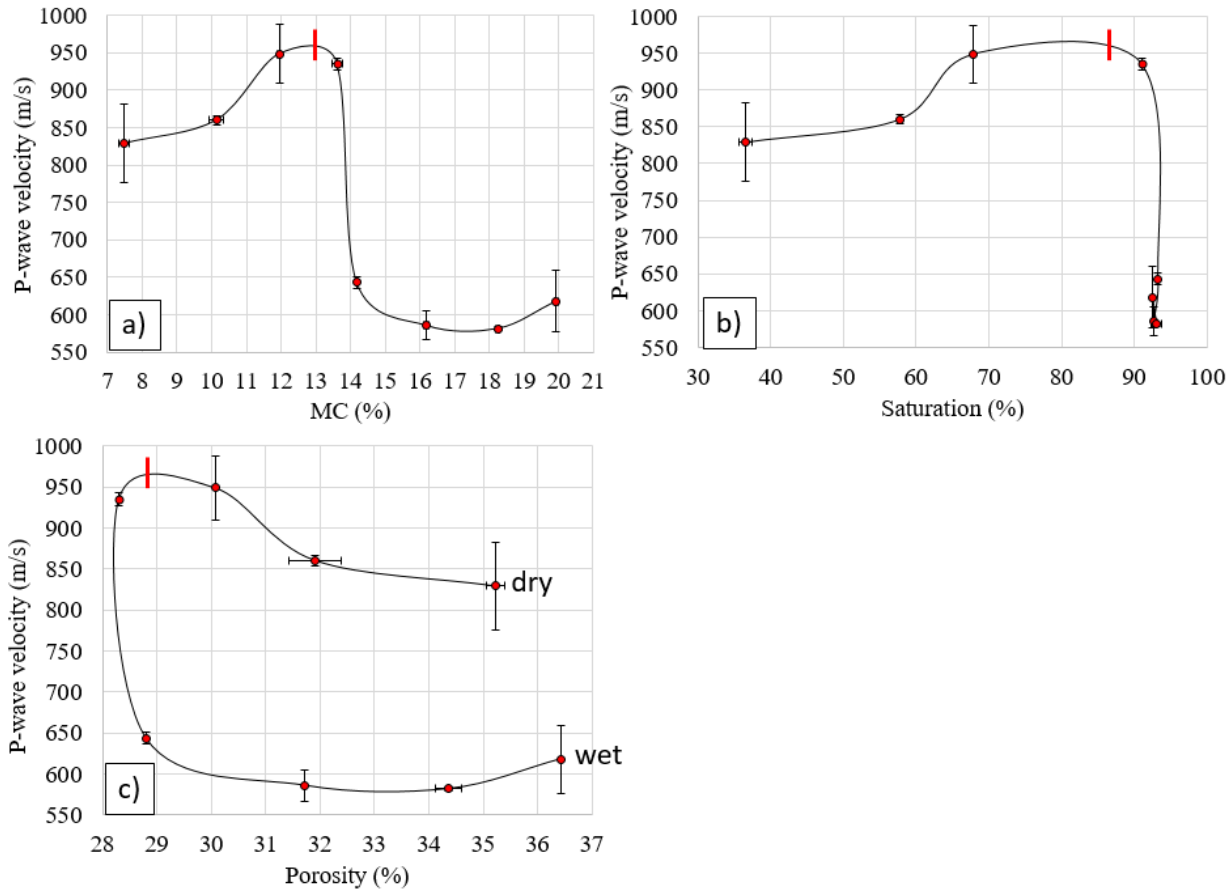

Figure 5.14: a) P-wave velocity vs. moisture content, b) p-wave velocity vs. saturation, and c) p-wave velocity vs. porosity for Stillwater clay loam. The red line markers in each figure indicate the OMC.

Electrical resistivity laboratory measurement results for the Stillwater clay loam shown in Figure 5.15 is monotonic with a minimum near OMC . Electrical resistivity at the OMC of 13% is 9.8 Ohm-m and 13 Ohm-m at 10% moisture content (Figure 5.15a). In Figure 5.15c, electrical resistivity decreases rapidly when approaching OMC and then slightly increases above OMC. Below OMC, electrical resistivity decreases with decreasing porosity, which is unexpected. However, the saturation is also changing, and the change in electrical resistivity is dominated by the change in saturation. Above OMC, the saturation is constant (Figure 5.15b), and an increase in porosity results in electrical resistivity that increases slightly. The increase in electrical resistivity

with increase in porosity at constant saturation is again not what is expected. Compaction above optimum moisture is most likely changing the connectivity of the pores.

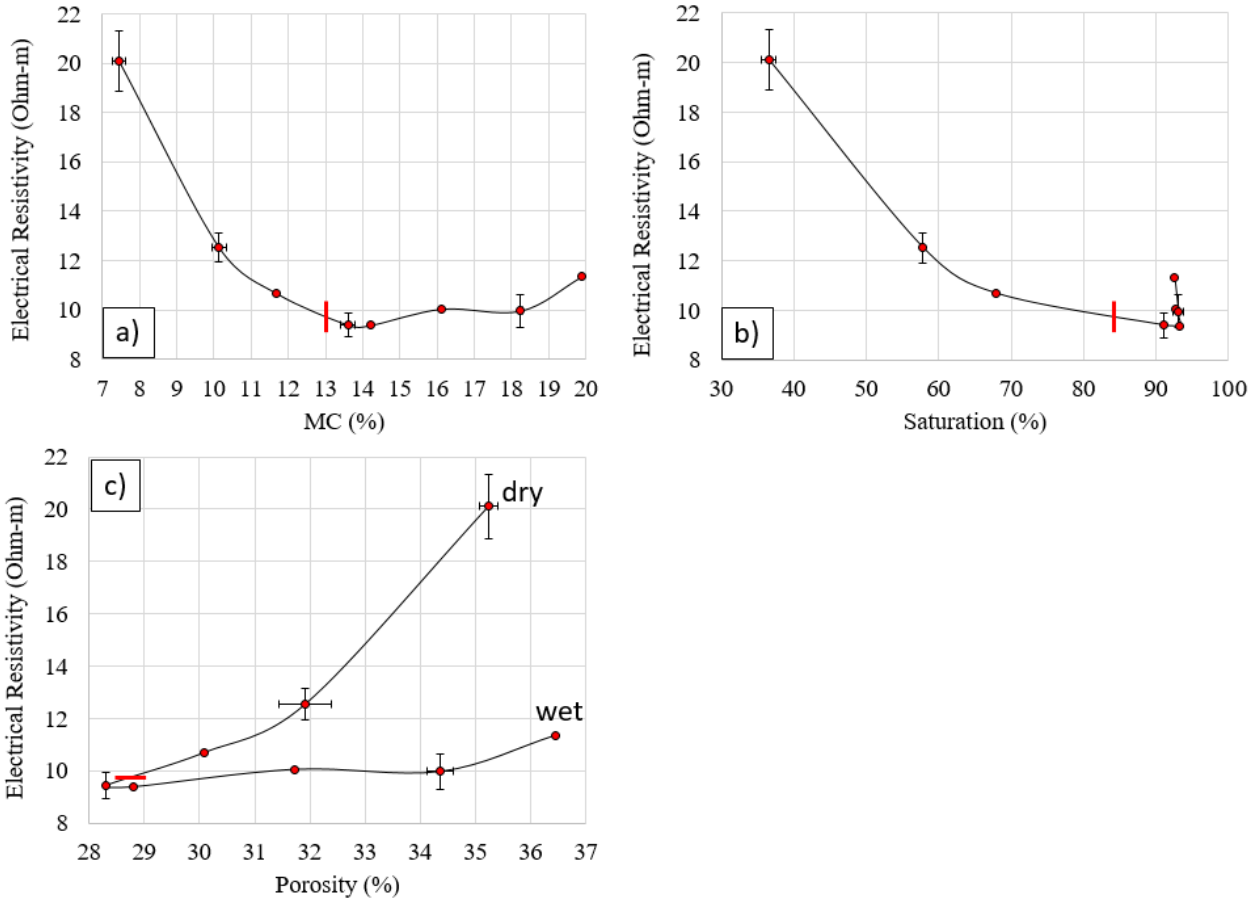

Figure 5.15: a) Electrical resistivity vs. moisture content, b) electrical resistivity vs. saturation, and c) electrical resistivity vs. porosity for Stillwater clay loam. The red line markers in each figure indicate the OMC.

5.3.4 Lab measurements on the Stillwater loamy sand

The Proctor curve plot for the Stillwater loamy sand is shown in Figure 5.16. The soil has an OMC of 11.75% and a maximum dry density of 1826 Kg/m^3.

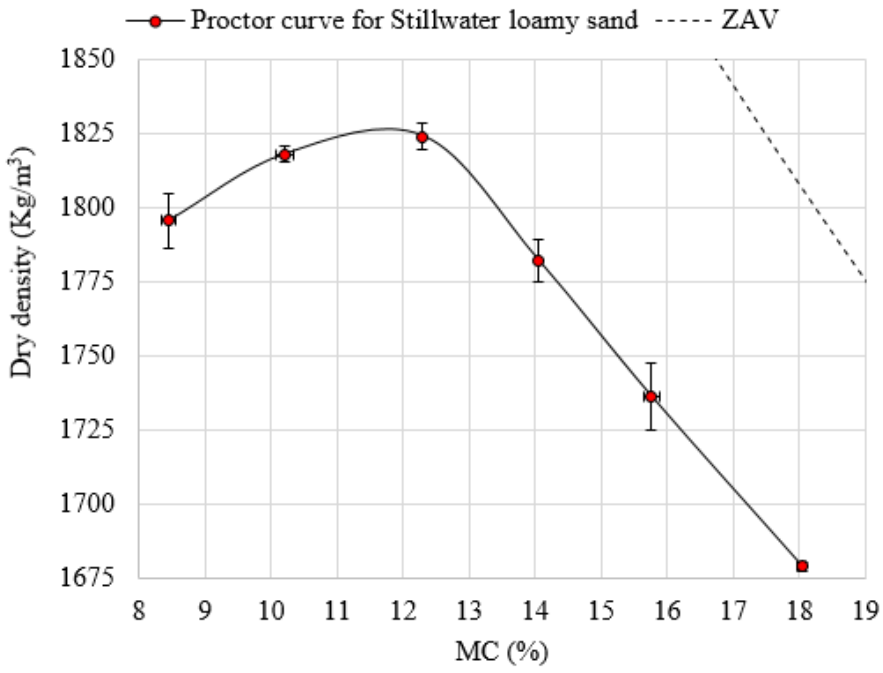

Figure 5.16: Proctor curve plot for the Stillwater loamy sand.

P-wave velocity results for the loamy sand are shown in Figure 5.17. P-wave velocity at the OMC of 11.75% is 426 m/s. In contrast to the clay loam, the loamy sand has a minimum p-wave velocity near the OMC (Figure 5.17a). Above the OMC, p-wave velocity increases with increasing moisture content and saturation (Figure 5.17b), which is different than the clay loam. Addition of water to loamy sand increases capillary suction, which in turn pulls the soil particles together increasing the shear strength and seismic velocity of the loamy sand (Lu et al., 2009).

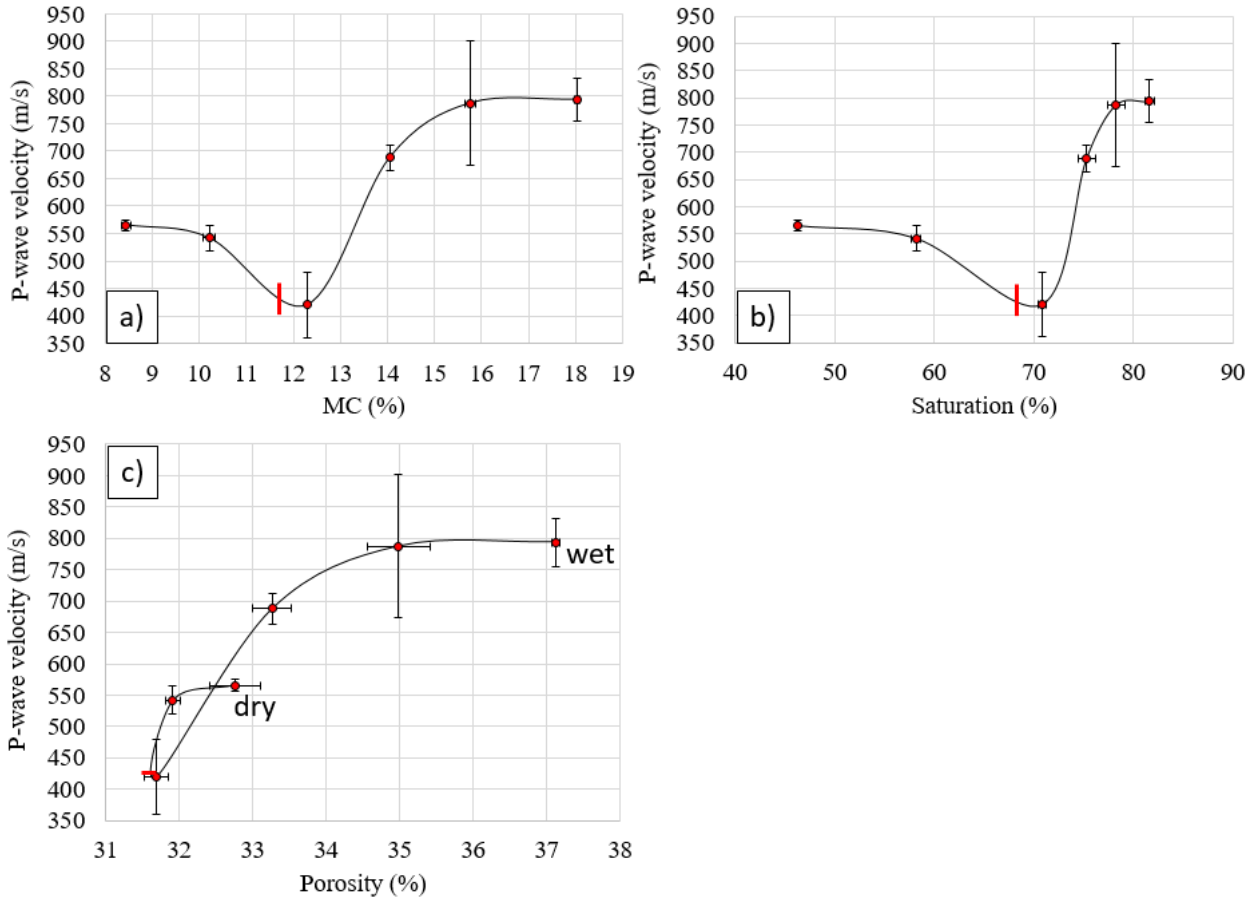

Figure 5.17: a) P-wave velocity vs. moisture content, b) p-wave velocity vs. saturation, and c) p-wave velocity vs. porosity for Stillwater loamy sand. The red line markers in each figure indicate the OMC.

Electrical resistivity results for the loamy sand is shown in Figure 5.18. Electrical resistivity at the OMC of 11.75% is 62 Ohm-m. Figure 5.18c shows a sharp decrease in resistivity below OMC which could be due to the sharp increase in saturation. The slow decrease in electrical resistivity above the OMC could be associated with the slow increase in saturation (Figure 5.18b).

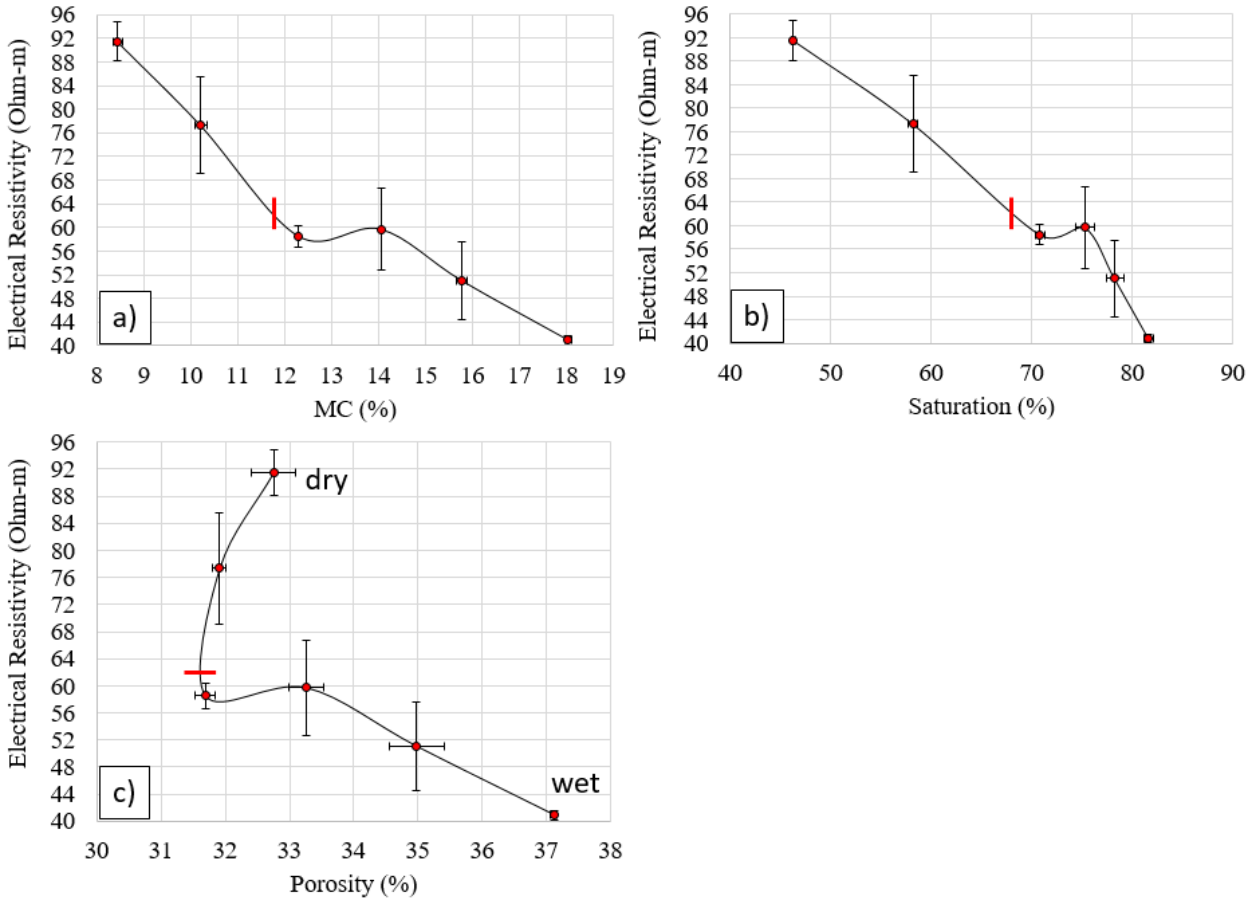

Figure 5.18: a) Electrical resistivity vs. moisture content, b) Electrical resistivity vs. saturation, and c) Electrical resistivity vs. porosity for Stillwater loamy sand. The red line markers in each figure indicate the OMC.

5.3.5 Comparison between Laboratory and Field Measurement of Seismic Velocity and Electrical Resistivity

Comparison between lab measured and field measured p-wave velocities is shown in Table 5.3. For the field measurements, average values for each of the three zones (loamy sand zone, clay loam, and dry compacted clay loam) are calculated from p-wave velocity tomograms from the November cyclic loading surveys. For the lab measurements, p-wave velocity and electrical resistivity values at OMC of 11.75% for loamy sand and 13% for clay loam are taken. For the dry compacted clay loam, values at 10% moisture content are taken.

Table 5.3: Comparison between laboratory and field measured p-wave velocities.

Soil type	Field measured p-wave velocity (m/s)	Lab measured p-wave velocity (m/s)	% change from field to lab measurements
Loamy sand	200	426	113
Clay loam	281	955	240
Dry compacted clay loam	195	855	338

Laboratory measured p-wave velocities for the loamy sand, clay loam, and dry compacted clay loam are significantly higher than values obtained from the field measurements (tomograms). This could be due to the difference in the state of stress between the in situ (field) and lab measurements. P-wave seismic velocity increases with increasing effective confining pressure (Christensen et al., 1985, Prasad et al., 1997, Lokajicek et al, 2015). While the field soil is confined by overburden pressure, the lab soil is confined by the acrylic mold. The effective pressure, which is the difference between confining pressure and pore pressure, could be higher in the lab soil leading to higher p-wave velocity.

Another possible reason for the significant difference in p-wave velocity is the difference in frequency of the seismic waves. In the field measurements, a sledgehammer is used to generate a seismic wave of less than 100 Hz. For the lab measurements, a half cycle pulse of 3 kHz is used. Due to the high frequency of the source wave, the soil does not have enough time to relax and effectively becomes more stiff leading to a higher p-wave velocity.

Comparison between lab measured and field measured electrical resistivity is shown in Table 5.4. The variations in the field and laboratory measured electrical resistivity values could be associated with multiple soil property differences in field and lab measurements. Differences in degrees of saturation, temperature, porosity, connectivity of pores, and pore size distribution could

cause variations in electrical resistivity (Samouëlian et al., 2005). Although the laboratory and field compaction are made with the same compaction effort, maintaining similar porosity, connectivity of pores, and pore size distribution is difficult.

Using models such as Archie's laws and Waxman-Smits models, saturation and porosity values calculated from laboratory electrical resistivity measurements can be used to calculate the changes in electrical resistivity associated with longer wetting time. An example of such an application was shown in the cross-plot analysis targeting the loamy sand using preliminary measurements.

Table 5.4: Comparison between laboratory and field measured electrical resistivity.

Soil type	Field measured ele. resistivity (Ohm-m)	Lab measured ele. resistivity (Ohm-m)	% change from field to lab measurements
Loamy sand	42	62	48
Clay loam	17	9.8	-42
Dry compacted clay loam	13	13	0

Therefore, in order to utilize laboratory measurements for determining cross-plot boundaries, further study is required to represent field conditions in the lab. This is especially important in p-wave velocity measurements. In addition to field compaction effort and moisture content, important factors, such as level of confining stress, seismic wave frequency, and temperature, should be well represented in the lab.

5.4 Seismic Velocity and Electrical Resistivity Laboratory Measurements using Synthetic Soils

In this section, results from seismic velocity and electrical resistivity laboratory measurements on different soil types based on the USDA soil texture triangle are presented. The

objective of the study is to examine if seismic velocity and electrical resistivity laboratory measurements can differentiate between three groups of soil types on the USDA soil texture triangle. The three groups of soils are based on regions of recommended and not recommended soil types for earthen dam construction.

5.4.1 Suitable soil types for earthen dam and levee constructions

When constructing dams and levees, the proximity and accessibility of material are the controlling factors in the decision of the soil type. Except for a few soil types, almost any soil can be used for the construction of levees and earthen dams. The US Army Corps of Engineers manual on the design and construction of levees states that any type of soil except very wet, fine-grained or highly organic soil can be used for the construction of levees (USACE EM 1110-2-1913, 2000). The general design and construction considerations for earth and rock-fill dams (USACE EM 1110-2-2300, 2004) states that soils with a wide grain size distribution (well graded) are preferable as long as they are insoluble and inorganic. It also states that rock flours and clays with liquid limits above 80 should not be used for earth-fill dams.

According to the United States Society on Dams (USSD) (2011), broadly (well) graded soil types that are not entirely fine grained or entirely coarse-grained are recommended for earthen dams. In the United States, well-graded soils with a minimum 20% and a maximum of 71% passing the No. 200 sieve (0.074mm sieve opening) are used for embankment dams.

Hanson et al., (2005) studied internal erosion and impact of erosion resistance by constructing two model embankment dams. The two model dams were constructed using two different soil types. Dam 1 was constructed with sandy loam (64% sand, 7% clay, and 29% silt) while Dam 2 was constructed using loam (25% sand, 26% clay, and 49% silt). The study showed that Dam 2 was more erosion resistant than Dam 1.

In general, using soil types with too much sand or too much fine is not suitable for earthen dam and levee construction. Soils with a wide range of grain size are less susceptible to piping, erosion, and seepage (USACE EM 1110-2-2300).

Seismic velocity and electrical resistivity laboratory measurements were conducted on different soil types based on the USDA soil texture triangle shown in Figure 5.19. This classification is based on three soil particle sizes (sand, clay, and silt). For a given soil mass, the soil texture classification is based on the weight of a given particle mass of the overall soil mass. These percentages by mass are measured using soil samples dried slightly above 100 ^{o}C (Moyes, 2014).

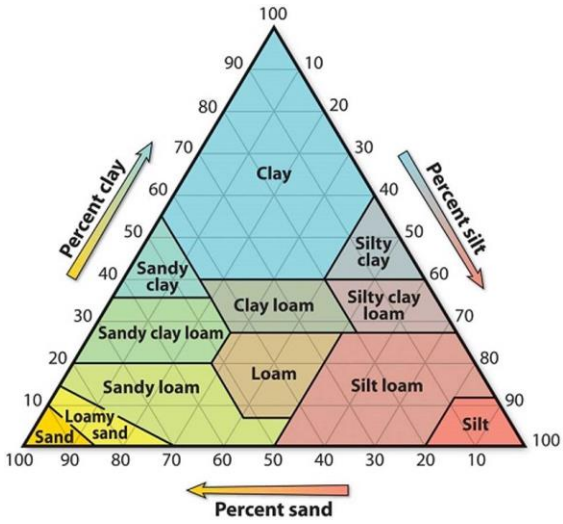

Figure 5.19: USDA soil texture triangle (https://www.nrcs.usda.gov).

Based on the United States Society on Dams (USSD), a well-graded dam with a minimum of 20% and a maximum of 71% soil passing the No. 200 sieve is recommended. The No. 200 sieve divides sands from silts and clays. Therefore, a minimum of 20% silt and clay means a maximum of 80% sand, and a maximum of 71% silt and clay means a minimum of 29% sand is recommended for earthen dams. Figure 5.20 shows the region of recommended soil types for earthen dam

construction on the USDA soil texture triangle. The figure shows there are multiple soil types both within and outside the recommended range.

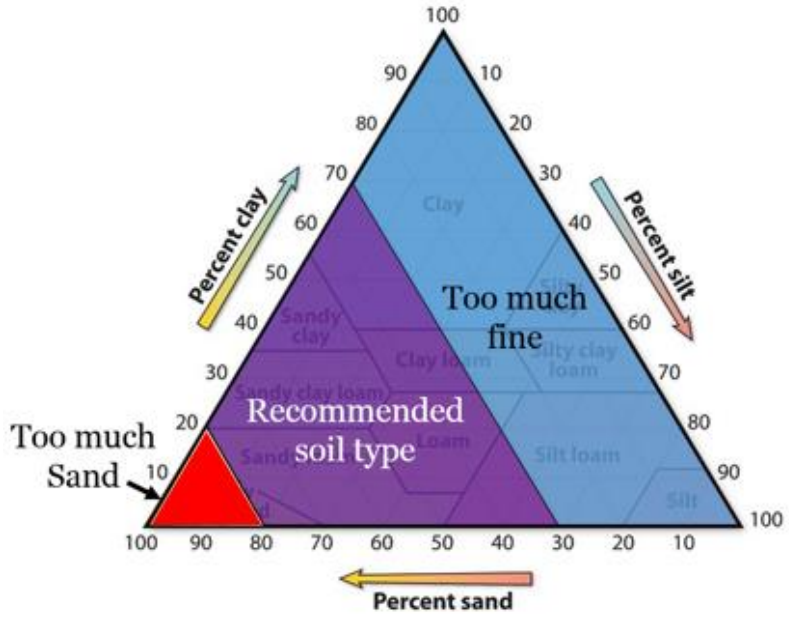

Figure 5.20: Regions of recommended soil types for earthen dam construction (https://www.nrcs.usda.gov).

5.4.2 Laboratory measurements on synthetic soil samples

To evaluate if laboratory seismic velocity and electrical resistivity measurements can differentiate between the three regions in Figure 5.20, measurements were conducted in the lab using different soil types. The different soil types (samples) used for the lab measurements are shown in Table 5.5. The soil type classification is based on the USDA soil texture triangle. Synthetic soil samples were prepared in the laboratory using sand, silt, and clay minerals (kaolinite and bentonite). The clay fraction in all the soil samples was 90% kaolinite and 10% bentonite by mass of clay. These values are chosen to match the kaolinite and bentonite percentage fraction in the Stillwater clay loam. It should be noted that the objective of this study is not to differentiate between the ten soil samples in Table 5.5, but the three color-coded regions in Figure 5.20.

Table 5.5: Soil types (samples) for lab measurement.

Sample	Soil type	Sand (%)	Silt (%)	Clay (%)	Remark
1	Sandy clay loam	60	10	30	Too much sand
2	Sandy clay	50	10	40	
3	Sandy loam	75	10	15	
4	Loamy sand	85	10	5	
5	Loam	30	45	25	Recommended soil type
6	Clay loam	35	30	35	
7	Clay	20	10	70	Too much fine
8	Silty clay loam	10	55	35	
9	Silty clay	10	45	45	
10	Silty loam	10	75	15	

The p-wave velocity and electrical resistivity scatter plot with the ten soil samples is shown in Figure 5.21. The samples are color-coded to match the three groups in Figure 5.20. For each soil type, seismic velocity and electrical resistivity values at optimum moisture content are measured in the laboratory. Except for one data point with high resistivity, all three groups are between electrical resistivity of 10 – 25 Ohm-m. P-wave velocity has a wider range of 420 – 680 m/s. There is no clear differentiation between the three zones on the p-wave velocity versus electrical resistivity scatter plot.

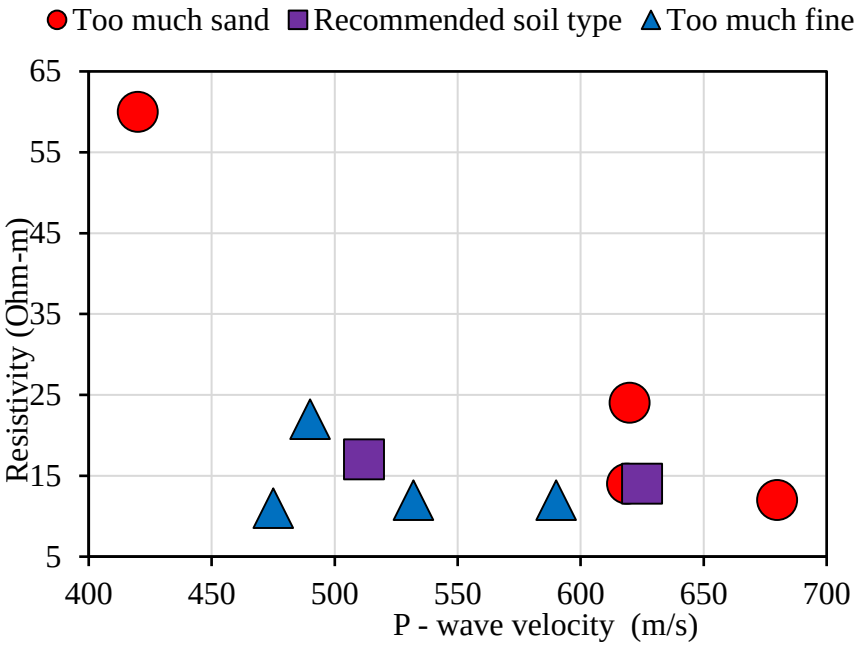

Figure 5.21: P-wave velocity vs resistivity scatter plot for the ten soil samples.

An s-wave velocity and electrical resistivity scatter plot is shown in Figure 5.22. S-wave velocity ranges from 200 m/s to 340 m/s with no clear distinction between the three soil groups.

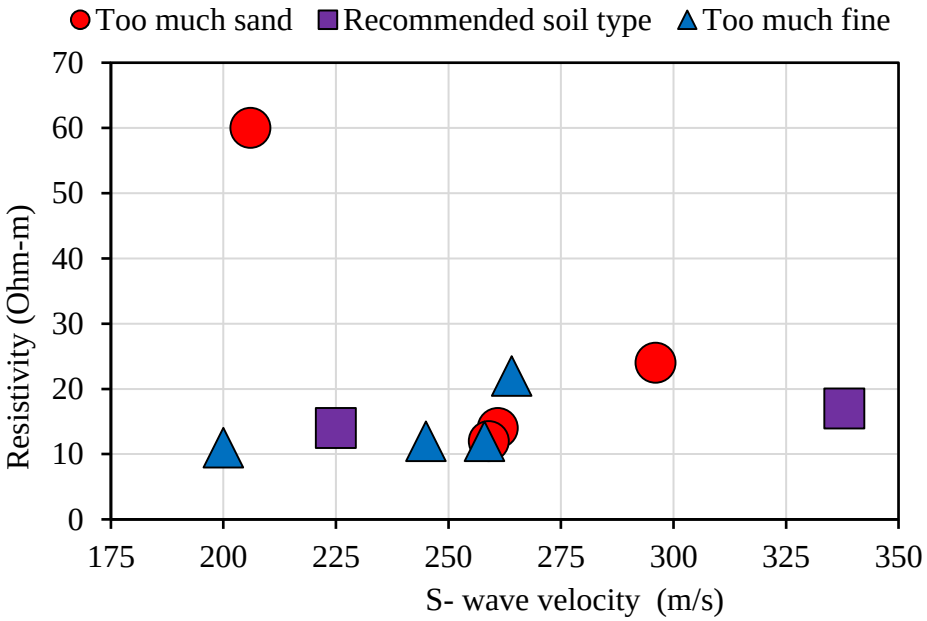

Figure 5.22: S-wave velocity vs resistivity scatter plot for the ten soil samples.

Overall, laboratory seismic velocity and electrical resistivity measurements using synthetic soil samples cannot clearly differentiate soil types recommended for dam construction based on the USDA soil classification.

5.5 Summary

Cross-plot analysis using preliminary measurements on clay loam leads to a conservative constraint (high degree of safety) where most of the dam is classified as probably compromised. Preliminary field measurement on the loamy sand does not account for wetting associated with longer loading time. In order to target saturated loamy sand, a reduction in the electrical resistivity of the loamy sand from the preliminary value should be determined with the help of laboratory measurements. By combining saturation adjusted preliminary measurements on the loamy sand and preliminary measurements on the clay loam, cross-plot boundaries based on a factor of safety and on how tightly the saturated loamy zone is targeted can be chosen.

The preliminary electrical resistivity value of the dry compacted clay loam is high and does not place the field measured dry compacted clay into the compromised quadrant. This is because the field measurements were conducted after the dry compacted clay loan was affected by wetting. Therefore, the drop in the preliminary electrical resistivity associated with wetting should be determined for the dry compacted clay.

Laboratory measured p-wave velocities for the loamy sand, clay loam, and dry compacted clay loam, are significantly higher than values obtained from the field measurements (tomograms). This could be due to differences in confining stress and seismic wave frequency between the laboratory and field measurements. Differences in electrical resistivity between laboratory and field measured values is smaller compared to differences in p-wave velocity. The variations in

electrical resistivity could be associated with differences in degree of saturation, temperature, porosity, connectivity of pores, and pore size distribution.

For better application of cross-plot analysis, an improved identification of compromised zones in their actual (field) geotechnical state is important. Preliminary and laboratory measurements fail to capture the field stress state of both compromised and safe zones. In addition to that, differences in the frequencies of field and laboratory seismic waves can lead to differences in p-wave velocity results. For cross-plot analysis on actual dams and levees, where preliminary measurement is not usually available, geophysical field measurements and theoretical models could be used.

Using synthetic soil samples, seismic velocity and electrical resistivity laboratory measurements were conducted on three groups of soil types based on their suitability for dam construction. Results from scatter plot analysis showed that laboratory seismic and electrical resistivity measurements could not clearly separate between the three groups of soils. This could be due to the general overlap of geophysical values in soils. When using synthetic soil samples to represent actual soil samples, effects of rarely considered factors, such as iron oxide, clay mineralogy, and organic content, on the geotechnical and geophysical properties should be examined.

CHAPTER 6

6. APPLICATION OF EXTERNAL PHYSICAL CONSTRAINTS USING GEOPHYSICAL SURVEYS AND THEORETICAL MODELS AT FRANCIS LEVEE SITE *

6.1 Introduction

In Chapter 5, one important observation derived from the preliminary and laboratory geophysical measurements on the Stillwater dam was that these measurements fail to capture the confining field stress condition. Therefore, theoretical models that correctly represent the field state of possible compromised zones could be used to identify similar locations within the dam or levee.

In Chapter 6, a new method of establishing cross-plot analysis constraints using external physical constraints derived from geophysical surveys and theoretical models is presented. The method is applied to identify locations of preferential flow paths through the subsurface of the Francis levee site that might have led to the formations of the three sand boils.

6.2 Introduction to Francis Levee Site

The 2011 flood report by the Mississippi Levee Board identified as many as twelve areas associated with seepage within the state of Mississippi (Nimrod, 2011). The Francis Levee site is one of the locations affected by the flood.

∗ A book section on this study is currently under peer-review. Wodajo, L.T., Hickey, C.J., Brackett, T.C., "Application of Seismic Refraction and Electrical Resistivity Cross-plot Analysis: A Case Study at Francis Levee Site", *Levee and Dams: Advances in Geophysical Monitoring and Characterization*, Springer.

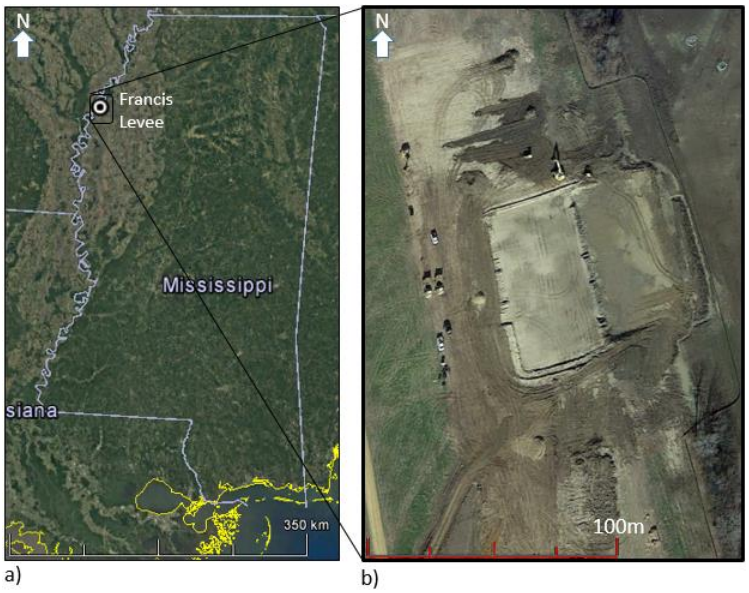

Figure 6.1: a) Francis levee site (34° 5'9.48"N, 90°51'52.56"W) located 0.8 km west of Francis (Google Earth, 2015), b) aerial photography taken during mitigation of the levee (Google Earth, 2013).

During the 2011 flood event, three main sand boils were observed and mitigated by the construction of sandbag berms (Nimrod, 2011). After the first sand boil (green dot on Figure 6.2) was mitigated, two more sand boils (red dots on Figure 6.2) surfaced approximately 90 m landward in the field. After the initial mitigation, the US Army Corps of Engineers (USACE) extended the berm of the levee and constructed 16 relief wells.

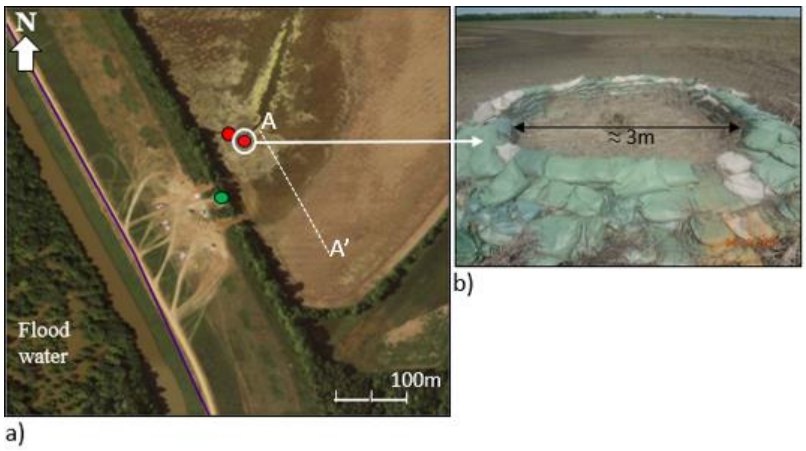

Figure 6.2: a) Location of the three sand boils (Nimrod, 2011), and b) mitigation of sand boil with sand bags (Nimrod, 2011).

The Francis Levee site is located in the Mississippi River flood plain, which is composed of Holocene and Pleistocene-aged meander deposits formed by the migration of the Mississippi River across its floodplain. The fluvial depositional environments include point bars, channel-fill deposits, natural levees and back swamp deposits (Saucier, 1994). Saucier (1994) notes that the convex portion of meander bends typically host point bar deposits near the channel with overbank/back swamp deposits occurring further away. As the distance from the meander increases, it is expected that deposits will decrease in grain size (Brackett, 2012). The three sand boil formations at the Francis Levee Site fall within an old channel or an oxbow as shown in Figure 6.3. The different colors in Figure 6.3a) indicate the stage of the river at the time. The broken blue lines indicate meander belt around the Francis Levee site.

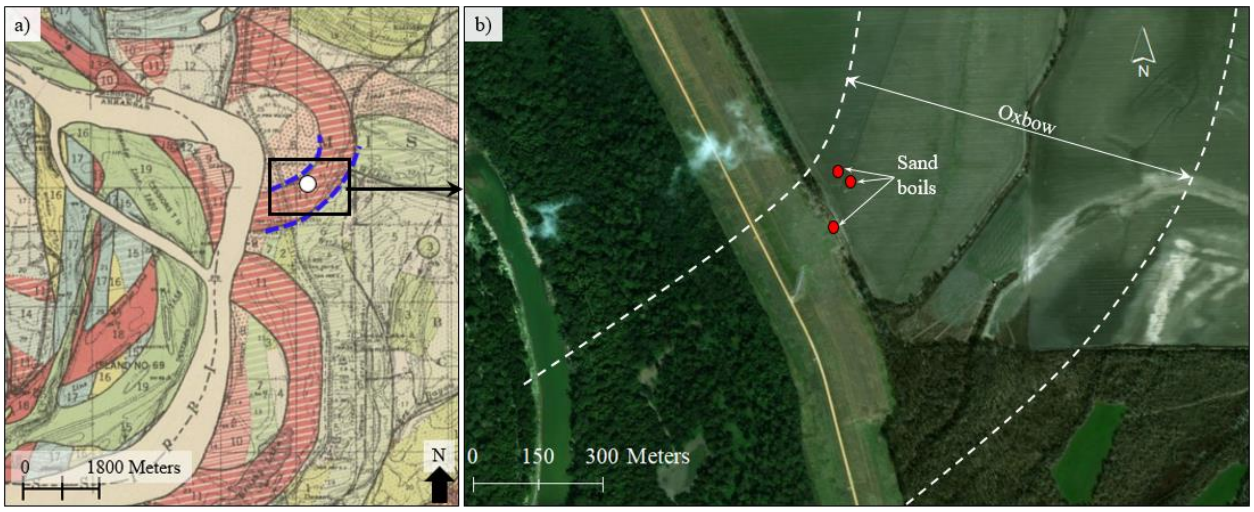

Figure 6.3: a) Ancient courses of the Mississippi River reconstructed from multiple aerial photographs (Fisk, 1944), b) relative location of the sand boils (red dots) and meander belt edges (broken white line) (Google Earth, 2015).

Cross section A-A' in Figure 6.2 indicates that the levee is underlain by a clay-rich overburden averaging 3m thick (Figure 6.4). Below the clay overburden, the sediment coarsens into silt, and eventually a thick sand unit, which is assigned to the permeable substratum (Brackett, 2012). A similar cross section is observed on the waterside of the levee with a sand layer

connecting the waterside to the landside. With adequate water pressure, water can flow from the waterside to the landside through the permeable sand substratum.

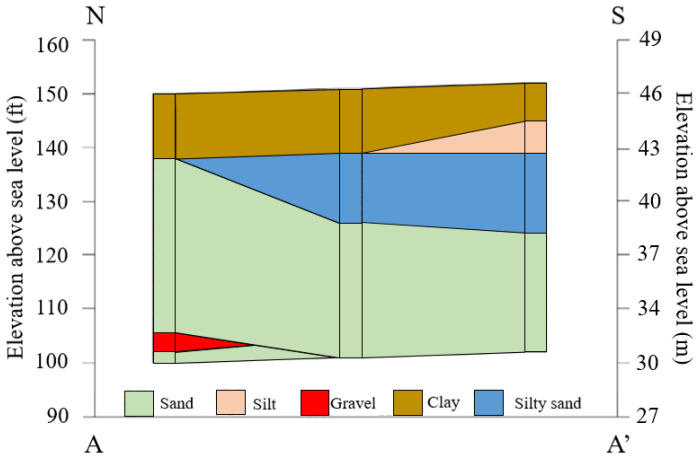

Figure 6.4: Cross section A-A' (Figure 6.2) shows a pinching-out of the silt and silty sand to the north of the site, yielding a direct sand to clay contact (Brackett, 2012).

A possible model for the sand boil formations is preferential flow through the coarser grained sands that filled an old oxbow (Figure 6.5). This coarse-grained high permeability sand layer acts as a flow channel for sub-surface seepage connecting the waterside to the landside. High water level on the waterside due to flood events generates enough hydraulic head to initiate seepage. This seepage then appears on the surface as a sand boil where the upper confining clay layer is the weakest.

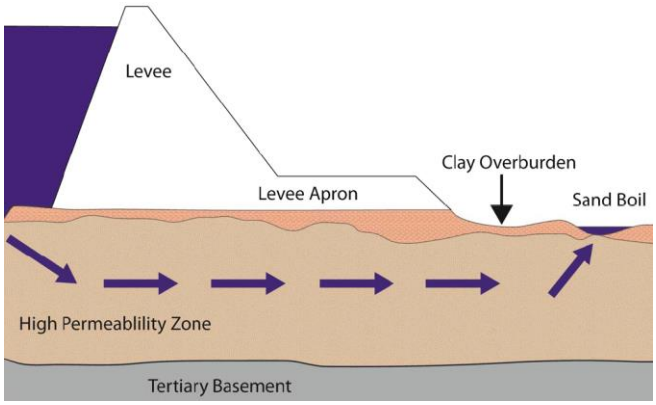

Figure 6.5: Possible model for sand boil formation at Francis Levee Site.

The objective of this field study is to implement a method of cross-plot analysis using two geophysical methods, seismic refraction tomography (SRT) and electrical resistivity tomography (ERT), in order to identify locations of preferential flow paths through the subsurface of the Francis levee that might have led to the formations of the three sand boils. A method of using theoretical models, Archie's first law, and effective fluid velocity model to determine the seismic velocity and electrical resistivity bounds of the cross-plot is presented.

6.3 Study Area and Survey Parameters

Three locations were selected to conduct both seismic and electrical resistivity measurements. Survey line 1 is on the waterside of the levee, survey line 2 is on the berm of the levee, and survey line 3 is on the landside of the levee between the first sand boil and the two sets of sand boils. Each survey line is 478 m long and starts at the northern end and progresses southward parallel to the levee. Figure 6.6 shows the location of the three survey lines and the sand boils.

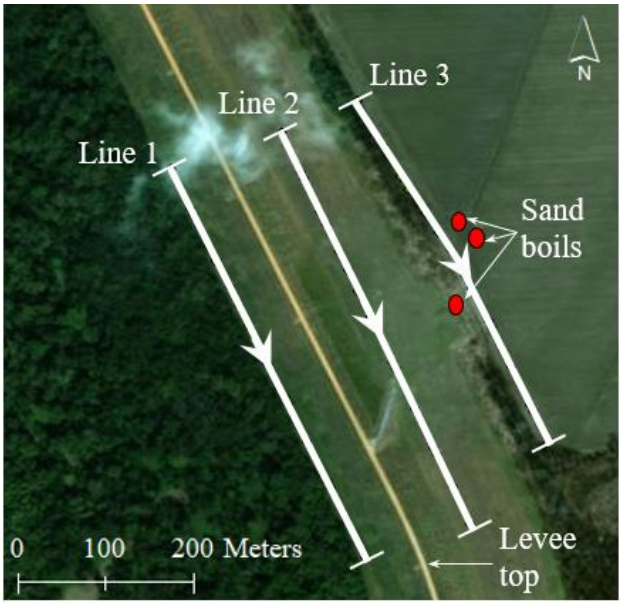

Figure 6.6: Locations of p-wave seismic refraction and electrical resistivity survey lines. The arrows on the lines indicate direction of surveys.

For the p-wave seismic refraction surveys, the whole length of each survey line is covered using a 24-geophone roll-along. Shot records were collected at 1 m offset from the first and last geophones and in between all geophones. For electrical resistivity surveys, the whole length of each survey line is covered using a 56-electrode roll along. Additional survey parameters are summarized in Table 6.1.

Table 6.1: Seismic refraction and electrical resistivity survey parameters used at Francis Levee Site.

Seismic refraction		
Number of geophones	48	10Hz vertical component
Geophone spacing	2	m
sample interval	0.125	msec
record length	2	sec
Electrical Resistivity		
Number of electrodes	112	
electrode spacing	1	m
Survey configuration	Dipole-dipole	

Rayfract™ software (Intelligent Resources, 2018) is used for the inversion of all seismic refraction data. Surfer™ imaging software (Golden Software, 2018) is used to build the tomograms after processing. EarthImager2D™ inversion software (Advanced Geosciences, 2018) is used for the inversion and imaging of all the electrical resistivity data.

A sample of p-wave seismic refraction end shot gather on survey line 1 (waterside 0m – 47m) is shown in Figure 6.7. The red line indicates the first arrival picks for the shot gather. A sample of the measured apparent resistivity pseudosection for survey line 3 (landside 0m – 167m) is shown in Figure 6.8.

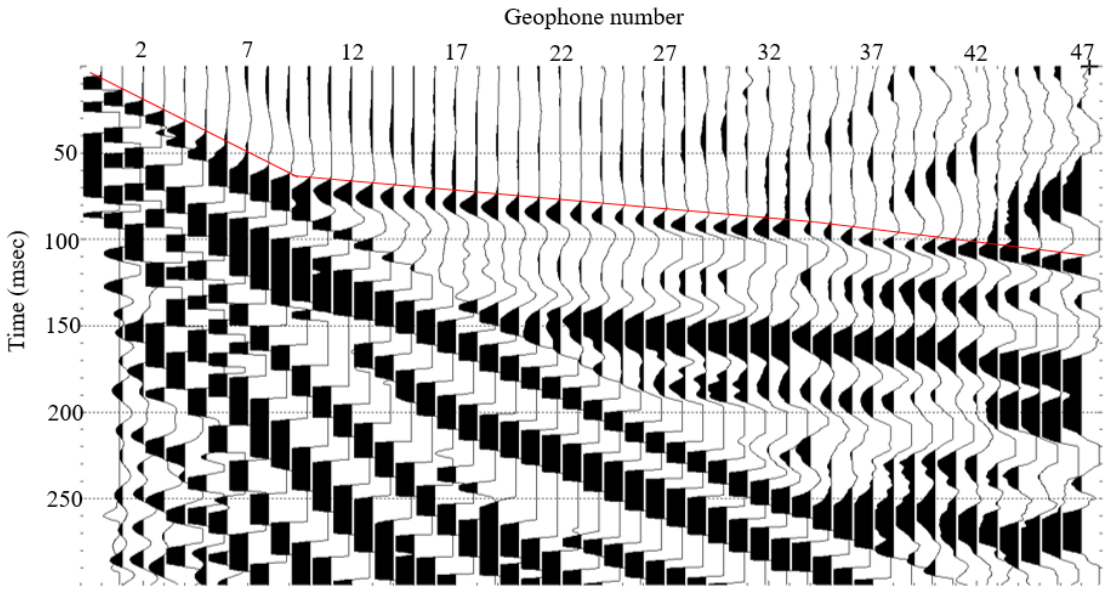

Figure 6.7: P-wave seismic refraction end shot gather at Francis Levee site (Line 1, waterside, 0m – 47m).

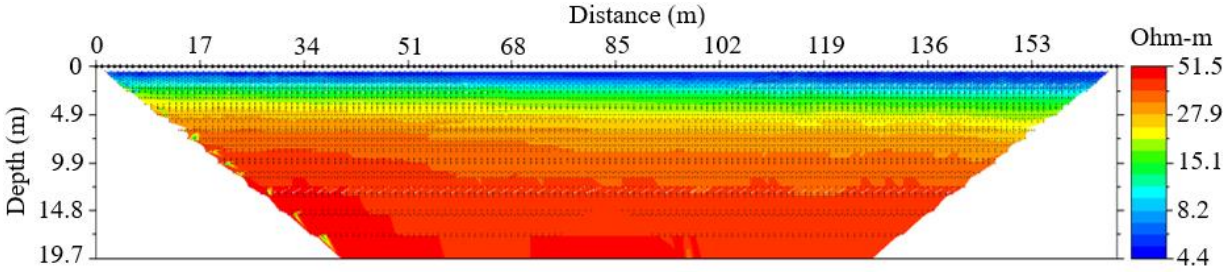

Figure 6.8: Measured apparent resistivity pseudosection for Francis Levee site survey line 3 (landside 0m – 167m).

6.4 Survey Result and Analysis

After the completion of all the seismic refraction and electrical resistivity surveys, seismic velocity and electrical resistivity tomograms are produced. Electrical resistivity survey on the berm (Line 2) was not usable due to poor data quality. A layer of sand was placed on the berm during the rehabilitation of the dam. Sand has high electrical resistivity, which leads to high contact resistivity at the electrodes hindering the transmission of electric current into the ground. Therefore, cross-plot analysis was only conducted for surveys on the waterside (line 1) and on the landside (line 3).

6.4.1 Waterside (Line 1)

The electrical resistivity tomograms for line 1 (waterside) are shown in Figure 6.9. Available borehole information is shown on the tomograms to aid with interpretation. Based on borehole data, all eleven high resistivity anomalies (E1-E11) indicated by the broken line circles on Figure 6.9 are located in the sand zone. Ground water level (GWL) is at 4.7 m depth indicating that the sand zone is saturated.

A possible seepage zone has high permeability. The permeability of soil depends on porosity and grain size distribution. High permeability corresponds to high porosity, which leads to low p-wave velocity. High permeability also implies coarse soil or low clay content which leads to high resistivity.

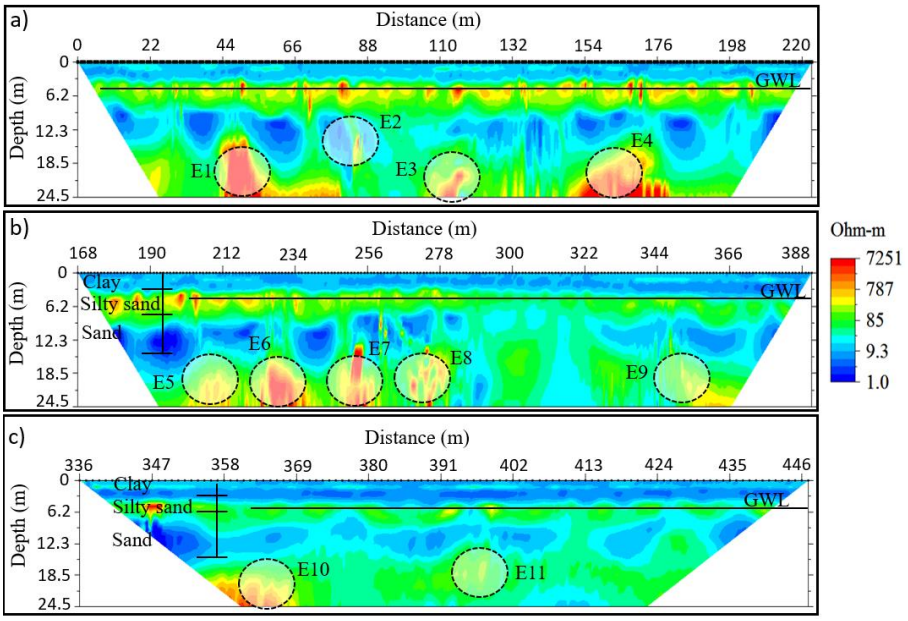

Figure 6.9: Line 1 (waterside) electrical resistivity tomogram, a) 0m - 220m distance, b) 168m – 388m distance, and c) 336m – 446m distance.

Therefore, in order to reduce the number of anomalies in the ERT tomograms, the next step is to identify locations of low-velocity anomalies in the seismic refraction tomograms that are

collocated with high resistivity anomalies. The p-wave seismic velocity tomograms for line 1 (waterside) are shown in Figure 6.10. Six seismic anomalies (S1 – S6) with low p-wave velocities, all located in the sand zone, are identified having low p-wave velocity compared to their background.

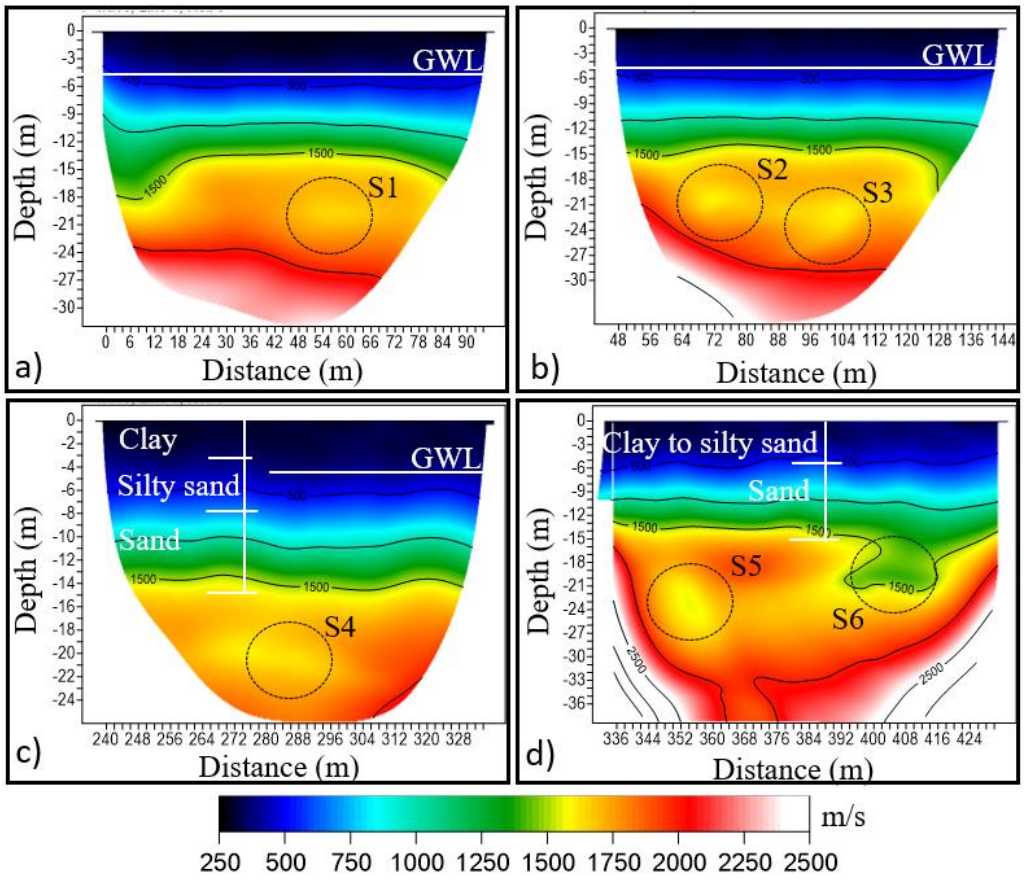

Figure 6.10: Line 1 (waterside) p-wave tomogram, a) 0m - 96m distance, b) 48m – 144m distance, c) 240m – 336m distance, and d) 336m – 432m.

6.4.2 Identification of True Compromised Zones Using Theoretical Models

In order to identify true compromised zones out of the six possibilities shown in Figure 6.10, an effective fluid velocity model (Eq. 6.1a) and (Eq. 6.1b), is used to model the seismic velocity of the sand zone and to calculate porosity ($\phi_{velocity}$) from p-wave velocity tomograms.

$$K_{sat} = (V_p{}^2)[(1 - \phi_{velocity})\rho_o + (\phi_{velocity})\rho_w] \qquad 6.1(a)$$

$$K_{sat} = \frac{(K_s \cdot K_w)}{(1 - \phi_{velocity})K_w + (\phi_{velocity})K_s} \qquad 6.1(b)$$

where K_{sat} is the saturated bulk modulus of the soil, K_s is the sand grain bulk modulus (36.6 GPa), K_w is the bulk modulus of water (2.20 GPa), V_p is p-wave velocity (m/s), ρ_w is density of water (1000 Kg/m^3), ρ_s is the sand grain density (2650 Kg/m^3), and $\phi_{velocity}$ is porosity calculated from p-wave velocity. Since average p-wave velocity (V_p) can be obtained from the tomograms in Figure 6.10, porosity ($\phi_{velocity}$) for each of the six seismic anomalies can be calculated by equating Eqs. 6.1a and 6.1b.

Archie's first law for a fully saturated clean sand,

$$\rho_o = \rho_w \cdot \phi_{resistivity}^{-m}, \qquad (6.2)$$

is used to model the electrical resistivity of a fully saturated clean sand and to calculate porosity ($\phi_{resistivity}$) where ρ_o is the bulk resistivity, ρ_w is the resistivity of the pore fluid, $\phi_{resistivity}$ is porosity calculated from electrical resistivity, and cementation factor (m) is taken as 1.8 for sand.

From the seismic refraction tomogram (Figure 6.10) and electrical resistivity tomograms (Figure 6.9), the sand zone (excluding the anomalies) has an average p-wave velocity of 1750 m/s and an average electrical resistivity of 415 Ohm-m. Porosity of the sand zone is determined by using Eq. 6.1 and the average p-wave velocity of the sand zone. The average resistivity of the sand zone is then used to determine the resistivity of the pore fluid (ρ_w) using Eq. 6.2. Resistivity of the pore fluid (ρ_w) is assumed to remain constant and porosity ($\phi_{resistivity}$) for each of the six seismic anomalies can be calculated using Eq. 6.2. Once the porosities of the six anomalies are calculated using the two models, their consistency is compared as shown in Table 6.2. Seismic anomaly 5 (S5), located 18 m to 27 m below the surface, has both calculated porosities within an acceptable

range (< 0.5) and is the most consistent between the two models (Table 6.2). Therefore, seismic anomaly 5 (S5) is considered an area most probably associated with a seepage path.

Table 6.2: Average p-wave velocity and electrical resistivity values for the six anomalies on the waterside, summary of values and consistency in the calculated porosity of the six anomalies.

Anomalies (Figure 6.10)	**Velocity (m/s)**	**Resistivity (Ohm-m)**	**$\phi_{velocity}$ (Effective fluid velocity model)**	**$\phi_{resistivity}$ (Archie's first law model)**	**$\Delta\phi = \phi_{res} - \phi_{vel}$**
S1	1656	160	0.35	0.49	0.14
S2	1597	133	0.40	0.54	0.14
S3	1597	63	0.40	0.82	0.42
S4	1646	15	0.35	1.82	1.47
S5	1639	218	0.36	0.41	0.05
S6	1430	29	0.71	1.26	0.55

6.4.3 Landside (Line 3)

The electrical resistivity tomograms for line 3 (landside) are shown in Figure 6.11. The survey for Figure 6.11a was conducted in May whereas the survey for Figure 6.11b and 6.11c were conducted in December. Surveys conducted during wet season have lower electrical resistivity compared to surveys conducted in dry season. In Figure 6.11, the broken line boxes indicate locations of electrical resistivity anomalies (EA1 – EA8) with high resistivity all located in the sand zone. The red and blue lines at the top of the figures indicate areas of overlap. The small red

boxes at the top of the tomograms indicate the relative locations of the three sand boils. GWL represents ground water level from well readings.

Anomaly EA2 in Figure 6.11b is not present in Figure 6.11a, which could be an effect of seasonal change. Even though the surveys for Figure 6.11b and 6.11c are conducted at the same time, they do not indicate anomaly EA7 in a similar fashion. In general, since anomaly EA3 and EA4 are collocated, ERT survey on line 3 (landside) indicates seven distinct anomalies where all the high resistivity anomalies are located in the sand zone.

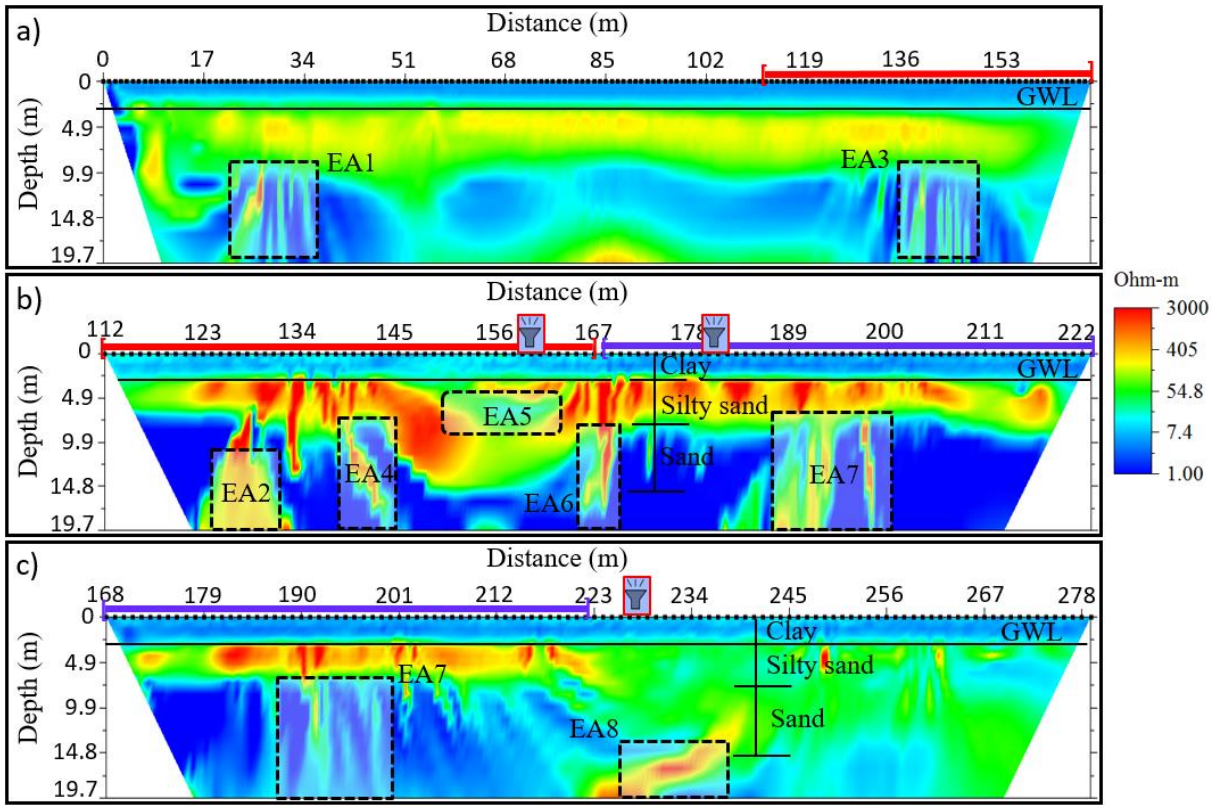

Figure 6.11: Electrical resistivity tomograms for line 3 (landside). a) 0m - 170m distance, b) 112m – 222m distance, and c) 168m – 278m distance.

The p-wave velocity tomogram for landside, Figure 6.12, indicates three distinct seismic anomalies (SA1, SA2, and SA3) having low p-wave velocity compared to their background and all located in the sand zone. The broken circles indicate locations of the seismic anomalies, all

located in the sand zone. The small red boxes at the top of the tomograms indicate the relative locations of the three sand boils.

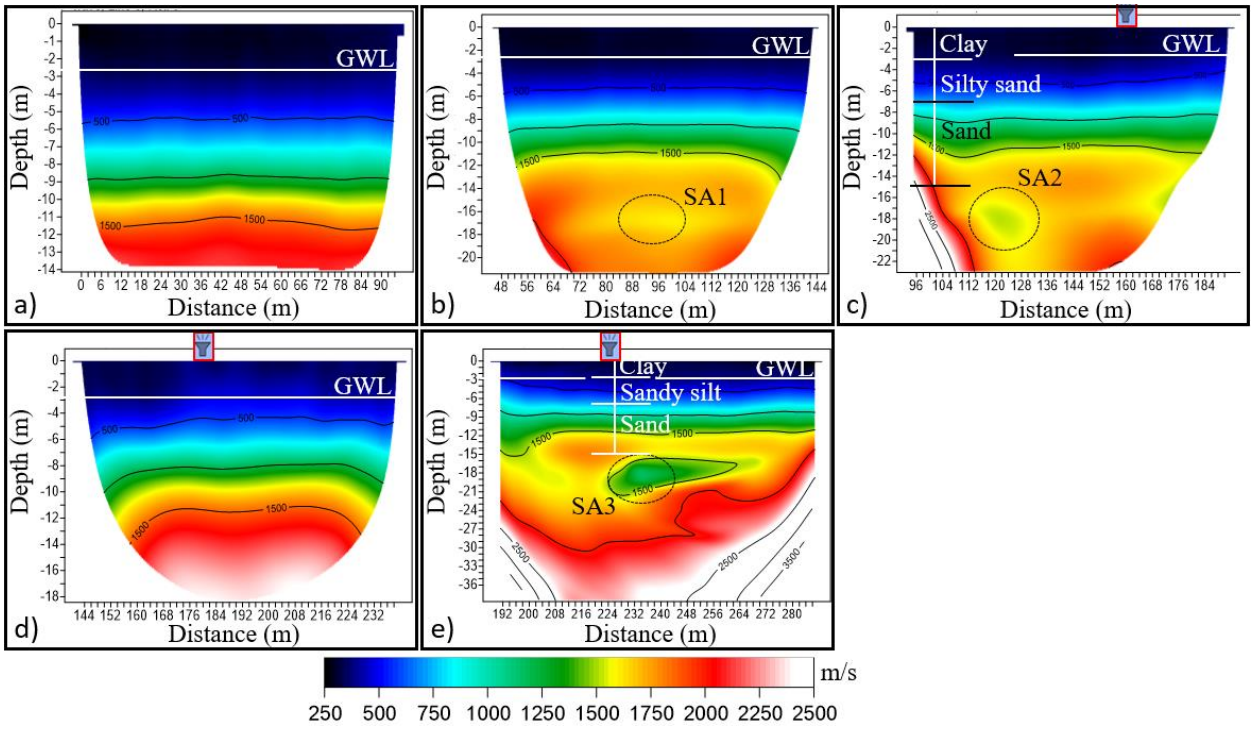

Figure 6.12: Line 3 (landside) p-wave velocity tomograms. a) 0m - 96m distance, b) 48m – 144m distance, c) 96m – 192m distance, d) 144m – 240m distance, and e) 192m – 288m distance.

The location of all the electrical resistivity anomalies (Figure 6.11) and all seismic velocity anomalies (Figure 6.12) are obtained from the tomograms and indicated across line 3 (landside) as shown in Figure 6.13. Seismic anomalies 2 and 3 have a corresponding anomaly in the ERT tomograms. Seismic anomaly 2 (SA2) is collocated with ERT anomaly 3 (EA3) and seismic anomaly 3 (SA3) is collocated with ERT anomaly 8 (EA8). Since seismic anomaly 1 (SA1) has no corresponding high resistivity anomaly, it can be omitted.

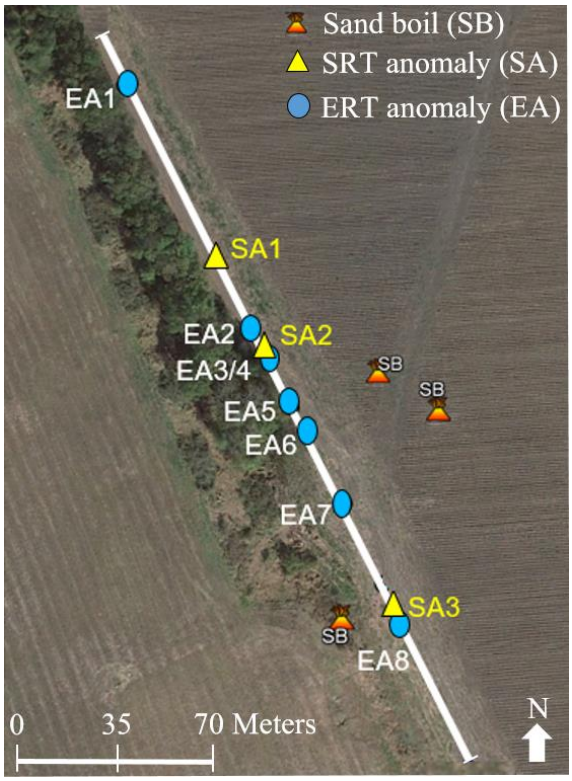

Figure 6.13: An aerial image of survey line 3 (landside) with locations of SRT and ERT anomalies indicated along the survey line.

6.5 Cross-Plot Analysis

In order to identify which of the remaining two pairs of collocated anomalies, ([SA2 and EA3] and [SA3 and EA8]), is associated with the formation of the sand boils, a cross-plot analysis based on the seismic velocity and electrical resistivity of anomaly number 5 (S5) on the waterside is performed. Cross-plot analysis using the seismic velocity (1639 m/s) and electrical resistivity (218 Ohm-m) values of anomaly number 5 (S5) (Table 6.2) on the waterside can be used to identify similar anomalous locations on the landside (line 3). This is a variant of standard cross-plot analysis where prior information is used as the boundary of the cross-plot analysis.

The cross-plot analysis of seismic anomaly 2 (SA2) and electrical anomaly 3 (EA3) is shown in Figure 6.14. The blue boxes on both the ERT (Figure 6.14a) and SRT (Figure 6.14b) indicate a background area selected covering both anomalies (SA2 and EA3). The size (area) of the blue boxes are the same on both ERT and SRT tomograms. Each grid point in the ERT tomogram has a corresponding grid point in the SRT tomogram. All electrical resistivity and p-wave velocity pairs within the blue boxes (background) are cross-plotted on a resistivity versus p-wave velocity plot and shown with blue dots (Figure 6.14c). Similarly, the cross-plot for the SA2 (black points) and EA3 (purple points) are shown in Figure 6.14c. The cross-plot boundary values of 1639 m/s and 218 Ohm-m are shown with the red lines on the cross-plot Figure 6.14c. Analysis of the cross-plot indicates that neither SA2 nor EA3 fall in the compromised quadrant.

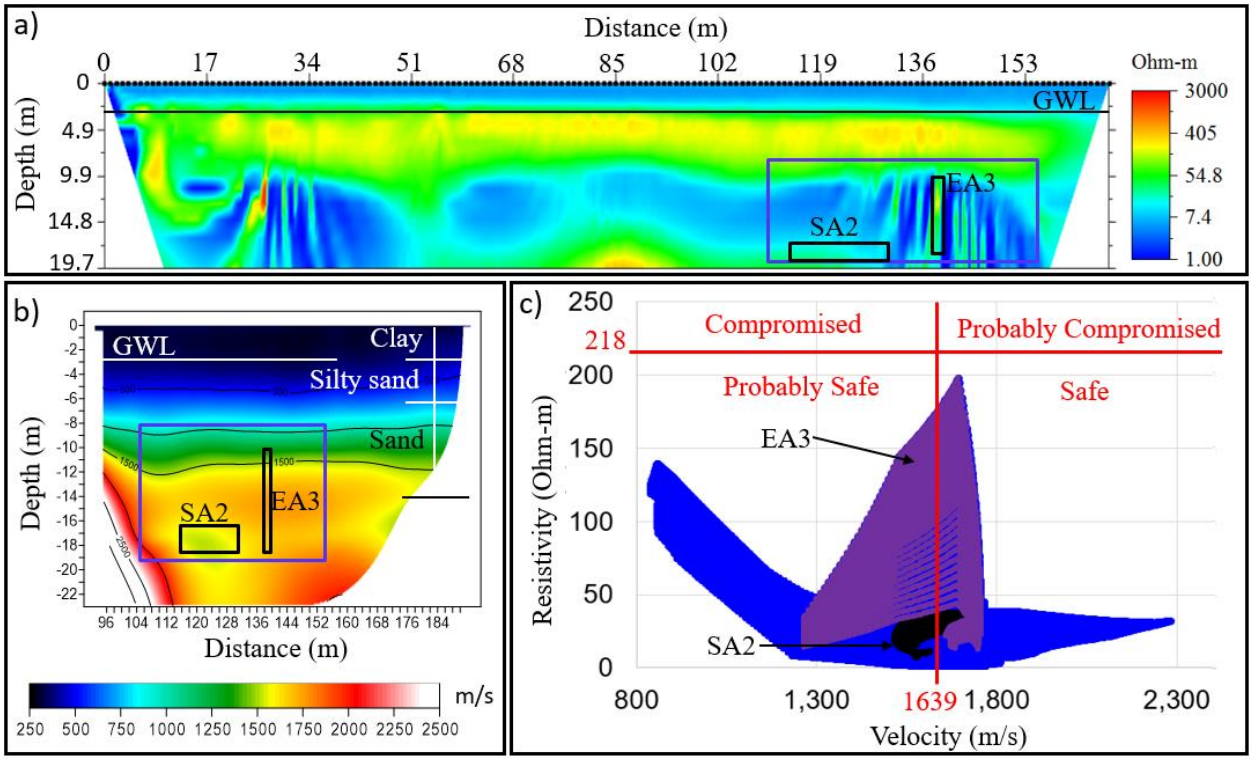

Figure 6.14: a) Electrical resistivity tomograms for line 3 (landside) for 0m to170m distance, b) line 3 (landside) p-wave velocity tomograms for 96m to 192m distance, c) cross-plot analysis using SA2 and EA3.

Similarly, the cross-plot analysis for SA3 and EA8 is shown in Figure 6.15c. A smaller area shown with a white box on both tomograms is picked by focusing on the high resistivity area within SA3 (black box). The cross-plot of this smaller area is shown by the light blue dots on the cross-plot (Figure 6.15c). The cross-plot analysis shows that the majority of SA3/EA8 falls within the compromised quadrant. This is an indication that the combination of SA3 and EA8 have similar features to anomaly number 5 (S5) on the waterside (Figure 6.10d) and could be associated with the formation of the three sand boils.

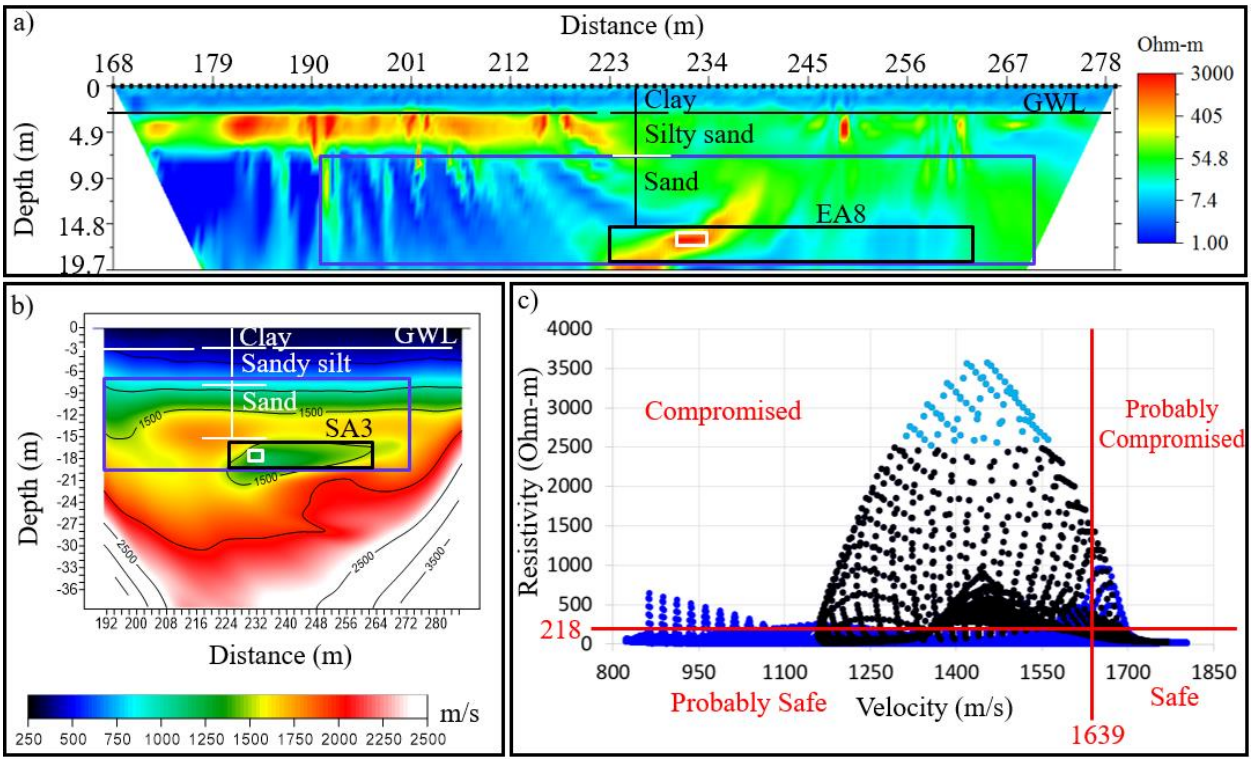

Figure 6.15: a) Electrical resistivity tomograms for line 3 (landside) for 168m to 278m distance, b) line 3 (landside) p-wave velocity tomograms for 168m to 278m distance, c) cross-plot analysis using SA3 and EA8.

6.6 Possible Seepage Path

In order to identify a possible seepage path, the location of the sand boils, the six anomalies on the waterside, and the three anomalies on the landside are plotted on an aerial image of Francis Levee Site as shown in Figure 6.16. A possible seepage line parallel to the northern edge the meander belt is drawn passing through anomaly S5 on the waterside and anomaly SA3/EA8 on the landside. The projection of this possible seepage path passes through the three sand boils. Flow path parallel to the meander is expected because the soil deposit inside the meander has low compaction and high permeability compared to the native ground. Water can flow through the highly permeable sand and gravely sand and cause sand boil formations at locations where the overburden clay layer is thin. The anomaly on the landside is located 18m to 27m below the surface whereas on the waterside the anomaly is between 15m to 21m below the surface.

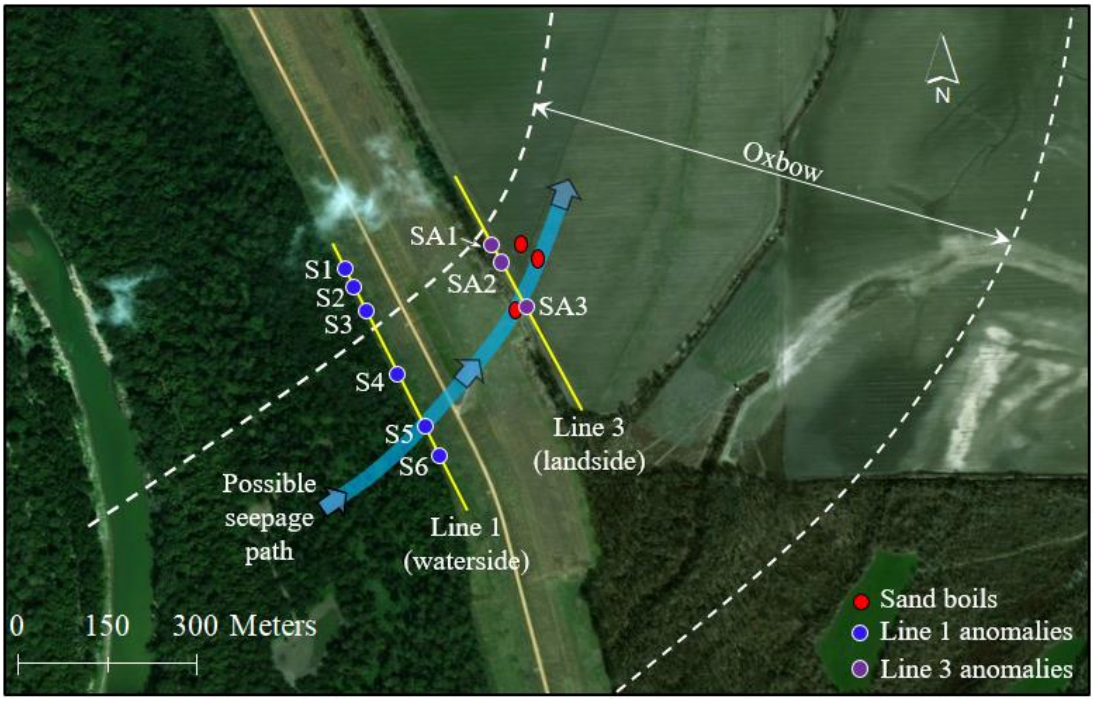

Figure 6.16: Possible seepage path (blue line) going parallel to the northern edge the meander belt and passing through anomaly S5 on the waterside and anomaly SA3/EA8 on the landside.

6.7 Summary

Results from seismic refraction and electrical resistivity surveys conducted at Francis Levee Site indicated seven distinct anomalies that might be associated with seepage. For both surveys on the waterside and landside, applying the restriction that velocity of a seepage zone should be lower than the background velocity reduces the number of anomalies in the ERT tomograms.

The location (depth from the surface) of the anomalies, associated with the proposed seepage paths, support the idea that the preferential flow occurs within the sand layer in the old oxbow. The location of the sand boils is along the proposed trajectory but most likely outcrops where the overlying impermeable clay layer is thin or the weakest. The predicted subsurface pathway is reasonable because it follows the contour of the meander and it passes through the location of the sand boils.

The study showed that theoretical models, along with available geotechnical data, could be used to determine cross-plot analysis bounds. These bounds are based on field measured seismic and electrical resistivity values of anomalies that are identified in the individual geophysical methods.

CHAPTER 7

7. CONCLUSIONS

7.1 Summary

Geophysical investigations such as seismic refraction tomography and electrical resistivity tomography can play an important role in the assessment of earthen dams and levees. Conducting integrity assessment of earthen dams and levees usually involves proceeding straight from visual inspection to invasive geotechnical drilling. However, geophysical methods can be used as subsurface inspection tools to guide engineers to locations that have a higher probability of being compromised. The advantages of geophysical surveys are high spatial subsurface sampling (both 2D and 3D), non-invasive acquisition allowing for repetitive measurements to monitor changes over time, and less expense than traditional boring programs. The impediments of incorporating geophysical information are that the data is represented in terms of geophysical parameters not commonly used by engineers and that the natural heterogeneity of dams and levees can produce geophysical anomalies; as such, not all geophysical anomalies are indicative of compromised zones.

The goal of this research was to advance geophysical measurement use for the preliminary investigation of dams and levees to guide the more invasive geotechnical investigations. This work focuses on ranking geophysical anomalies with respect to their likelihood of representing certain types of compromised zones within dams and levees. One approach for establishing a better correlation between geophysical anomalies and compromised zones is to utilize data from two

geophysical methods. Cross-plot analysis is being developed to merge seismic velocity and electrical resistivity for identifying compromised zones. Through cross-plot analysis, the subsurface conditions are divided into different integrity classes based upon geophysical values. This work advances the use of cross-plot analysis by better understanding the dividing boundaries of the integrity classes and developing additional external constraints.

In conclusion, geophysical surveys are valuable subsurface inspection tools that should be adopted for the integrity investigation of earthen dams and levees. However, these methods are not a replacement for geotechnical surveys and drilling is required for the confirmation of true compromised zones.

7.2 Contributions

The use of cross-plot analysis for identifying two types of compromised zones within a dam was examined using a field experiment. A quarter-size model embankment dam was constructed at Stillwater, OK, with two compromised zones placed within the dam. The two compromised zones were a dry compacted clay loam compacted at 10% moisture content, and a loamy sand zone. The remaining "safe" parts of the dam were constructed from clay loam compacted at OMC. This was the first time that such a study was conducted over a period of two years to monitor changes in geophysical properties associated with reservoir loading conditions, seasonal changes, internal erosion, and seepage.

Based on conventional cross-plot analysis, compromised zones are generally associated with low p-wave velocity and high electrical resistivity. Results from this study showed that this generalization does not work for all cases. When a dry compacted clay loam becomes saturated, its electrical resistivity can drop below that of the dam body (i.e. the safe part). Therefore, in order

to identify dry compacted clay loam when it is saturated, a cross-plot analysis with a compromised quadrant of low p-wave and low electrical resistivity should be used. Using the Stillwater field data, the loamy sand zone was detected using conventional cross-plot analysis and boundaries selected from field data.

Different approaches for defining the cross-plot boundaries were investigated. The selection of the cross-plot bounds for the Stillwater experiment were based on prior information on the location of the zones and visual inspection of the scatter plots of known safe and compromised locations. However, even in this well-controlled experiment, proper adjustments were required to address depth accuracy issues in the seismic refraction tomography. This shows that cross-plot analysis does not remedy problems that are inherent to seismic refraction and electrical resistivity surveys. If proper adjustment is not made to address depth accuracy issues of seismic refraction tomography, cross-plot analysis could provide misleading information due to mismatching locations of anomalies on seismic refraction and electrical resistivity tomograms.

Lateral resolution of both seismic refraction and electrical resistivity surveys are better with the new approach of using a lateral plan view derived from cross-plot analysis maps. With the adaptation of this method, cross-plot analysis results can be easily georeferenced and presented on aerial maps to guide engineers on where to place boring locations along miles of levees.

Cross-plot boundaries were also defined using p-wave velocity and electrical resistivity measurements during construction. On real dams and levees, this information could be obtained by conducting geophysical measurements and confirming compromised locations by drilling select anomalies. The “safe” criteria could be established by estimating the average behavior of the dam in locations absent of anomalies. Cross-plot boundaries using measurements on clay loam (dam body) leads to a conservative constraint (high degree of safety). The predicted state of the dam will

have more anomalies and differentiating true anomalies from false alarms would require further investigation. Cross-plot boundaries based on compromised zones leads to a low factor of safety. The predicted condition of the dam will have fewer anomalies but with the possibility of missing compromised zones. Cross-plot boundaries selected between these two cases are analogous to selecting an intermediate factor of safety and should be adopted when using preliminary geophysical values.

Compromised zones will change as a function of time, and measurement at a particular time may not account for the wetting condition during a survey. Therefore, time-lapse measurement and laboratory measurements are required to establish the relationship between geophysical properties and wetting condition. Relationships between geophysical properties and wetting condition can be obtained by conducting laboratory measurements on soil samples at different moisture contents.

An attempt was made to establish cross-plot boundaries based solely on laboratory experiments. A new laboratory apparatus for measuring the seismic velocity and electrical resistivity during a proctor compaction was designed and constructed. Results from the laboratory measurements on the Stillwater loamy sand and clay loam showed that p-wave velocities were significantly higher than values obtained from the field measurements. This discrepancy must be resolved before these values can be used for cross-plot boundaries. However, laboratory measurements showed a significant change in p-wave velocity and electrical resistivity during the proctor compaction process. This could be a future approach for studying geophysical properties of dams and levees. These types of studies would be valuable for establishing relationships between geophysical and engineering parameters.

Based on the time-lapse seismic refraction and electrical resistivity measurements that were conducted on the model embankment dam, a new approach of adding an external constraint further enhanced the location of the loamy sand. In this case, an additional restriction that electrical resistivity should decrease with increased loading time was used. Additionally, results from this time lapse study showed that compromised zones such as dry compacted clay loam and loamy sand can be identified using geophysical anomalies for surveys conducted during certain time periods. This suggests that the timing of geophysical surveying can be important for enhancing the sensitivity of the measurements to certain compromised zones. For example, the preferred time to identify dry compacted clay loam is when the dam has been loaded for an extended amount of time. When the dam is not loaded, since the dry compacted clay and the dam body have the same mineralogy and only a 3% moisture content difference, electrical resistivity lacks the resolution to differentiate them. When the dam is loaded for an extended time, water seeps more easily into the dry compacted clay loam reducing its electrical resistivity. On the other hand, the best time to identify the loamy sand is when the dam is unloaded or at dry season, when there is an overall moisture decrease in the dam. Identifying loamy sand when it is wet becomes difficult because water infiltrates into the loamy sand and reduces its electrical resistivity close to the base line resistivity of the dam. These observations show that conducting time-lapse geophysical measurements is very important in reducing the chance of missing anomalies associated with compromised zones.

Geophysical surveys were conducted at the Francis Levee site to assist in understanding the formation of sand boils at this location. As expected, the geophysical data had numerous anomalies that could be associated with possible seepage paths. The number of anomalies was reduced by using collocation of anomalies from seismic and electrical surveys. To further reduce

the number of anomalies, a new approach based upon external physical constraints calculated from field geophysical data and theoretical models was developed. In this case, the constraint is based upon the predicted porosity using the seismic and electrical data. The anomaly with the most consistent porosity was considered to be characteristic of a compromised zone (in practice, a drilling investigation would be required to confirm the anomaly is associated with a compromised zone). The geophysical data of this anomaly is then used to develop cross-plot boundaries to classify other anomalies with a low factor of safety. An application of this method at the Francis Levee site showed promising results in identifying paths that led to the formation of the sand boils.

7.3 Recommendations for Further Research

An attempt to use laboratory measured p-wave velocity and electrical resistivity measurements to establish cross-plot analysis boundaries was not successful. Similarly, laboratory measurements on synthetic soil samples failed to differentiate between different soil groups based on suitability for dam construction. Laboratory measured p-wave velocities were significantly higher than values obtained from the field measurements. Two possible reasons are the differences in seismic wave frequency between laboratory and field measurements and the variations in confining stress on laboratory compacted soil samples and field soil. Laboratory electrical resistivity measurements are relatively better than p-wave velocity values when compared to field measured values. More research on how to determine laboratory geophysical properties under field representative stress conditions is needed. One method of approaching this is to incorporate well-established geotechnical measurements of confining stress, such as a tri-axial test, during seismic velocity and electrical resistivity laboratory measurements. Study of methods of converting seismic velocity results from high frequency laboratory measurements to more field representative low frequency measurements is also required. This might require conducting laboratory

measurements at different frequencies on the same soil sample and studying variations in measured velocities. Understanding these variations could be used to deduce p-wave velocity values for low frequency field measurements from high frequency laboratory measurements.

Cross-plot analysis targeting the dry compacted clay loam zone did not clearly differentiate the zone from the clay loam compacted at OMC. Although the two zones were separated in p-wave velocity, electrical resistivity lacked the resolution to differentiate the two zones. This could be due to similarity in the mineralogy of the two zones. Extended loading time might be required for the electrical resistivity of the dry compacted clay loam to drop much further than the resistivity of the dam body. Therefore, for identifying under compacted clay zones, study on the application of cross-plot analysis over a much longer loading time is required. Measurements on a loaded dam over a year could be required to provide good insight to changes in geophysical properties associated with extended loading time and seasonal changes.

Time-lapse measurements on the Stillwater model embankment dam showed that a p-wave seismic refraction survey has a consistent problem of showing known features shallower than expected. Improving the depth accuracy of seismic refraction methods by incorporating known depth information in the data processing stage is also required. Improvement of existing processing software is required to allow users to input depth and geometry of known features in dams and levees. Examples of input data for real dams and levees include location and size of principal spillways (for dams), geometry from design (as-built) drawings, ground water elevation from well data, and borehole information.

BIBLIOGRAPHY

Aal, G., Ismail, A., Anderson, N., and Atekwana, E., (2013), "Geophysical investigation of seepage from an earth fill dam, Washington County, MO," *Journal of Applied Geophysics*, 44, pp. 167-180.

Abu-Hassanein, Z. S., Benson, C. H., and Blotz, L. R., (1996), "Electrical resistivity of compacted clays," *Journal of Geotechnical Engineering*, 122, pp. 397-406.

Abuzeid, N., (1994), "Investigation of channel seepage areas at the existing Kaffrein dam site (Jordan) using electrical-resistivity measurements," *Journal of Applied Geophysics*, 32, pp. 163-175.

Advanced Geosciences Inc., (AGI), 2018. http://www.agiusa.com/index.shtml, access date: April 07, 2018.

Al-Fares, W., (2014) "Application of electrical resistivity tomography technique for characterizing leakage problem in Abu Baara Earth Dam, Syria," *International Journal of Geophysics*, 2014, Article ID 368128.

Ammerlaan, P.R.M., (2007) *Levees and levee evaluation: The Dutch and US practice compared, MSc. Thesis*, Delft University of Technology.

Anyiam, O. A., Mode, A. W., Okara, E. S., (2017), "The use of cross-plots in lithology delineation and petrophysical evaluation of some wells in the western Coastal Swamp, Niger Delta," *Journal of Petroleum Exploration and Production Technology*, 8, pp. 61-71.

Archie, G. E., (1942), "The electrical resistivity log as an aid in determining some reservoir characteristics," *American Institute of Mining, Metallurgical, and Petroleum Engineers*, 146, pp. 54–62.

Bedrosian, P. A., Burton, B. L., Powers, M. H., Minsley, B. J., Philips, J. D., and Hunter, L. E., (2012), "Geophysical investigations of geology and structure at the Martis Creek Dam, Truckee, California," *Journal of Applied Geophysics*, 77, pp. 7-20.

Bassell, B., (1904), *Earth Dams: A study*, The Engineering News Publishing Company, New York.

Biswas, A. K. and Chatterjee, S., (1971), "Dam disasters – an assessment," *Engineering Journal (Canada)*, 54, pp. 3– 8.

Black, C. A., (1965), *Methods of Soil Analysis: Part I Physical and mineralogical properties*, American Society of Agronomy, Madison, Wisconsin, USA.

Borsic, A., Comina, C., Foti, S., Lancellotta, R., and Musso, G., (2005), "Imaging heterogeneities with electrical impedance tomography: Laboratory results," *Geotechnique*, 55, pp. 539-547.

Brackett, T. C., (2012), Use of Geophysical Methods to Map Subsurface Features at Levee Seepage Locations, Master's thesis, University of Mississippi.

Brosten, T. R., Llopis, J. L., and Kelley, J. R., (2005) "Using geophysics to assess the condition of small embankment dams," USACE Engineering Research and Development Center, ERDC/GSL TR-05-17.

Bryson, L.S., (2005), "Evaluation of geotechnical parameters using electrical resistivity measurements," *Engineering and Soil Dynamics,* ASCE, GSP 133, pp. 1-12.

Bryson, L.S., and Bathe, A., (2009), "Determination of selected geotechnical properties of soil using electrical conductivity testing," *Geotechnical Testing Journal*, 32, pp. 252-261.

Butler, D. K., Llopis, J. L., Dobecki, T. L., Wilt, M. J., Corwin, R. F., Olhoeft, G., (1990), "Comprehensive geophysical investigation of an existing dam foundation," *The Leading Edge*, 9, pp. 44-53.

Case, J. S., (2012), *Inspection of earthen embankment dams using time lapse electrical resistivity tomography*, Master's Thesis, University of Mississippi.

Chan, C. M., (2012), "Variations of shear wave arrival time in unconfined soil specimens measured with bender elements," *Geotechnical and Geological Engineering,* 30, pp. 461-468.

Chan, K. H., Boonyatee, T., and Mitachi, T., (2010), "Effect of bender element installation in clay samples," *Geotechnique,* 60, pp. 287–291.

Chinedu, A. D., and Ogah, A. J., (2014), "Electrical resistivity imaging of suspected seepage channels in an earthen dam in Zaria, North-Western Nigeria," *Open Journal of Applied Sciences*, 3, pp. 145-154.

Cho, I., and Yeom, J., (2007), "Crossline resistivity tomography for the delineation of anomalous seepage pathways in an embankment dam," *Geophysics*, 72, pp. G31–G38.

Christensen, N. I., and Wang, H. F., (1985), "The influence of pore pressure and confining pressure on dynamic elastic properties of Berea sandstone," *Geophysics,* 50, 2, pp. 207-213.

Clayton, C. R., (2011), "Stiffness at small strain: research and practice," *Geotechnique*, 61, pp. 5-37.

Cosenza, P., Marmet, E., Rejiba, F., Cui, Y. J., Tabbagh, A., and Charlery, Y., (2006), "Correlation between geotechnical and electrical data: a case study at Garchy in France," *Journal of Applied Geophysics,* 60, pp. 165-178.

Cullen, A. H., (1962), *Rivers in Harness: The Story of Dams,* Chilton Books Publishing, New York.

Dahlin, T., and Johansson, S., (1995), "Resistivity variations in an earth embankment dam in Sweden," *1st EEGS Meeting, Environmental Risk and Planning*.

Dam, T. T., Pisaniello, J. D., and Burritt, R. L., (2011) “Small dam safety problems in Vietnam and associated responsibility and accountability: evidence from a rural commune,” Journal of Asia-Pacific Center for Environmental Accountability, 17, pp. 154-181.

Das, B.M., (2009), *Soil mechanics laboratory manual*, Oxford University Press, Inc, Oxford.

Deniz, R. O., (2008), *Bender elements and bending disks for measurement of shear and compressional wave velocities in large sand specimens*, Master's Thesis, Northeastern University.

Department of Ecology for the State of Washington, (2007), Dam Safety: Notable Dam Failures, http://www.ecy.wa.gov/programs/wr/dams/failure.html, access date March 20, 2017.

Drnevich, V., Evans, A., and Prochaska, A., (2007) “A study of effective soil compaction control of granular soils,” Indiana Department of Transportation and the U.S. Department of Transportation Federal Highway Administration, FHWA/IN/JTRP-2007/12, Final report.

Dyvik, R., and Madshus, C., (1985), “Lab measurements of G_{max} using bender elements,” *ASCE Geotechnical Engineering Division, Proceedings of the conference on the advances in the art of testing soil under cyclic conditions*, pp. 186–196.

Fertl, W. H., (1981), “Openhole cross-plot Concepts – a powerful technique in well log analysis,” *Journal of Petroleum Technology*, 33, doi:10.2118/8115-PA.

Fioravante, V., and Capoferri, R., (2001), “On the use of multi-directional piezoelectric transducers in triaxial testing,” *ASTM Geotechnical Test Journal*, 24, pp. 243–255.

Garcia Bengochea, I., Lovell, C.W., and Altschaeffl, A.G., (1979), “Pore distribution and permeability of silty clays,” *ASCE, Journal of Geotechnical Engineering Division*, 105, pp. 839–856.

Golden software (2018), http://www.goldensoftware.com/products/surfer

Han, D., and Batzle, M. L., (2004) “Gassmann’s equation and fluid-saturation effects on seismic velocities,” *Geophysics*, 69, pp. 398-405.

Hanson, G. J., Tejral, R. D., Hunt, S. L., and Temple, O. M. (2005) “Internal erosion and impact of erosion resistance,” Collaborative Management of Integrated Watersheds. http://ussdams.com/ proceedings/773-784.pdf.

Hayashi, K., and Konishi, C., (2010), “Joint use of a surface-wave method and a resistivity method for safety assessment of levee systems,” *ASCE, GeoFlorida 2010*, pp. 1340-1349.

Hayashi, K., and Suzuki, H., (2004) “CMP cross-correlation analysis of multi-channel surface-wave data,” *Exploration Geophysics*, 35, pp. 7-13.

Hickey, C. J., (2012), *Rapid assessment of potential hazards in levees and earthen dams*, SERRI project final report, August 2012.

Hickey, C. J., Eikmov, A., Hanson, G. J., and Sabatier, J.M., (2009), "Time lapse seismic measurements on a small earthen embankment during an internal erosion experiment," *Symposium on Applications of Geophysics to Environmental and Engineering Problems (SAGEEP),* Fort Worth, TX, pp. 144-156.

Hickey, C. J., Mathias, J. M., Robert, R. W., and Wodajo, L. W., (2015), "Geophysical methods for the assessment of earthen dams," *Advances in Water Resources Engineering,* Springer, USA (book chapter).

Holmes, M., Holmes, A. M., & Holmes, D. I., (2017), "Mixed Reservoir Wetting in Unconventional Reservoirs and Interpretation of Porosity/Resistivity Cross Plots, Derived From Triple-Combo Log Data," *Society of Petrophysicists and Well-Log Analysts (SPWLA) 58th Annual Logging Symposium,* Oklahoma City, OK, June 17-21, 2017.

https://www.nrcs.usda.gov, access date: April 07, 2018.

Imamura, S., Tokumaru, T., Mitsuhata, Y., Hayashi, K., and Inazaki, T., (2007) "Application of integrated geophysical techniques to vulnerability assessment of levee," *Proceeding of the 116th SEGJ Conference*, pp. 120-124.

Inazaki, T., and Hayashi, K., (2011), "Utilization of integrated geophysical surveying for the safety assessment of levee systems," *Symposium on Applications of Geophysics to Environmental and Engineering Problems (SAGEEP),* Charleston, South Carolina.

Inazaki, T., (2007), "Integrated geophysical investigation for the vulnerability assessment of earthen levee," *Symposium on Applications of Geophysics to Environmental and Engineering Problems (SAGEEP),* Denver, Colorado.

Intelligent resources INC (2018). http://www.rayfract.com/

IR (International-Rivers), (2009) *Dam performance and safety*, http://www.internationalrivers.org.

Ivanov, J., Miller, R. D., Stimac, N., Ballard, R. F., Dunbar, J.B., and Smullen, S., (2006), "Time-lapse seismic study of levees in southern New Mexico," *SEG expanded abstract.*

Ivanov, J., Johnson, C. D., Lane, J. W., and Miller, R. D., (2009), "Near-surface evaluation of Ball Mountain Dam, Vermont, using multi-channel analysis of surface waves (MASW) and refraction tomography seismic data methods on land-streamer data," *SEG expanded abstract.*

Ivanov, J., Miller, R. D., Xia, J., Dunbar, J. B., (2007), "Application of the JARS method to study levee sites in southern Texas and southern New Mexico," *Society of Exploration Geophysics,* 6, pp. 1725-1729.

Johansson, S., and Dahlin, T., (1996), "Seepage monitoring in an earth embankment dam by repeated resistivity measurements," *European Journal of Engineering and Geophysics*, 1, pp. 229-247.

Jovicic, V., Coop, M. R., and Simic, M., (1996), "Objective criteria for determining G_{max} from bender element tests," *Geotechnique,* 46, pp. 357–362.

Kalinski, R.J., and Kelly, W.E., (1993), "Estimating water content of soils from electrical resistivity," *Geophysical Testing Journal,* 16, pp. 323-329.

Keith, M., Kristina, C., Donna, C., (2012), *Ensuring public safety by investing in our nation's critical dams and levees*, Center for American Progress.

Kilty, K. T., Norris, R. A., McLamore, W. R., Hennon, K. P., and Euge, K., (1986), "Seismic refraction at Horse Mesa Dam: an application of the generalized reciprocal method," *Geophysics,* 51, pp. 266-275.

Kim, H. S., Oh. S. H., Park, H. G., Chung, H. J., Shon, H. W., Kim, K. S., Lim, H. D., (2004), "Electrical resistivity imaging for comprehensive evaluation of earth-rock dam seepage and safety," *Procs. International Commission on Large Dams (ICOLD),* 72th Annual Meeting, Seoul, Korea, pp. 123-134.

Kim, J. H., Yi, M. J., Song, Y., Seol, S. J., Kim, K. S., (2007), "Application of geophysical methods to the safety analysis of an earth dam," *Journal of Environmental Engineering Geophysics,* 12, pp. 221-235.

Kim, K. Y., Jeon, K. M., Hong, M. H., and Park, Y., (2011), "Detection of anomalous features in an earthen dam using inversions of p-wave first-arrival times and surface-wave dispersion curves," *Exploration Geophysics*, 42, pp. 42-49.

Krief, M., Garat, J., Stellingwerff, J., and Ventre, J., (1990), "A petrophysical interpretation using the velocities of p- and s- waves (full-waveform sonic)," *Society of Petrophysicists and Well-Log Analysts,* 1990, ID: SPWLA-1990-v31.

Lee, J. S., and Santamarina, J. C., (2005), "Bender elements: performance and signal interpretation," *Journal of Geotechnical and Geo-environmental Engineering*, 131, pp. 1063-1070.

Leong, E. C., Cahyadi, J., and Rahardjo, H., (2009), "Measuring shear and compression wave velocities of soil using bender-extender elements," *Canadian Geotechnical Journal*, 46, pp. 792–812.

Liechty, D. J., (2010), "Geophysical surveys, levee certification geophysical investigations, DC resistivity," *23rd EEGS Symposium on the Application of Geophysics to Engineering and Environmental Problems.*

Lim, H. D., Kim, K. S., Kim, J. H., Kwon, H. S., Oh, B. H., (2004), "Leakage detection of earth dam using geophysical methods" *Procs. International Commission on Large Dams (ICOLD), 72th Annual Meeting*, Seoul, Korea, pp. 212-224.

Lin, C. P., Hung, Y. C., Wu, P. L., and Yu, Z. H., (2014), "Performance of 2-D ERT in investigation of abnormal seepage: a case study at the Hsin-Shan earth dam in Taiwan," *Journal of Environmental and Engineering Geophysics*, 19, pp. 101-112.

Lin, C. P., Hung, Y. C., Yu, Z. H., and Wu, P. L., (2013), "Investigation of abnormal seepages in an earth dam using resistivity tomography," *Journal of GeoEngineering*, 8, pp. 61-70.

Liu, C., and Ghosh, D. P., (2016), "AVO and spectral cross-plot: a case study in the Malay basin," *Offshore Technology Conference*, doi:10.4043/26482-MS.

Lokajicek, T., and Svitek, T., (2015), "Laboratory measurement of elastic anisotropy on spherical rock samples by longitudinal and transverse sounding under confining pressure," *Ultrasonic*, 56, pp. 294-302.

Loke, M. H., (1999), "Electrical imaging surveys for environment and engineering studies (A practical guide to 2D and 3D surveys)," *Earth Sciences*, 6574525, No. 1999.

Loke, M. H., (2004), "Tutorial: 2D and 3D electrical imaging surveys," University of Montana.

Loke, M. H., and Barker, R. D., (1995), "Least-square deconvolution of apparent resistivity pseudosections," *Geophysics*, 60, pp. 1682-1690.

Lu, Z., and Sabatier, J. M., (2009), "Effects of Soil Water Potential and Moisture Content of Sound Speed." *Soil Science Society of America Journal*, 73, No. 5, pp. 1614-1625.

Loperte, A., and Soldovieri, F., (2015), "Monte Cotugno dam monitoring by the electrical resistivity tomography," *IEEE Journal of Selected Topics in Applied Earth Observations and Remote Sensing*, 8, 11, pp. 5346-5351.

Mattsson, H., Larsson, R., Holm, G., Dannewitz, N., and Eriksson, H., (2005), "Down-hole technique improves quality control on dry mix columns," *Proceedings of the international conference on deep mixing best practice and recent advances*, 1, pp. 581–592.

McCarter, W. J., (1984), "The electrical resistivity characteristics of compacted clays," *Geotechnique*, 34, pp. 263-267.

Morgan, F. D., (2001), *Self-potential and resistivity for the detection and monitoring of earthen dam seepage*, Massachusetts Institute of Technology: Department of Earth, Atmospheric and Planetary Sciences, Earth Resources Laboratory.

Moustafa, S. S., Ibrahim E. H., Elawadi, E., Metwaly, M., and Agami, N., (2012), "Seismic refraction and resistivity imaging for assessment of groundwater seepage under a dam site, southwest of Saudi Arabia," *International Journal of the Physical Sciences*, 7, pp. 6230-6239.

Moyes, J., (2014) "The soil texture wizard: R functions for plotting, classifying, transforming and exploring soil texture data." https://cran.r-project.org/web/packages/soiltexture/vignettes/soiltexture_vignette.pdf, access date: April 07, 2018.

National Inventory of Dams, (2009), US Army Corps of Engineers (USACE), CorpsMap, http://geo.usace.army.mil/pgis/f?p=397:5:0::NO, access date: March 15, 2015.

National Committee on Levee Safety (NCLS), (2009), Recommendations for a national levee safety program, http://www.leveesafety.org/, access date: April 2, 2009.

Nimrod, P., (2011) *2011 Flood Report, A Success Story*, Mississippi Levee Board.

Nicholson, P. G., (2015) *Soil improvement and ground modification methods*, Elsevier Inc. USA.

Okko, O., Hassinen, P., Korkealaakso, J., (1994), "Location of leakage paths below earth dams by geophysical techniques," *Proceedings International Conference on Soil Mechanics and Foundation Engineering (ICSMFE)*, New Delhi, pp. 1349-1352.

Panthulu, T. V., Krishnaiah, C., Shirke, J. M., (2001), "Detection of seepage paths in earth dams using self-potential and electrical resistivity methods," *Engineering Geology*, 59, pp. 281-295.

Pennington, D. S., Nash, D. F., and Lings, M. L., (2001), "Horizontally mounted bender elements for measuring anisotropic shear moduli in triaxial clay specimens," *ASTM Geotechnical Test Journal*, 24, pp. 133–144.

Prasad, M., and Manghnani, H., (1997), "Effects of pore and differential pressure on compressional wave velocity and quality factor in Berea and Michigan sandstone," *Geophysics*, 62, 4, pp. 1163 – 1176.

Rhoades, J.D., Kaddah, M.T., Halvorson, A.D., and Prather, R.J., (1997), "Establishing soil electrical conductivity-salinity calibrations using four-electrode cells containing undisturbed soil cores," *Soil Science Society of America Journal*, 123, pp. 137-141.

Samouëlian, A., Cousin, I., Tabbagh, A., Bruand A., and Richard G., (2005), "Electrical resistivity survey in soil science: a review," *Soil and Tillage Research*, 83, pp. 173-193.

Saucier, R. T., (1994), Geomorphology and quaternary geologic history of the lower Mississippi 554 valley, U*.S. Army Engineer Waterways Experiment Station*, Volume 1.

Seed, R. B., Nicholson, P. G., Dalrymple, R. A., Battjes, J., Bea, R. G., Boutwell, G., Bray, J.D., Collins, B. D., Harder, L.F., Headland, J.R., Inamine, M., Kayen, R.E., Kuhr, R., Pestana, J. M., Sanders, R., Silva-Tulla, F., Storesund, R., Tanaka, S., Wartman, J., Wolff, T. F., Wooten, L., and Zimmie, T., (2005), "Preliminary report on the performance of the New Orleans levee systems in Hurricane Katrina on August 29, 2005," Report No. UCB/CITRIS-05/01.

Shahin, A., Stoffa, P. L., Tatham, R. H., and Sava, D., (2009), "Multicomponent seismic time-lapse cross-plot and its applications," Society of Exploration Geophysicists (SEG) International Exposition and Annual Meeting, Houston, TX.

Sheehan, J. R., Doll, W. E., and Mandell, W. A., (2005), "An evaluation of methods and available software for seismic refraction tomography analysis," *Journal of Environmental and Engineering Geophysics*, 10, pp. 21-34.

Sjödahl, P., Dahlin, T., Johansson, S., and Loke, M. H., (2008), "Resistivity monitoring for leakage and internal erosion detection at Hällby embankment dam," *Journal of Applied Geophysics,* 65, pp. 155–164.

Song, S. H., Song, Y., and Kwon, B. D., (2005), "Application of hydrogeological and geophysical methods to delineate leakage pathways in an earth fill dam," *Exploration Geophysics,* 36, pp. 92-96.

Sreedeep, S., Reshma, A.C., and Singh, D.N., (2005), "Generalized relationship for determining soil electrical resistivity from its thermal resistivity," *Experimental Thermal and Fluid Science,* 29, pp. 217-226.

United States Society on Dams (USSD) (2011) "Materials for embankment dams," prepared by the USSD committee on materials for embankment dams.

US Army Corps of Engineers (USACE) EM 1110-1-1802 (1995) *Geophysical exploration for engineering and environmental investigations,* Engineer Manual.

US Army Corps of Engineers (USACE) EM 1110-2-1913 (2000) *Design and construction of levees,* Engineer Manual.

US Army Corps of Engineers (USACE) EM 1110-2-2300 (2004) *General design and construction considerations for earth and rock-fill dams,* Engineer Manual.

Uyanik, O., (2011), "The porosity of saturated shallow sediments from seismic compressional and shear wave velocities," *Journal of Geophysics,* 73, pp. 16-24.

Van Baars, S., and Van Kempen, I. M., (2009) "The causes and mechanisms of historic dike failures in the Netherlands," *European Water Association,* ISSN 1994-8549.

Van Der Meer, M. T., Woldringh, R. F., Knuuti, K., (2009) "Comparison of the Dutch and American levee safety approach," ASFPM Conference, Orlando, USA.

Waxman, M. H., and Smits L.J. M., (1968) "Electrical conduction in oil-bearing sands," *Society of Petroleum Engineers Journal,* 8, pp. 107-122.

Wodajo, L. T., (2011) *Seismic tomography for the integrity assessment of earthen dams and levees*, Master's thesis, University of Mississippi.

Yuan, H., Xiang, Y., Wang, Z., Li, J., and Li, Z., (2012), "Three-dimensional seismic refraction to image dam structure," *ASCE, Hydraulics and Earth Structures,* pp. 1104-1109.

Zhou, B., and Dahlin, T., (2003), "Properties and effects of measurement errors on 2D resistivity imaging surveying," *Near Surface Geophysics,* 1, pp. 105-114.

VITA

Leti Wodajo graduated from Jimma University, Ethiopia, with a Bachelor of Science in Civil Engineering in July 2007. From August 2007- June 2009, he worked as a Junior Site Engineer at Sunshine Construction PLC in Addis Ababa, Ethiopia. He entered The University of Mississippi, Oxford, Mississippi, in August 2009, and received a Master of Science Degree in Civil Engineering in May 2011. After his graduation, he decided to continue his education at the University of Mississippi by enrolling in a Civil Engineering Doctorate program. During his graduate study, he worked at the National Center for Physical Acoustics as a graduate research assistant from August 2009 to November 2016, and as an Associate Research and Development Engineer beginning December 2016.

His experience includes conducting research in near surface geomaterials when subjected to mechanical deformations, developing seismic measurements for monitoring spatial and temporal changes in soil properties, conducting seismic refraction, MASW, and electrical tomography methods for the investigation of earth embankment dams, levees and tunnel detection. He has excellent working experience with multiple seismic and electrical resistivity tomography inversion and imaging software.